2013

Risk-based security-constrained optimal power flow: Mathematical fundamentals, computational strategies, validation, and use within electricity markets

Qin Wang
Iowa State University

Risk-based security-constrained optimal power flow: Mathematical fundamentals, computational strategies, validation, and use within electricity markets

by

Qin Wang

A dissertation submitted to the graduate faculty

in partial fulfillment of the requirements for the degree of

DOCTOR OF PHILOSOPHY

Major: Electrical Engineering

Program of Study Committee:
James D. McCalley, Major Professor
Venkataramana Ajjarapu
Ian Dobson
Leigh Tesfatsion
Lizhi Wang

Iowa State University

Ames, Iowa

2013

TABLE OF CONTENTS

LIST OF TABLES

LIST OF FIGURES

ACKNOWLEDGEMENTS

I would like to express my most sincere gratitude to my major professor, Dr. James D. McCalley, for his guidance, patience and support throughout this research and the writing process of this dissertation. His professional accomplishments and dedications have been a tremendous source of inspiration for me, and will inspire me to go ahead on my future academic career. I enjoyed working under his supervision very much.

I greatly appreciate my committee members, Dr. Venkataramana Ajjarapu, Dr. Ian Dobson, Dr. Leigh Tesfatsion, and Dr. Lizhi Wang for their efforts and generously providing time and assistance in the completion of this work. I would also like to thank Dr. Tongxin Zheng and Dr. Litvinov Eugene at ISO New England for their help to my research, and Prof. Fushuan Wen for his guiding of me to enter the door of academia.

In addition, I would also like to thank my friends, colleagues, the department faculty and staff for making my time at Iowa State University a wonderful experience. Without your help, I wouldn't be where I am now.

Finally, thanks to my family for their encouragement and to Wanning Li for her hours of patience, respect and love.

ABSTRACT

This dissertation contributes to develop the mathematical fundamentals and computational strategies of risk-based security-constrained optimal power flow (RB-SCOPF) and validate its application in electricity markets. The RB-SCOPF enforces three types of flow-related constraints: normal state deterministic flow limits, contingency state deterministic flow limits (the "N-1" criteria), and contingency state system risk, which depends only on contingency states but not the normal state. Each constraint group is scaled by a single parameter setting allowing tradeoffs between deterministic constraints and system risk. Relative to the security-constrained optimal power flow (SCOPF) used in industry today, the RB-SCOPF finds operating conditions that are more secure and more economic. It does this by obtaining solutions that achieve better balance between post-contingency flows on individual circuits and overall system risk. The method exploits the fact that, in a SCOPF solution, some post-contingency circuit flows which exceed their limits impose little risk while other post-contingency circuit flows which are within their limits impose significant risk. The RB-SCOPF softens constraints for the former and hardens constraints for the latter, thus achieving simultaneous improvement in both security and economy. Although the RB-SCOPF is more time-intensive to solve than SCOPF, we have developed efficient algorithms that allow RB-SCOPF to solve in sufficient time for use in real-time electricity markets. In contrast to SCOPF, which motivates market behavior to offload circuit flows exceeding rated flows, the use of RB-SCOPF provides price signals that motivate market behavior to offload circuit flows and to enhance system-wide security levels. Voltage stability testing has demonstrated that the dispatch result based on RB-

SCOPF has higher reactive margins at normal state and after a contingency happens, thus has better static voltage stability performance.

CHAPTER 1. INTRODUCTION

1.1 The Need of Risk-based Approach in Electric Power Systems

Risk assessment (RA) has been widely used in other industries such as nuclear, aerospace, oil, food, public health, information technology and financial engineering. It is an emerging new topic in power engineering. Although the successful application of RA in other areas could provide valuable experience for the implementation of risk-based approach in power systems, the definition as well as the meaning of risk is quite different. In fact, risk assessment has a wide-ranging content. Traditional popular RA methods such as mean-variance, Value-at-Risk and real operation approaches have been used in business and finance areas—this kind of risk approach primarily takes an angle from the economic perspective. The intent of this dissertation, however, is to discuss the models, methods and applications of engineering risk in physical power systems. The major difference of engineering risk and financial risk lies in their sources of uncertainties. For example, the financial risk is rooted from uncertainties of credit, investment, and market liquidity, et al., while the engineering risk comes from failures of equipment, behaviors of persons and conditions of weather, et al. In addition, the engineering risk should be in accordance with the physical law of power systems.

According to an IEEE standard, risk could be calculated as the product of the probability a contingency occurs multiplied by the consequence of that contingency. In real world, both the probability and the consequence of an event occurrence are difficult to quantify. Thus, the risk management (RM) method, whose purpose is to identify, assess and prioritize risk, should be researched to minimize, monitor and control the probability and/or sequence of

unexpected events. There should be at least three tasks for risk management in power system:

- Setting up standards or measures of quantifying the risk
- Determining acceptable risk levels for power system operation or planning
- Finding effective mechanisms to reduce the risk

The application of risk management in power system is motivated by a perceived increase in the frequency at which power system operators are encountering high stress in bulk transmission systems and the corresponding need to improve security monitoring of these networks. Traditional security assessment approach in power system tries to capture risk with rules like the so-called "N-1 security criteria", but does not do a good job at it. During the past years, the power system outage events have occurred a lot all around the world. According to a report by Ernest Orlando Lawrence Berkeley National Laboratory ("*Understanding the Cost of Power Interruptions to U.S. Electricity Consumers*", 2004), the national cost of power interruptions in USA is about $80 billion annually. Some severe power outages have happened recently. For example, the Northeast Blackout occurred on August 14, 2003 in North America area affected an estimated 10 million people in Canada and 45 million people in eight states of USA. On November 10, 2009, a power outage occurred throughout much of Brazil and entirety of Paraguay (for a short time) affected an estimated 60 million people. These severe outages of power system lead us incentives to re-examine the single-contingency criterion (N-1 principle) that has served the industry for the past decades. The N-1 criterion may not be sufficient to guarantee the system be within a reasonable security level. On the other hand, it is generally accepted that to implement N-2 or even higher N-k ($k \geq 3$) security principle may cause excessive financial and

computational costs for utility companies. Consequently, one attractive and applicable alternative is to adopt risk-based approach in the planning and operations of power system. We think that the risk-based approach will reduce the frequency and severity of high consequence events, but it is not clear if it would have eliminated these particular events.

Risk is a measure of uncertainties. Another motivation of risk-based approach lies in the fact that the power industry is facing increasingly more uncertainties, which have brought great challenges to the security of power system. In July 21, 2011, the FERC (Federal Energy Regulatory Commission) issued Order 1000 which supports many states in USA to focus upon the following three topics of future power system: energy efficiency, demand response, and smart grid. All of them will increase the uncertainties of the system. Energy efficiency means using less energy to provide the same service. Some activities suggested by the IEA (International Energy Agency) to save energy, such as "*turning off the lights when not using it*" and "*using a power strip to turn off stand-by power in electronics and appliances* [1]," will increase the uncertainty on human's usage of electricity. Demand response is a mechanism to encourage customers reducing their electricity consumption in response to market prices. The ISOs (Independent System Operators) may even execute load shedding when necessary according to the demand side bidding price. The uncertainties, from both customer's behaviors and demand side load forecasting, will make the operation of power system more complicated. Smart grid has a broad range of contents. Although its definition is various, the following characteristics are generally accepted to form the future smart grid environment: higher penetration of renewable generation resources, deployment of advanced electricity storage and peak-shaving technologies including plug-in hybrid electric vehicles (PHEVs), provision to consumers with timely

information and control options, increased use of information technology to improve reliability, security and efficiency of the electric power grid. Obviously, the smart grid environment will bring new challenges to the operation of power system. All these factors will force power utilities to operate and plan the system closer to the limits, thus lead to more stressed operation conditions.

The risk-based approach is an emerging new direction that is studied and beginning to be used in power system planning [2][3] and maintenance [4][5]. Most of the previous work focuses on Risk-based Security Assessment (RBSA). Research on the application of risk-based approach for real-time operation is rare. The major reasons are that the "N-1 principle" applied in RBSA is simple to implement and to understand, and our operating paradigm and tools have not evolved to enable observation of its weakness. Reference [6][7] proposed the frameworks of risk-based approach application for power grid, but did not provide details on how to realize it. A risk-limiting dispatch under smart-grid environment was proposed in [8]. Although it has provided models taking into account the stochastic nature of renewable sources and the demand response, it is difficult to extend the model in real-world large-scale power systems. Thus, the following problem becomes critical:

- How to embed risk and the benefits of its use into the real-time operation software of today's ISO-based power system while maintaining it to be mathematically rigorous and computationally tractable, without decreasing the system's overall security level?

The purpose of our work is to motivate the application of risk-based operation approach in ISO's real-time dispatch procedure. To this end, the proposed approach should be able to satisfy the operational requirements of a large power system. For example, it is not a good idea to apply chance-constrained programing model in power system operation. The chance-constrained programing is a popular risk management method. A generally used approach to solve the model is Monte Carlo simulation. However, the Monte Carlo simulation is an experiment-based computational algorithm that relies on repeated random samplings. Usually large amount of original sample is needed to get the desired results. It would be too time consuming to be applied in power system operation.

Considering the above requirements on the ISOs-oriented dispatch software, we proposed a so-called Risk-based Security-Constrained Optimal Power Flow (RB-SCOPF) model for the purpose of replacing the current SCOPF model. In the following chapters we will present the mathematical fundamentals, the computational strategy and the industrial applications of RB-SCOPF model. The RB-SCOPF has an alternative name of RB-SCED (Risk-based Security-Constrained Economic Dispatch), which may appear in the following chapters. A key challenge to implement RB-SCOPF is its high computational dimensionality, as introduced in what follows.

1.2 Literature Review

1.2.1 Definition of power system security

To ensure the reliable operation is a critical task for the safe and economic operation of power systems. The NERC (North American Electric Reliability Council) defines power system reliability as follows [9]:

"*Reliability, in a bulk power system, is the degree to which the performance of the elements of that system results in power being delivered to consumers within accepted standards and in the amount desired. The degree of reliability in operations may be measured by the frequency, duration and magnitude of adverse effects on consumer service. The degree of reliability in operational and long-term planning is measured by the predicted performance of the system in studies to provide acceptable performance for credible contingencies while considering sensitivity in the assumptions that define the operational state being studied.*"

The reliability of bulk power system can be addressed by considering two basic and functional aspects [9]:

- **Adequacy** is the ability of the bulk power system to supply the aggregate power and energy requirements of the consumers at all times, taking into account scheduled and unscheduled outages of the system components.
- **Security** is the ability of the bulk power system to withstand sudden disturbances such as electric short circuits or unanticipated loss of system components.

The adequacy is usually interpreted as the system's ability to supply the load without violating the circuits and bus voltage ratings, while the security is interpreted as the system's ability to withstand sudden disturbances in a short-term, which is the so-called transient effect. In this dissertation, we address the security of power system with the manner in which the potential of outage events have impacts on operation and planning decisions. The disturbances introduced here include 3 types of problems: overload of circuits, low voltages and cascading. We do not assess and control dynamic security, which

refers to transient instability and oscillatory instability, in this dissertation. It is another important topic to be addressed in future work.

Traditionally, the NERC standard requires that electric transmission systems be operated under *disturbance-performance criteria*, where a disturbance resulting in loss of any single component such as transmission line, transformer or generator (NERC class B) or simultaneously loss of two components (NERC class C) will result in performance that is within stated criteria. Typical criteria includes branch flows within designated ratings, bus voltage variations are within a certain range, voltage stability margins are above specified thresholds, no cascading, and no out-of-step conditions. To accomplish the NERC disturbance-performance criteria, the control center must continuously assess the conditions of power system to detect if the system operation condition is unacceptable, monitor security assessment to decide when actions need to be taken and what actions to take. All these will be helpful to maneuver the system back into acceptable conditions.

In today's control center, the assessment, monitoring, and decision are based on the security analysis function within the Energy Management System (EMS), where the pre-contingency activities and predicted violations are its basis. For example, security assessment results are used to monitor the predicted post-contingency performance of elements. A decision making process begins as soon as any single contingency is predicted to violate the performance criteria. Overload on transmission lines generally require generation re-dispatch, and voltage instability on buses is usually addressed by increasing reactive power supply.

However, there are at least 3 other influences that are not addressed in the above decision making process: 1) The likelihood of contingencies: loss of a 100 mile length transmission

line at severe weather is more likely than loss of a 10 mile length line at normal weather—traditional assessment approach treats them equally. 2) The extend of violations: a 10% post-contingency overload on a 500 Amperes rated line may be of less concern than a 5% post-contingency overload on a 1000 Amperes rated line. 3) The number of violations: an operating condition whereby one "N-1" contingency results in a single post-contingency violations is of less concern than an operating condition whereby several different "N-1" contingencies result in multiple post-contingency violations.

Today's EMS security assessment functionality does not have the ability to provide automated decision-supports in ways that account for the above influences. This leads to an important motivation for our research—to develop approaches and tools that are able to provide quantifiable results to account for some or all of the above influences.

Fig. 1.1 indicates the power system operating states [10]. Five operating states are described for the power system conditions: normal, alert, emergency, in extremis (or extreme emergency), and restorative. There are two types of constraints for power system operation: equality constraints, which refer to the power balance equation, and the inequality constraints, which generally means the system variables must not exceed the practical limitations. In the normal state, all the constraints are satisfied. The system is secure and is able to withstand the loss of any one pre-defined contingencies. The system enters the alert state if the system security level falls below a certain limit, or if the probability of a disturbance increases due to adverse weather conditions. The system may enter emergency state or *in extremis* state from the alert state if a sufficiently severe disturbance really occurs, depending on the severity degree of the disturbance: in emergency state only inequality constraints are not satisfied, while in *in extremis* state both inequality and equality

constraints are not satisfied. The restorative state stands for such a condition that control action is being taken to reconnect the facilities and to restore the system load. Only equality constraints are not satisfied in restorative state. The system may transits from restorative state to either normal or alert states.

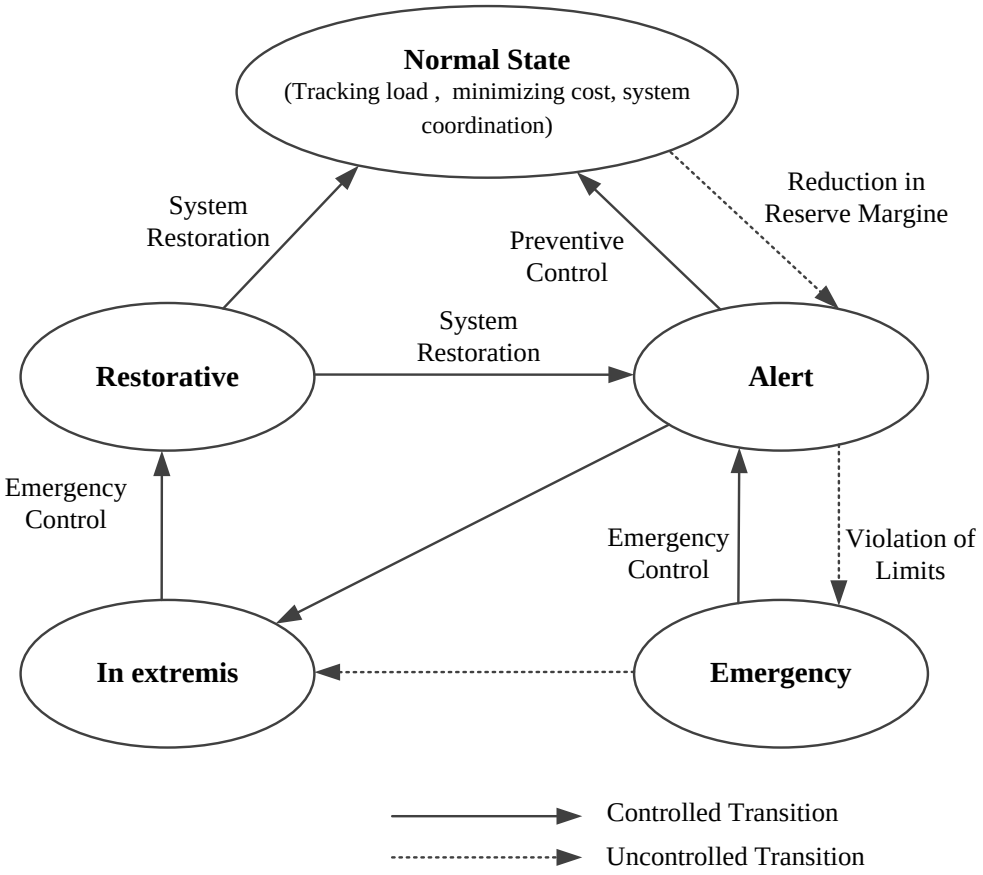

Fig. 1.1. Power system operating states

Traditional security-based decision such as the "*N-1*criteria" is a worse-scenario approach that any normal state is acceptable, and the other states are not acceptable. The weakness of the traditional approach is that it lacks a quantitative method to measure the security level and distinguish between the states. Consequently, rough rules of thumb are adopted in the

decision process. Most importantly, lack of a security level index disguises the fact that it is hard to distinguish the alert state and the normal state, in both of which the equality and inequality constraints are satisfied and unexpected events may cause undesirable consequences. Thus, the risk index is a good metric to distinguish the operating conditions of different states, and quantify the likelihood and/or severity of undesirable consequences.

1.2.2 Power System Security Assessment

Security has costs. A higher security level generally means higher costs, and vice versa. References [11]-[12] proposed the framework on computing the value of security. Security assessment (SA) refers to the analysis that is required to determine if the system can fulfill specified criteria in reliability and security for both transient and steady-state conditions under all credible contingencies [13]. Historically, there are two types of power system security assessment: deterministic approach and probabilistic approach. The deterministic approach generally refers to the "N-1" criterion applied in the operation and planning procedure of power industry, while the probabilistic approach accounts for the probabilistic nature of system conditions and is able to quantify and manage system risk.

The deterministic approach has been applied in the industry for a long time [14]-[17]. Under the deterministic framework, system security analysis is performed in terms of the thermal loading of system elements [18], voltage and frequency variations for both transient and steady states [19]. The basic idea is that the system is able to withstand a set of selected contingencies, which are supposed to have a significant likelihood of occurrence. Although the deterministic approach has well-served the industry on supporting the economic and secure operation of power system in the past decades, there has been a tangible price to pay

for applying it: the solution tends to be conservative because it tends to focus on the most severe events. Consequently, it may lead to such situations that existing facilities cannot be fully explored (in operation), or system resources be overbuilt (in planning). Another weakness of deterministic approach is that there is no index to measure the system's security level, thus it is difficult to integrate security into the economic decision-making process.

The probabilistic approach roots from the nature of probabilistic behaviors in power system. For example, the random failure of power equipment is usually beyond the control of system personnel; loads will always be uncertain and it is impossible to forecast the load exactly precise. It is known that the probabilistic methods have been used as powerful tools in various kinds of decision-making process [20]-[28]. In the works from [29] to [33], the authors focus on developing risk indices, which consider both the likelihood and the severity of events, to capture the probabilistic nature of power system. One of the most attractive implementation of the proposed methodology is to perform the on-line risk-based security assessment (RBSA) [34]-[37]. Compared to traditional online security assessment who always performs security assessment on a past condition (i.e., the last state-estimation), the RBSA has the feature that it performs security assessment on a near-future condition. One significant advantage of this feature lies in that information on which the decision is based, from the assessment, corresponds to the time frame in which the decision is effective [36]. Although the deterministic methods are still dominated in the industry, there is consensus that using probabilistic approach has great potential to improve on analysis and decision-making.

1.2.3 Security Control and Optimization

Power system control usually includes the following actions: prime mover and excitations controls, system frequency control by unit commitment and MW outputs, reactive power and voltage controls, transformer taps controls, shut reactors and capacitors control, and line or bus-bar switching control. The security control is an important function in today's EMS control centers to guarantee the secure operation of power systems. Two kinds of security controls are generally applied:

- **Preventive Control**, which generally includes actions like generation rescheduling and selecting reasonable reserve margins. The preventive control will restore the system from alert state to normal state, as shown in Fig. 1.1.
- **Corrective Control,** which is established to restore the system after the post-contingency events occurs. The corrective controls are usually employed to restore the system from emergency state to alert state.

In power system operation and planning procedure, we usually need to optimize an objective function, such as the generation costs or the control changes from base-case, along with scheduling control actions to achieve the system being operated at a desired security level. This leads to the development of "optimal power flow (OPF)" problem. Literatures on solving OPF problem could generally be summarized into 4 major types: 1) linear programming (LP) and successive linear programming (SLP). Linear programming was used at the early stage due to the limitations on computer hardware [38]-[39]. Successive linear programming is a technique to approximately solve nonlinear optimization problems. Reference [40] introduces the application of SLP in the procedure of solving nonlinear OPF problem by iterations between AC power flow and linearized LP optimization. 2) Interior

point method, which has been generally applied in power system to solve both linear and nonlinear optimization problems [41]–[43]. Due to its speed of convergence and convenience of handling inequality constraints, the interior point method has become a very appealing approach to the OPF problem. 3) Quadratic programming (QP), which is a special form of nonlinear programming with the objective function being quadratic and constraints be linear. The QP has higher accuracy than pure LP. Its advantage is that the objective function is convex, thus a global optimal solution could be guaranteed [44][45]. 4) Heuristic method. It is a technique of searching in the solution space by moving around the neighbors of a known solution in a certain direction such as the steepest ascent [46]. The major heuristic method includes evolutionary algorithm, simulated annealing, tabu search, ant colony search and fuzzy programming.

Security-constrained OPF (SCOPF) problems are a special class of OPF problems. It iterates between a base-case OPF problem and a set of predefined contingency system states. To ensure the security of system, a so-called "N-1 criteria" is applied, i.e. there should be no violations after the outage of any single element I the system. This leads to the implementation of preventive mode of SCOPF. Since it does not allow the post-contingency control capabilities, the preventive mode is usually conservative. If we allow rescheduling to the N-1 security concept, it leads to the corrective mode of SCOPF. The preventive mode is the most secure yet the most expensive solution mode. The corrective mode is less secure but with lower cost since it allows the rescheduling of resources at post-contingency states. It is usually more difficult to solve than the preventive mode. Sometimes people use a combined preventive/corrective mode — some of the violations are relieved in preventive mode, and the rest in corrective mode.

In previous literatures, numerous works have been focused on how to reduce CPU times and computer memory so as to improve the efficiency of SCOPF problem [47]-[49], which indicates that the computation of SCOPF is arduous. Attempting to solve the SCOPF problem directly by simultaneously imposing all post-contingency constraints might lead to unacceptable CPU time and memory. Alternatively, the Benders Decomposition [50], and its general form [51] has been used widely to solve SCOPF problems. For example, the application of BD to preventive and corrective SCOPF was described in [47] and [48], respectively.

1.3 Current Industry Real-time Procedures

The objective of establishing an electricity market is to facilitate an economical operation while ensuring the security of the system. Two major components are included for the operation of today's ISO-based electricity markets: day-ahead market clearing process and real-time market operation. Their structures are indicated in Fig. 1.2 and Fig. 1.3, respectively.

Fig. 1.2 shows the clearing process of day-ahead electricity market. The market participants submit their supply and demand bids to the ISO. At first, a pure unit commitment problem (without network constraints) is solved in the Resource Commitment application (RSC) procedure. This generally involves solving a mixed integer programing (MIP) problem. The resources commitment (on and off status) result is sent to the market clearing engine (MCE) to identify the optimal dispatch (MW and PAR angle) of resources. Then the dispatch result is sent to the Network Security Analysis procedure to check if there is overload violation on the circuits for both normal and post-contingency states. This is

called the simultaneous feasibility test (SFT) [52] process. If there are no violations, the market clearing result is obtained. Otherwise, the SFT will generate generic constraints that will eliminate the violations. The generic constraints are fed back to the MCE to re-dispatch the resources. If the MCE finds that the current resource commitments are not sufficient to support the secure dispatch, the UC problem is solved again to recommit the available resources. Otherwise, the MCE will find the optimal result thus the market clearing results could be obtained.

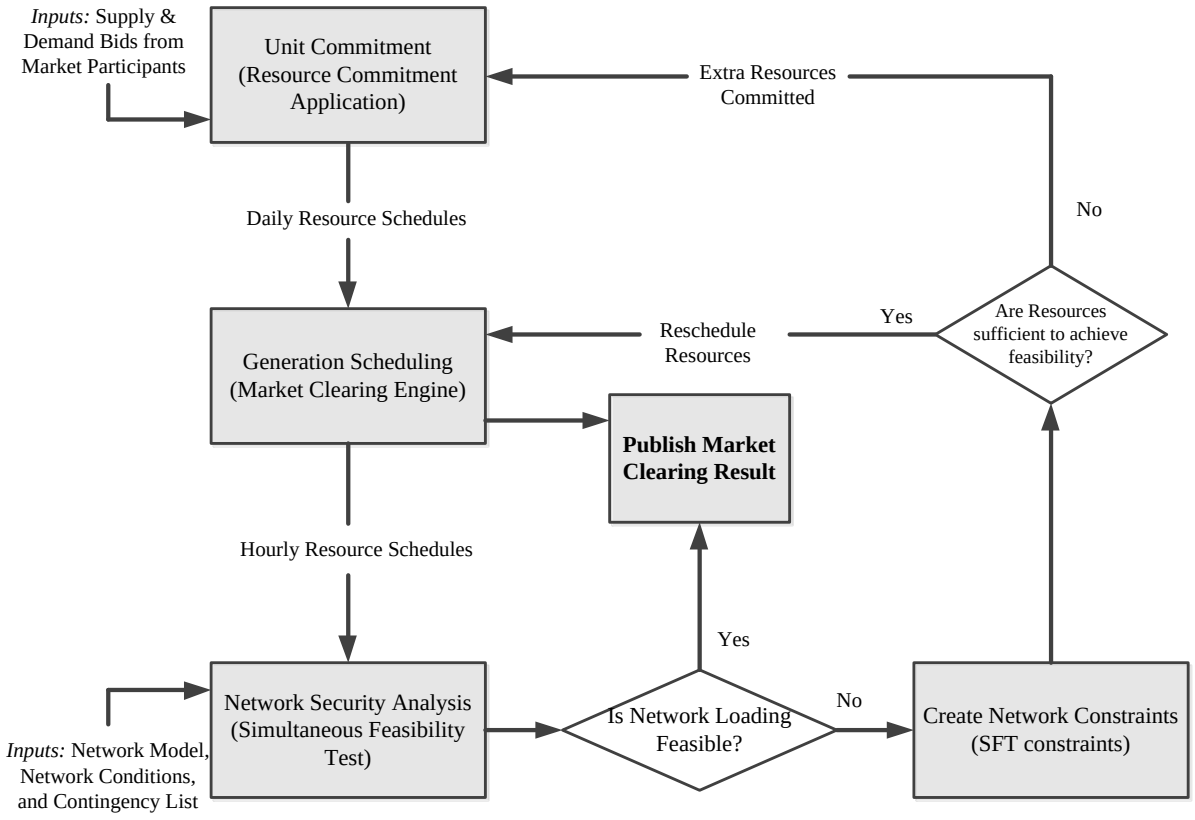

Fig. 1.2. The clearing process of day-ahead electricity market

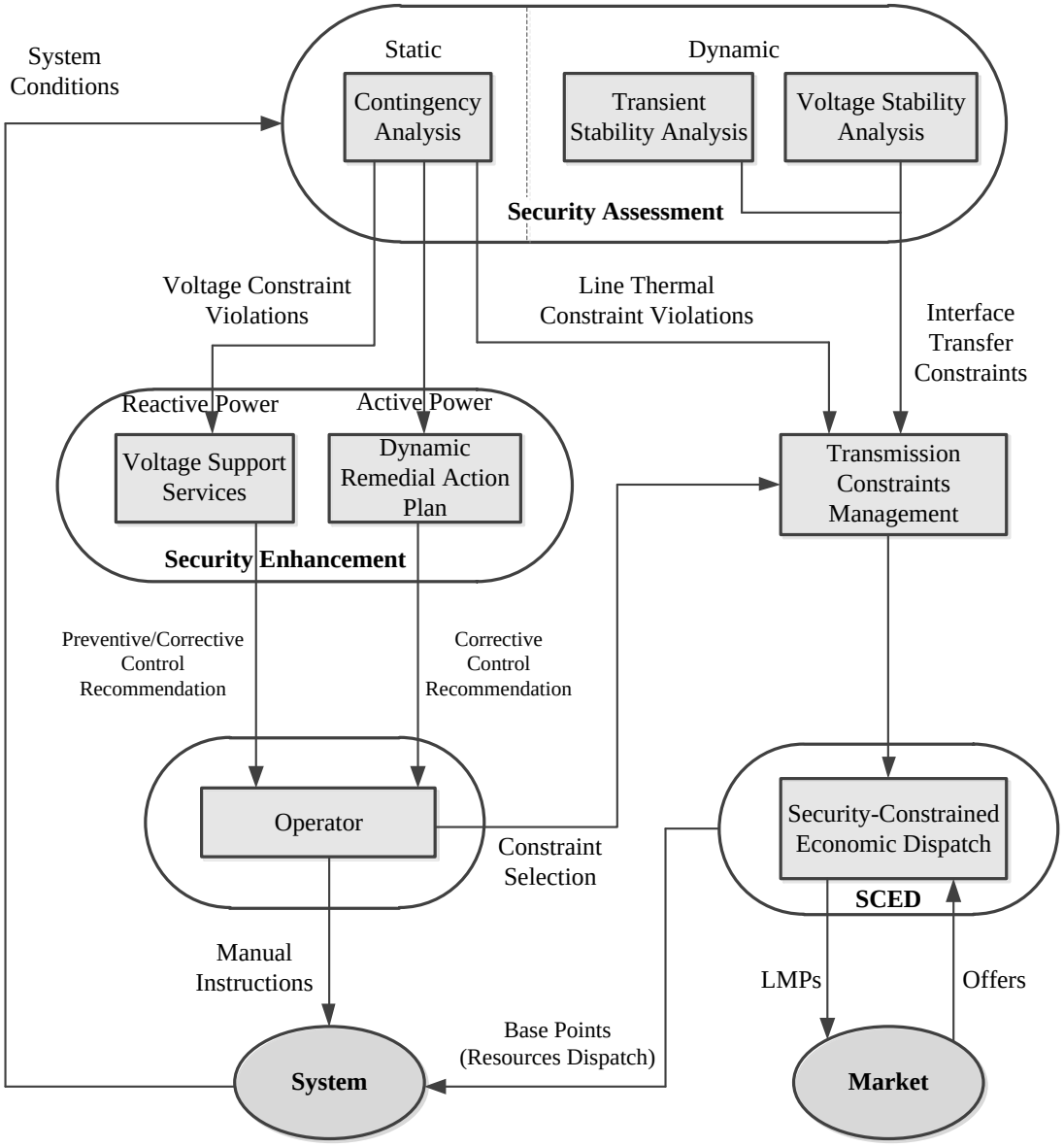

Fig. 1.3. Real-time operation of power system and electricity market

Fig. 1.3 demonstrates how the real-time power system and electricity market are operated [53]. The system and the market are two interconnected components in the operation of ISOs. Historically, ensuring secure operation of the system has always been a critical task. Thus, the system conditions are sent to a so-called Security Assessment (SA) procedure to examine if the current system is secure. The SA includes static security assessment, which

includes contingency analysis (CA), and dynamic security assessment (DSA), which includes transient stability analysis and voltage stability analysis. The static security assessment will generate thermal constraints, which are able to protect the transmission facilities from thermal overload. The dynamic security assessment will generate generic constraints, which are able to protect the transmission system from transient instability and voltage collapse. On the other hand, the CA result will be sent to a Security Enhancement procedure to generate control recommendations to operators. The purpose of security enhancement is to implement control actions to enhance the system's security level, which is realized through the security-constrained optimal power flow (SCOPF). The SCOPF formula is usually divided into two parts: the active power sub-problem and the reactive power sub-problem. The SCOPF is solved by LP optimization, with the objective function of minimizing the control changes from the base-case. The constraints generated in Security Enhancement procedure are selected by the system operators, and then sent to the Transmission Constraints Management (TCM), along with the thermal and generic constraints generated in SA. The TCM will determine activated constraints for the security-constrained economic dispatch (SCED). Based on market participants' offers, SCED produces a least cost dispatch of resources to meet the system requirements including the transmission constraints and resource limit constraints. The SCED generates LMP for the market and base points for system operation.

1.4 Basic Concept of Risk-based OPF

In this section we will present the basic concept of RBOPF, without exploring the details of formulations and computational strategies. At first we introduce the so-called *security*

diagram proposed in [54], as shown in Fig. 1.4 (a) and (b). The information provided in these figures is described as follows:

- **Security regions:** There are three regions: emergency region, highly-stressed region, and less-stressed region, corresponding to the areas with red, yellow and while colors, respectively. If only overload violations are considered, the less-stressed region refers to the circuit loading less than 90% of the emergency rating; the highly-stressed region corresponds to loadings less than 90% of the emergency rating; the emergency region corresponds to loadings in excess of emergency rating.
- **Probability sectors:** Suppose for this particular system, there are five post-contingencies: C1 to C5. Note that the contingency set in real power system is very large, and we may just list the contingencies that bring the system to emergency or highly-stressed regions. The angular spread of each sector is proportional to the contingency probabilities. For example, C4 has the largest probability among the five.
- **Severity circles:** The small circles L1, L2, L5, L8 and L9 represents circuits with post-contingency overload violation or near-violation. In this system, some circuit numbers such as L3, L4, L6 and L7 are not listed in the figure because these circuits will not cause highly-loaded conditions. Radial distance from the center of the diagram to each small circle is proportional to the extent (severity) of the violation. For example, L1 in Fig. 1.4 (a) means flow at circuit L1 is 97.5% of its emergency rating under contingency C4.

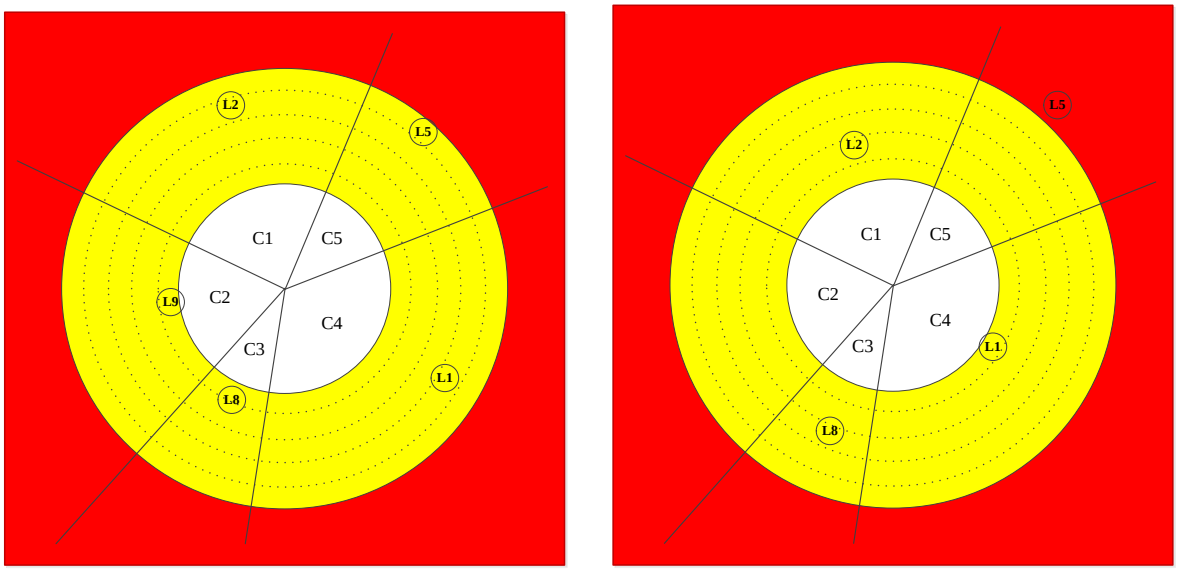

(a) Security diagram for the solution to SCOPF

(b) Security diagram for the solution to RBOPF

Fig. 1.4. Security diagram, C1, C2, C3, C4 and C5 are contingencies; L1, L2, L5, L8 and L9 are lines with post-contingency flow over 90% of their emergency ratings

Fig. 1.4 (a) and (b) demonstrate the benefits of RBOPF over SCOPF. In (a), all the post-contingency circuit flows will not exceed their contingency ratings, as is requirement of the "N-1 principle". However, this is a highly stressed system since some high-probability circles are located close to the red zone. In contrast, the RBOPF result in (b) shows high-probability circles L1, L2 and L9 move closer to the white zone, at the cost of moving low-probability circles L5 and L8 closer to the red zone. By this way, lower risk is achieved by decreasing severity on high probability violations L1, L2 and L9 while increasing severity of low probability violations L5 and L8. Although one violation L5 exceeds its deterministic limit, the overall system risk is lower.

1.5 How RB-SCOPF fits into real-time procedures

As shown in Fig. 1.3, the current industry is using SCED in the real-time electricity market to minimizing the bidding costs, and using Security Assessment and Security Enhancement to guarantee the secure operation of system. If we replace SCED with RB-SCED, the following components should be changed/improved to fit into the new real-time dispatching pattern:

- Replace SCED with RB-SCED. This will require developing new algorithms to solve the RB-SCED problem, as the work done in the following chapters. The corresponding components in the EMS should be modified as well. Since the RB-SCED is more computationally intensive than SCED, thus there is higher requirement on hardware. This is possible with today's computing and analysis tools.
- New market clearing mechanism. In current electricity markets, LMPs are obtained by solving the SCED problem. The LMP at a location is defined as a cost of supplying an increment of load at this location. It could be split into three components: energy component, loss component, and congestion component. If RB-SCED is applied, the three components will have some modifications in their form. In addition, there should be an additional risk component.
- Change of Security Assessment module. The major change comes from there is need to use Adaptive Emergency Transmission Rates (ATR) [55], since we allow a certain degree of post-contingency overloading in RB-SCED model. Although ATR permits post-contingency violations within a certain time interval, the system

reliability is not degraded because the system could be recovered to normal state in reasonable time.

- Modification for the reporting results in Contingency Analysis (CA) process. In current ISO software, the CA process only reports the shift factors and contingency numbers related to the overloading (>100% limit) circuits. The set for these circuits is usually not large. However, if RB-SCED is applied, there is need to report/save shift factors and contingency numbers for the highly-stressed (>90% limit) circuits. There is an increase in the computational burden.
- Set up a new module with the function of computing the contingency probabilities. There does not exist such a module in the real-time electricity market, since the deterministic approach has been applied. To fully address the benefits of probabilistic approach, we need to compute the probability that a contingency may occur by comprehensively considering the real-time information of the system's operational condition and the weather, as well as the historical outage data information.

1.6 Structure of Dissertation

The structure of this dissertation is summarized as follows.

- In chapter 2, we proposed a computational strategy to solve preventive RB-SCOPF model. The benefit of Risk-based (RB) security-constrained optimal power flow (SCOPF) model lies in its ability to improve the economic performance of a power system while enhancing the system's overall security level. However, the RB-SCOPF model is difficult to solve due to the following two characteristics: a) the

overload severity of a circuit changes with the loading condition on it, thus is hard to express with a deterministic function, and b) the risk index is a function of the state variables in both normal and contingency states, which greatly increases the scale of optimization. To handle the first issue, a new expression of severity function is proposed so that it is possible to decompose the model into a SCOPF subproblem and a risk subproblem. To deal with the second issue, a nested Benders decomposition with multi-layer linear programming method is proposed. Illustrations use the ISO New England bulk system is provided to demonstrate the feasibility of the proposed method. Analysis is presented to demonstrate the merits of the RB-SCOPF over the traditional SCOPF model.

- Chapter 3 demonstrates how to use Lagrangian relaxation and Benders decomposition to solve corrective RB-SCOPF. This chapter presents an efficient decomposition based algorithm to solve the corrective risk-based security-constrained optimal power (CRB-SCOPF) problem. The mathematical formulation was proposed imposing, in addition to the traditional post-contingency corrective constraints, risk constraints related with both single circuits (type I risk constraints) and the whole system (type II risk constraints). To solve CRB-SCOPF model is very difficult since the risk index is a function of state variables in all normal and contingency conditions, thus greatly increases the optimization problem size. The proposed approach applies Lagrangian relaxation to the type II risk constraints so as to manage the coupling risk index over the entire system. The remaining problem, called the Lagrangian dual problem (DP), can be solved by the Benders decomposition method. The master problem in DP is a ‘base-case’ economic

dispatch problem associated with corresponding type I risk constraints, and the subproblems are independent contingency analysis with generation rescheduling to eliminate constraint violations. The iterative process will terminate until a converged optimal solution to DP is found. An updated Lagrangian multiplier could be obtained based on the optimal solution. The whole algorithm will be stopped when the multiplier difference between two consecutive iterations is below a pre-specified threshold. The proposed approach has been test on the IEEE 30-bus system and the ISO New England bulk system.

- Chapter 4 presents the framework of applying RB-SCED in the industry by embedding the algorithm into commercial software. The work presented in this chapter was motivated by a perceived increase in the frequency at which the power system operators are encountering higher stressing operation conditions, especially with the increasing uncertainties in power system due to the integration of renewable resources and price responsive demand. To deal with the emerging challenges, we propose a novel risk-based security-constrained economic dispatch (RB-SCED) for the online operation of power system. The RB-SCED model is able to control the system's overall loading stress while handling the uncertainties of post-contingency states. Three different operational conditions for RB-SCED model are provided, thus enables the system operators to make tradeoffs between the economy and security of the system. A combined use of Lagrangian relaxation and Benders decomposition was developed to solve the model. To improve computing efficiency for large system, we performs simultaneous feasibility test (SFT) to make the network sensitivity analysis. Test results based on ISO New England system are illustrated.

- Chapter 5 show how cost and risk change in RB-SCOPF and SCOPF, using coordination parameters in RB-SCOPF to effect tradeoffs between system risk and "N-1" criteria, and thereby characterize conditions under which RB-SCOPF outperforms SCOPF. The K_R-K_C coordination diagram is developed for decision-support that enables efficient security-economy tradeoff analysis. An efficient algorithm to find "breakpoints" in the K_R-K_C coordination diagram. In addition, this chapter shows how system risk and post-contingency overload levels on individual circuits can be coordinated to enhance both economy and security of a power system in real-time operations, and identifies types of conditions for which high-security and high-economy modes would be best suited.
- Chapter 6 develops a new pricing mechanism in electricity market, called the Risk-based LMP (RLMP). It is derived based on the RB-SCED model in Chapter IV. Traditionally, the LMP is calculated with three components: marginal energy, marginal loss and marginal congestion. The RLMP includes, in addition to the three components, a new component called marginal risk. The risk component is a price signal to reflect the system's overall security level. We have researched the features of RLMP on a six-bus system by answering the following three questions: 1) What is the meaning of the risk component? 2) Which generators/loads would likely see higher (or lower) prices? 3) How does the choice of KR and KC affect the RLMP? We have found in the test that RLMP can exclude some extremely high pricings in the system and make the price difference between nodes smaller.
- Chapter 7 compares the voltage stability performance of operating conditions obtained from RB-SCOPF and SCOPF, respectively, using a steady-state voltage

instability index. For both the RB-SCOPF and the SCOPF operating conditions, we model a fictitious synchronous condenser (SC) with very wide reactive limits (e.g., ±1000 MVARs) at one reactive-weak extra-high voltage (e.g., 345 or 500 kV) bus in the system. We use the SC to vary the voltage from its nominal value to a very low value, identifying the bus reactive injection necessary from the SC to hold the given voltage. All the evidences demonstrate that RB-SCOPF has better performance on voltage instability analysis than SCOPF.

- Chapter 8 summarizes the main contribution of the dissertation and proposes the future work.

CHAPTER 2. A COMPUTATIONAL STRATEGY TO SOLVE PREVENTIVE RISK-BASED SECURITY-CONSTRAINED OPTIMAL POWER FLOW

2.1 Introduction

Power system operation is essentially a decision-making process that meets the power demand in an economic way while maintaining system security [2], [56]-[58]. The power industry often adopts the so called "N-1 security criterion" that requires the system as a whole to sustain failure of any single element, such as generator, transformer, or transmission line [59], thus ensures the security of power system after the occurrence of any single contingency. This criterion leads to the implementation of a widely-used optimization problem called security-constrained optimal power flow (SCOPF) in power system [60]-[65]. The SCOPF approach treats the power system in a deterministic way: the system will be either secure or insecure – it cannot quantify how secure the system could be. For example, it is not able to distinguish between violations that occur from contingencies with different likelihood, nor is it able to distinguish between violations that occur with different severity. Hence, risk, a probabilistic index which captures event likelihood and consequence, is proposed in previous work [29] [36] to represent system health, and the corresponding risk-based optimal power flow (RBOPF) [54][66] was proposed to improve on the traditional SCOPF. The RBOPF could result in less cost and higher security operational level on power system than SCOPF [67][68]. In this chapter, we develop a new preventive risk-based security-constrained optimal power flow (RB-SCOPF) model, which coordinates the constraints associated with both the "N-1" contingencies—considered in SCOPF and the risk—considered in RBOPF. The RB-SCOPF model enables the system

operators to make tradeoffs between economy and security, and between system's security and circuit's security.

The major difficulty of RB-SCOPF problem lies in both high computing burden and model dimensionality, especially when the system is large and many contingencies are considered. Attempting to solve the problem by simultaneously imposing all the post-contingency constraints will cause prohibitive requirements on memory and CPU [48]. The objective of this chapter is to propose a computational strategy to solve preventive RB-SCOPF. The major contribution is that we propose a new expression of severity function and a nested Benders decomposition [50] [51] framework to solve the problem. By transferring the deterministic severity function into an optimization problem, it is possible to decompose the model into a SCOPF subproblem and a risk subproblem. In addition, the method does not rely on the form of the severity function, as long as it is convex. The nested Benders decomposition technique is inherently a two-layer linear programming. We provide the simulation results based on ISO New England bulk system using the proposed approach.

2.2 Benders Decomposition Method Introduction

The Benders decomposition (BD) algorithm was first proposed by [50] to solve large-scale, mixed-integer linear programming problems [MILP]. It divides the full problem into a master problem (which could be linear or nonlinear, and continuous or integer), and linear programming sub-problems. The method was further generalized by [51], thus extent to the so-called generalized Benders decomposition (GBD) and make it be able to solve nonlinear problems.

The structure of optimization problems that could be solved by Benders Decomposition is shown as follows:

$$z = \quad Min \quad c(x) + d(y) \tag{2.1}$$

$$s.t. \quad A(x) \ ^3 \ b \tag{2.2}$$

$$E \bullet x + F(y) \geq h \tag{2.3}$$

where constraint (2.3) is referred to as the *coupling constraint*, and matrix *E* is called the *coupler*. In the above form, *E* is a linear matrix, while matrix *A* and *F* could be non-linear.

The problem (2.1)-(2.3) could be decomposed into three easier-to-solve problems: master problem, feasibility sub-problem, and optimality sub-problem.

- **Master Problem**

The master problem is

$$\underline{z} = \quad Min \ \ c(x) + \alpha(x) \tag{2.4}$$

$$s.t. \quad A(x) \geq b \tag{2.5}$$

where $\alpha(x)$ is the estimated lower bound of the optimality sub-problem as a function of decision variable *x* in the master problem. $\underline{z}$ is the lower bound of the lower bound of the original problem and is iteratively updated by solving the optimality subproblems. The optimal solution x^* obtained from the master problem is used in the feasibility and optimality sub-problems.

- **Feasibility subproblem**

The function of feasibility sub-problem is to check if (2.3) is satisfied based on given x^* from the master problem. A slack vector denoted as *s* is usually introduced to formulate the feasibility-check sub-problem:

$$v = \quad Min \ 1^T \bullet s \tag{2.6}$$

$$s.t. \quad F(y) + s \geq h - E \bullet x^* \tag{2.7}$$

where 1^T is the vector of ones. Since $s \geq 0$ and could be large enough, the problem (2.6) - (2.7) should always be feasible. If the optimal solution *v* is greater than 0, it means there are violations in the subproblem. In order to eliminate the violations, the feasibility cut (2.8) should be added to the master problem:

$$v + \lambda E(x^* - x) \leq 0 \tag{2.8}$$

where λ is the Lagrangian multiplier vector for inequality constraints (2.7).

- **Optimality subproblem**

If for a given x^* from the master we have identified that constraint (2.3) is feasible, we need to solve a so-called *optimality-check subproblem* as follows:

$$w = \quad Min \ d(y) \tag{2.9}$$

$$s.t. \quad F(y) \geq h - E \bullet x^* \tag{2.10}$$

where optimal function value *w* is just the $\alpha(x)$ in equation (2.4) when $x = x^*$.

The optimality cut to be added to the master is shown as follows:

$$w + \pi E(x^* - x) \leq \alpha \tag{2.11}$$

where π is the Lagrangian multiplier vector of inequality constraint (2.10).

In the Benders decomposition scheme, the iterations between master problem and subproblem are shown as follows:

a) Start with an approximation $\hat{\alpha}(x)$ which is a lower bound to $\alpha(x)$.

b) Solve the master problem (2.4) – (2.5), obtain the optimal solution x^*.

c) It is possible to show that the optimal objective function value $\underline{z}$ of problem (2.4) – (2.5) is a lower bound to the original optimal solution.

d) Solve the feasiblility-check subproblem, as shown in (2.6) – (2.7). If *v* is greater than 0, add a feasibility cut (2.8) to the master problem, and go to b). Otherwise, go to step e).

e) Solve the optimality-check subproblem (2.9) – (2.10). If the optimal objective function value $w > \alpha(x)$, add a optimality cut (2.11) to the master problem, and go to step b). Otherwise, the optimal solution of the problem has been obtained, the algorithm stops.

2.3 General Formulation of Preventive RB-SCOPF

2.3.1 Overview of risk index

Risk is a probabilistic index defined to reflect the severity of the system's operation condition [36]. Commonly used indices include overload, cascading overload, low voltage and voltage instability [69]. Since the purpose of this chapter is to enhance computational efficiency of the RB-SCOPF for real-time operation, only the risk of overload is considered in the model. Define E_0 as the system's loading condition at normal state and E_i (i = 1, 2, .., N) at contingency states. The risk of the system at certain time t is then

$$Risk(t) = \sum_{i=0}^{N} Pr(E_i, t) Sev(E_i, t) \tag{2.12}$$

where $Pr(E_i, t)$ is the probability of state i at time t, and $Sev(E_i, t)$ is its severity at time t. We only consider a single time period, such as 1 hour, in this chapter. For multiple periods, the proposed method should be the same.

2.3.2 Probability of post-contingencies

We desire to measure risk associated with defined events that may potentially cause specific contingencies, which are associated with a given topological state of the system. Therefore, we assume that the topological state just previous to occurrence of the event, i.e., the normal state, is known with probability identical to one. In addition, in keeping with traditional "N-1" security criteria, we assume those events resulting in simultaneous loss of more than one component have probability zero. For the event "outage of circuit *i*", we may use Poisson process [70, pp. 246] to model it. The probability of a certain post-contingency event is the probability that it occurs at least one time in next hour, meanwhile all the other post-contingency events do not occur. Thus the probability for event E_i is [68]:

$$\Pr(E_i) = (1 - e^{-\lambda_i}) * \exp(-\sum_{j \neq i} \lambda_j) \tag{2.13}$$

where λ_i is the occurrence rate of contingency *i* per time interval. The statistical approach to compute λ_i is detailed in [71]-[72], in which λ_i is a function of weather, geography and voltage class.

The probability calculation for each operating point should be adapted to the market operation procedure. Fig. 2.1 indicates the timeline of market operation. The day-ahead market clears before T_0 of day 1, resulting in the UC and RB-SCED outcomes for the next day. Before the real-time operation hour *T* of day 2, the probability results need to be prepared for the real-time RB-SCED calculation. Thus, the procedure of probability calculating should be finished in time interval [t_{N-1}, t_N] based on the close real-time operation information of power system, such as the forecasted load, the physical condition of equipment, and the weather.

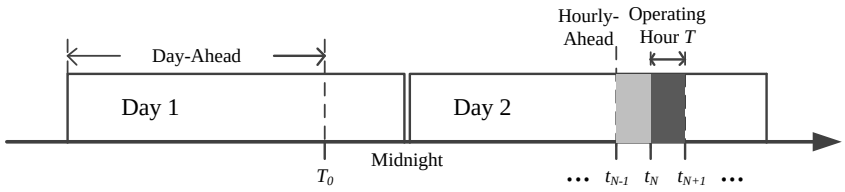

Fig. 2.1. Market operation timeline

2.3.3 Overload Severity

The overload severity function should quantify the consequence of the contingency and properly reflect the system loading condition. It is the fact that the power flow as percentage of rating (PR) of each circuit determines the overload severity of that circuit: the higher the PR is, the more severe the loading condition is, and vice versa [36]. Thus, a rational expression of overload severity function could be shown as the dashed line in Fig 2.2 It is a continuous differentiable function with severity value equal to 1 when PR is ±1, and with increasing slope with absolute value of PR. The benefits of using a continuous differentiable function lie in that it measures the loading condition of every circuit, rather than just measure those circuits with PR over 0.9 which was the case in references [67][68], hence improves the measurement accuracy. The only issue is that this function needs to consider every circuit at both normal and contingency states, and thus it may cause prohibitive computational burden. Consequently, we make a linear approximation for this function, as shown in the solid line of Fig. 2.2. The intersection with horizontal axis at point *c* denotes an expected severity threshold — for PR below this value the circuit is considered to have zero severity. The value of *c* could be adjusted based on the perspective of the operating

organizations. The expression of the piece-wise linearly overload severity function for a single circuit l is:

$$Sev_l = \begin{cases} (PL_l / PL_{l\max} + c_l)/(c_l - 1), & PL_l \le -c_l PL_{l\max} \\ 0, & -c_l PL_{l\max} < PL_l < c_l PL_{l\max} \\ (PL_l / PL_{l\max} - c_l)/(1 - c_l), & PL_l \ge c_l PL_{l\max} \end{cases} \quad (2.14)$$

where PL_l is the power flow of circuit l and PL_{lmax} is its transmission limit, and $PR = PL_l / PL_{l\max}$.The approach adopted here depends only on the severity function being convex.

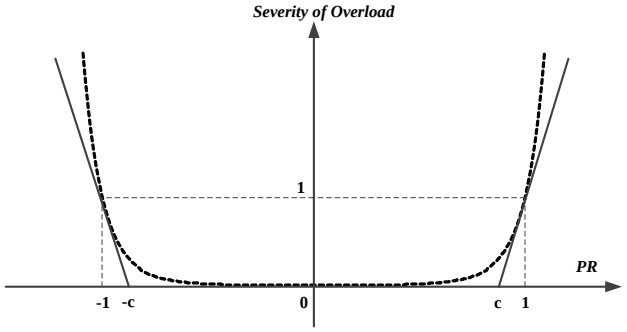

Fig. 2.2. Severity function of circuit overloading

The overload severity function as shown in Fig. 2.2 is applied in Chapter 2 and Chapter 3. A more practical severity function will be applied in Chapter 4, motivated by the concept of adaptive emergency transmission rates (ATR), which has been successfully applied in the control room of ISO New England [52]. The ATR is a novel concept of using continuous adaptive rates rather than discrete emergency rates. Fig. 2.3 illustrates the shape of calculating transient thermal rate as a function of time on the typical conductor DRAKE ACSR [73]. Traditionally, discrete rates are selected for the operational constraint of a line.

For example, the ISO New England operating procedure has defined 3 emergency ratings [74]: 1) Long time emergency (LTE) rating, which is intended to fit a daily load cycle for 4 hours in winter and 12 hours in summer. A facility may operate up to this rating provided that its loading could return to or below normal rating during off-peak hours. 2) Short time emergency (STE) rating, which is a 15 minute rating. A facility operates at this rate for more than 15 minutes will suffer thermal damage on equipment. 3) Drastic action limit (DAL), which is an immediate action rating. A facility operates at this rate for more than 5 minutes will cause thermal damage to equipment. The STE and LTE could be fixed or temperature dependent. The latter is called "dynamic rates" and is beginning to be used in the industry [75]-[77]. Typically, the system operator has to use conservative LTE as the post-contingency emergency rates, which may result in more than necessary restrictive transmission constraints. The ATR concept intends to adaptively select Emergency rating, which could be any point between STE and LTE, by utilizing the post-contingency system ramping capabilities and pre-contingency conductor loading.

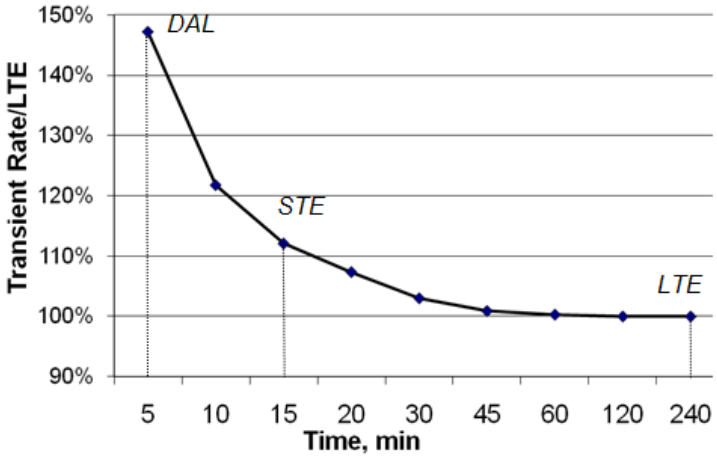

Fig. 2.3. Normalized transient emergency rate as a function of time on conductor DRAKE ACSR

An applicable overload severity function is proposed based on the ATR concept, as shown in Fig. 2.3. The flow on a circuit could be negative if it flows opposite to the pre-defined direction. We dismiss the flow under 90% LTE for post-contingency states, thus the severity value between [-0.9LTE, 0.9LTE] is zero. The severity value linearly increases if the flow is over 90% LTE and reaches 1 on LTE. If the flow is over LTE, the severe level is greater. Thus the curve between [LTE, STE] has lager slope than the one between [0.9LET, LTE]. Similarly, the curve between [STE, DAL] has lager slope than the one between [LTE, STE].

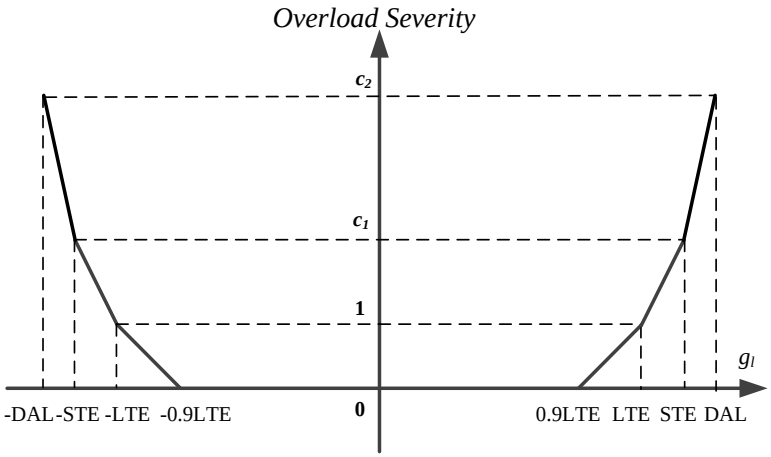

Fig. 2.4. Overload severity function for post-contingency states

In Fig. 2.4, g_l is the post-contingency circuit loading. Note that we do not use PR (as in Fig. 2.2) in the horizontal axis, for the purpose of better demonstrating the ATR concept. Parameters c_1 and c_2 are the corresponding values on the vertical axis. To ensure the convexity of the function, the following formulations should be satisfied:

$$c_1 > \max_l \left\{ 10P_{STE,l} / P_{LTE,l} - 9 \right\} \tag{2.15}$$

$$c_2 > \max_l \left\{ \frac{(c_1 - 1)P_{DAL,l} - c_1 P_{LTE,l} + P_{STE,l}}{P_{STE,l} - P_{LTE,l}} \right\} \tag{2.16}$$

2.3.4 Formulations of SCOPF, RBOPF and RB-SCOPF

The compact form of DC SCOPF could be formulated as follows:

$$\min \left\{ f(\underline{P_0}) \right\} \tag{2.17}$$

Subject to

$$\underline{h}(\underline{P_0}) = \underline{0} \tag{2.18}$$

$$\underline{g}_{\min} \le \underline{g}(\underline{P_0}) \le \underline{g}_{\max} \tag{2.19}$$

$$\underline{g'}_{\min} \le \underline{g}_k(\underline{P_0}) \le \underline{g'}_{\max}, \quad k = 1, ..., NC \tag{2.20}$$

where $\underline{P_0}$ are the real power injections at each node. Index k denotes system state, while k=0 represents the normal condition, and k>0 represents post-contingency conditions. Equation (2.17) optimizes an economic function $f(\underline{P_0})$ (e.g., supply offers less demand bids), (2.18) are the pre-contingency power flow equations, (2.19) are line loading constraints under normal (no contingency) conditions, and (2.20) are line loading constraints under each of NC contingencies. Under this preventive control model, the real power injections $\underline{P_0}$ do not change.

The benchmark RBOPF [78] problem can be formulated as follows:

$$\min \left\{ f(\underline{P_0}) \right\} \tag{2.21}$$

Subject to

$$\underline{h}(\underline{P}_0) = \underline{0} \tag{2.22}$$

$$\underline{g}_{\min} \le \underline{g}(\underline{P}_0) \le \underline{g}_{\max} \tag{2.23}$$

$$0 \le Risk(\underline{g}_1(P_0), \ldots \underline{g}_{NC}(P_0)) \le Risk_{\max} \tag{2.24}$$

where $Risk_{max}$ is the limit of *system* security level. Equation (2.24) is the risk constraint described in (2.25).

$$Risk(\underline{g}_1(P_0), \ldots \underline{g}_{NC}(P_0)) = \sum_{k=0}^{NC} \left(\Pr_k \, Sev(\underline{g}_k(P_0)) \right) \tag{2.25}$$

All the other nomenclatures are the same as in (2.17)-(2.20). Note that the flow constraints for individual circuits at post-contingency are not considered in the RBOPF model. Instead, it restrains the system's overall security level.

The preventive RB-SCOPF problem combines the above two models together by introducing two coordination factors K_C and K_R, formulated as follows:

$$\min \left\{ f(\underline{P}_0) \right\} \tag{2.26}$$

Subject to

$$\underline{h}(\underline{P}_0) = \underline{0} \tag{2.27}$$

$$\underline{g}_{\min} \le \underline{g}(\underline{P}_0) \le \underline{g}_{\max} \tag{2.28}$$

$$K_C \underline{g'}_{\min} \le \underline{g}_k(\underline{P}_0) \le K_C \underline{g'}_{\max}, \qquad k = 1, \ldots, NC \tag{2.29}$$

$$0 \le Risk(\underline{g}_1(P_0), \ldots \underline{g}_{NC}(P_0)) \le K_R \bullet Risk_{\max} \tag{2.30}$$

In formulations (2.29)-(2.30), it is the choice of K_C and K_R, and the coordination between them, through which one may impose control over a tradeoff between security and economy and also a tradeoff between *system* risk and individual circuit risk: the higher K_C and K_R are, the more economic and less secure the system is; and increasing K_C may decrease the security of individual circuit while decreasing K_R may increase the security of the system, and vice versa. We may have different approaches that are appropriate under different situations, as discussed in what follows:

- Highly secure mode (HSM): One may ensure that no control is performed which allows a post-contingency overload to occur. Setting K_C =1 achieves this, and then one can induce lower levels of system risk by adjusting K_R. This approach will never be more risky or more economic than the solution provided by SCOPF, but a given risk reduction, relative to that of the SCOPF solution, is achieved at maximum economic efficiency.
- Economic-secure mode (ESM): Setting K_C >1 allows individual circuit post-contingency loadings in excess of the LTE ratings. It is possible to provide modest reductions in system risk simultaneous with modest improvements in economic efficiency by permitting relatively small post-contingency overloads. Based on the ATR concept, we may select K_C such that $K_C \underline{g}'_{\max}$ equals to the STE in ESM.
- Highly economic mode (HEM): By permitting large post-contingency overloads, one may achieve larger reductions in system risk simultaneous with significant improvements in economic efficiency. The K_C is selected such that $K_C \underline{g}'_{\max}$ equals to the DAL. This approach should not be dismissed as overly-risky. In fact, this approach will yield significantly less risky operating points than the highly-secure

approach, an assertion that can be supported by assessing the different operating points using independent measures such as angular separation or cascading analysis, as shown in [68].

2.3.5 Transformation of severity function

The deterministic overload severity function indicated in Fig. 2.2, either in continuous differentiable or in piece-wise linear approximation form, could be transferred into equivalent optimization expression. The basic idea is that the minimization of a function over a convex area should be on the boundary of that area. A simple example is shown as follows:

$$\{x = 1\} \quad \xleftrightarrow{Equivalent} \quad \{Min\ x:\ x \geq 1\}$$

The equivalent form of (2.14) is:

$$\begin{aligned} &\min\ Sev_l \\ &\text{Subject to} \\ &Sev_l \geq (PL_l / PL_{l\max} + c_l)/(c_l - 1), \\ &Sev_l \geq 0, \\ &Sev_l \geq (PL_l / PL_{l\max} - c_l)/(1 - c_l). \end{aligned} \tag{2.31}$$

Since we try to control the system's risk as a whole in both normal and contingency states, formulation (2.31) might greatly increase the number of constraints when the system is large and many contingencies are considered. However, if Benders decomposition is applied, the PL_l in the right hand side of (2.31) is known from the result of the master problem. Also note that at given PL_l, only one of the three constraints in (2.31) is binding. These features make the problem easier to solve. Another benefit of using (2.31) is that there is no need to introduce integer variables when we treat the piecewise function as in (2.14).

2.4 Benders Decomposition Approach

2.4.1 Two-layer Benders decomposition method

Since the risk of a circuit is a function of the power flowing in it, we cannot compute the risk of the circuit until the dispatch result is known. Thus it is reasonable to divide the problem into two parts: the security-constrained optimal power flow (SCOPF) part without considering the risk and the risk control part based on the SCOPF scheduling result. Consequently, a two-layer Benders decomposition approach is proposed as follows:

- At the *external* layer, given the operating point $\boldsymbol{x_0}$ obtained from the master risk problem, find new operating points $\boldsymbol{x_i}$ that meet the constraint (2.30).
- At the *internal* layer, solve the modified SCOPF problem (including the Benders cuts from external layer BD). The master problem at this layer is the traditional OPF problem. The subproblems are to check the feasibility of transmission security constraints under both normal and contingency states. The obtained generation scheduling, which is locally optimized result, is then sent to the external layer.

The objective function is to minimize the operating cost f_0 at normal state while ensuring the post-contingency flows and the *system*'s overall risk level without violation. The decision process is illustrated in Fig. 2.5.

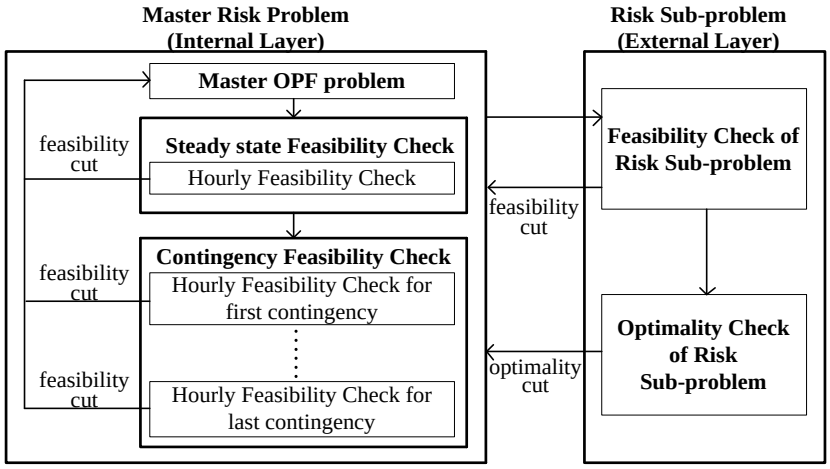

Fig. 2.5. RB-SCOPF problem with two-layer decomposition

2.4.2 Formulation of the preventive RB-SCOPF problem

As mentioned above, the objective of RB-SCOPF is to determine an hourly economic dispatch so as to minimize the operating cost of the system, while satisfying the prevailing constraints as follows:

1) Power balance

2) Hourly generation bids

3) Maximum and minimum limit of unit output

4) Reserve requirement of the system

5) Transmission flow limits in normal & contingency states

6) Limit on system's overall risk level

The objective function will be minimizing the bidding-based operation cost, as follows:

$$\text{Min} \sum_{i=1}^{NG} \sum_{j=1}^{NS_i} s_{i,j} P_{i,j} \tag{2.32}$$

where NG is the number of generation units. NS_i is the number of price bidding segments for unit i. $s_{i,j}$ is the jth segment of bidding price for unit i. $P_{i,j}$ is the real power output of unit i according to the jth segment bidding price.

Traditional SCOPF constraints include the system's power balance (2.33) and real power generation limits by segments (2.34):

$$\sum_{i=1}^{NG}\sum_{j=1}^{NS_i} P_{i,j} = \sum_{i=1}^{ND} P_{Di} + P_{Loss} \tag{2.33}$$

$$\underline{P}_{i,j} \le P_{i,j} \le \overline{P}_{i,j} \tag{2.34}$$

where ND is the number of load bus. P_{Di} is the load at bus i. P_{Loss} is the loss of the system. $\underline{P}_{i,j}$ and $\overline{P}_{i,j}$ are the lower and upper limits of real power output, respectively.

The circuit flows, expressed as linear functions of node power injections multiplied by power transfer distribution factors (PTDF), are enforced to within certain limits, as shown in (2.35) and (2.36):

$$-PL^0_{l,\max} \le PL^0_l = \sum_{i=1}^{NG} \mathrm{PTDF}^0_{l,i} \cdot P_i - \sum_{j=1}^{ND} \mathrm{PTDF}^0_{l,j} \cdot P_{Dj} \le PL^0_{l,\max}$$

$$l = 1, 2, \ldots, NL \tag{2.35}$$

$$-K_C PL^k_{l,\max} \le PL^k_l = \sum_{i=1}^{NG} \mathrm{PTDF}^k_{l,i} \cdot P_i - \sum_{j=1}^{ND} \mathrm{PTDF}^k_{l,j} \cdot P_{Dj} \le K_C PL^k_{l,\max}$$

$$l = 1, 2, \ldots, NL; \;\; k = 1, 2, \ldots, NC \tag{2.36}$$

where PL^k_l is the real power flow of lth circuit at kth contingency, NL is the number of circuits, $\mathrm{PTDF}^k_{l,i}$ is the power transfer distribution factor of bus i to circuit l for the kth contingency. Equation (2.35) denotes the normal state power flow limits, and (2.36) denotes the post-contingency states power flow limits. By using different values of K_C, we could identify various operating conditions for the system.

The DC-OPF can be expressed using balance of injection at each node, or, equivalently, it

can be expressed as a balance of generation and load for the entire system, while satisfying circuit power flow equations. We have chosen the latter approach, as was done in [79], with the system balance computed via equation (2.18) and the circuit power flows computed via equations (2.20) and (2.21) (the result enables computation of the injection at each node). The advantage of this approach is we can express the circuit power flow with the product of shift factors and generator outputs, which facilitates the processing of the feasibility check at the internal layer and improves the computational efficiency.

Many authors have researched on AC OPF model [80]-[83], which is more accurate, nevertheless more difficult to solve, especially for large systems. None of the ISOs in the USA are using ACOPF in their real-time electricity markets, (see page 35 of [34]). Our use of DCOPF is consistent with industry practice. ISO-NE is using DC OPF, with AC feasibility check. We are coordinating with ISO-NE and planning to use AC feasibility check in the next step.

The risk constraints are

$$Sev_{l,k} \geq 0,\ \ l = 1,2,...,NL; k = 0,1,2,...,NC \tag{2.37}$$

$$Sev_{l,k} \geq (PL_l^k / PL_{l,\max}^k + c_l) / (c_l - 1),\ l = 1,2,...,NL; k = 0,1,2,...,NC \tag{2.38}$$

$$Sev_{l,k} \geq (PL_l^k / PL_{l,\max}^k - c_l) / (1 - c_l),\ l = 1,2,...,NL; k = 0,1,2,...,NC \tag{2.39}$$

$$\sum_{k=1}^{NC} Pr_k \sum_{l=1}^{NL} Sev_{l,k} \leq K_R \times Risk_{max} \tag{2.40}$$

where (2.37)-(2.39) are the risk constraints for individual circuits, and (2.40) is the risk constraints for the whole system. The summation on the left side of (2.40) indicates that the risk of the system couples with every circuit at normal and contingency states.

2.4.3 Decomposition Strategy for the internal layer

Benders decomposition is a widely used decomposition technique to solve large-scale optimization problems. For the first-layer decomposition of RB-SCOPF, assuming that $\mathbf{x_1}$ represents the unit output vector $\boldsymbol{P}$ at normal state, and $\mathbf{y}_{1k}$ represents the flow on the circuit at kth contingency, we can write it into the following standard Benders decomposition form (k =0 denotes the variables and parameters at normal state):

$$\text{Min } \boldsymbol{c}^T \mathbf{x}_1 \tag{2.41}$$

Subject to

$$\boldsymbol{A}_1 \mathbf{x}_1 \geq \boldsymbol{b}_1 \tag{2.42}$$

$$\boldsymbol{E}_{1k} \mathbf{x}_1 + \boldsymbol{F}_{1k} \mathbf{y}_{1k} \geq \boldsymbol{h}_{1k}, k = 0,1,2,...,NC \tag{2.43}$$

where (41) represents the cost function (2.32). Equation (2.42) represents constraints (2.33) and (2.34) as well as the Benders cuts from the external layer. Equation (2.43) represents constraints (2.35) and (2.36). Thus, the master problem becomes:

$$\left\{ \text{Min } \boldsymbol{c}^T \mathbf{x}_1 : \boldsymbol{A}_1 \mathbf{x}_1 \geq \boldsymbol{b}_1 \right\} \tag{2.44}$$

The corresponding kth feasibility-check subproblem based on the optimal solution $\mathbf{x_1}^*$ from (2.44) is:

$$\begin{aligned} w_k(\mathbf{x}_1^*) = \text{Min } & \mathbf{1}^T \boldsymbol{s} \\ s.t. \ & \mathbf{F}_{1k} \mathbf{y}_{1k} + \boldsymbol{s} \geq \boldsymbol{h}_{1k} - \boldsymbol{E}_{1k} \mathbf{x}_1^* \qquad \boldsymbol{\lambda}_k \\ & k = 0,1,2,...,NC \end{aligned} \tag{2.45}$$

where $\mathbf{1}$ is the vector of ones, $\boldsymbol{s}$ is slack variables used to check the violation of constraints, and $\boldsymbol{\lambda}_k$ is the simplex multiplier vector of inequality constraints in (2.45). $w_k(\mathbf{x_1}^*) > 0$ means

there exists violation in the *k*th subproblem. To eliminate the violation, the following Benders cut is added to the master problem:

$$\boldsymbol{w}_k(\mathbf{x}_1) = \boldsymbol{w}_k(\mathbf{x}_1^*) - \boldsymbol{\lambda}_k^T \boldsymbol{E}_{1k}(\mathbf{x}_1 - \mathbf{x}_1^*) \le 0 \tag{2.46}$$

There is no optimality cut in the first-layer decomposition, because the optimal function in (2.41) is not interrelated with $\mathbf{y}_{1k}$, thus the subproblems are always optimal with objective values **0** as long as they are feasible. The first-layer optimization is inherently a traditional SCOPF problem, except that risk cut from the second layer is added to it at each iteration of the external loop, as shown in Fig. 2.5. The successful application of using Benders decomposition approach to solve SCOPF has been demonstrated in previous literatures [85]-[87]. Since this paper focuses on dealing with the risk constraints, we use DC model in the internal layer; however, an AC network model can also be used, as shown in Fig. 2.2 where an AC feasibility check can be applied in the "hourly feasibility check" block of the internal loop. The severity function is linear, thus the external loop algorithm remains the same.

2.4.4 Decomposition strategy for the external layer

Assume $\mathbf{x}_2$ represents the states of unit output **P** in normal state and the post-contingency circuit flow **PL**, $\mathbf{y}_2$ represents the states of overload severity at both normal and contingency conditions. We can write the problem into the following Benders decomposition form:

$$\text{Min } \boldsymbol{c}^T\mathbf{x}_2 + \boldsymbol{d}^T\mathbf{y}_2 \tag{2.47}$$

Subject to

$$\boldsymbol{A}_2\mathbf{x}_2 \ge \boldsymbol{b}_2 \tag{2.48}$$

$$\boldsymbol{E}_2\mathbf{x}_2 + \boldsymbol{F}_2\mathbf{y}_2 \geq \boldsymbol{h}_2 \tag{2.49}$$

where (2.47) is the modified objective function: the first part is the cost function in (2.32), and the second part, detailed in (2.50), is the sum of severity in the objective function of (2.31). Equation (2.48) represents constraints in (2.33)-(2.36) as well as the Benders cuts from subproblems, as shown in (2.60) and (2.61) from the following section. Equation (2.49) represents constraints in (2.37)-(2.40).

$$\boldsymbol{d}^T\mathbf{y}_2 = \sum_{k=0}^{NC}\sum_{l=1}^{NL} Sev_{l,k} \tag{2.50}$$

The master problem of Benders decomposition is:

$$\left\{\text{Min } \boldsymbol{c}^T\mathbf{x}_2 + \hat{u} : \boldsymbol{A}_2\mathbf{x}_2 \geq \boldsymbol{b}_2\right\} \tag{2.51}$$

where $\hat{u}$ represents an optimistic estimate of $\boldsymbol{d}^T\mathbf{y}_2^*$ in (2.47). It is a decision variable in the master problem. In theory, it could be any real value. However, in this problem the severity function is greater than or equal to zero, thus we constrain $\hat{u} \geq 0$. In the first iteration, there may be no constraints keeping it from approaching 0, thus we let $\hat{u}^*$ be 0 at the first iteration while minimizing the other constrained variables. The corresponding subproblem associated with the optimal solution $\mathbf{x_2}^*$ of master problem (2.51) is

$$\begin{aligned} \alpha(\mathbf{x}_2^*) = \text{Min } & \boldsymbol{d}^T\mathbf{y}_2 \\ s.t.\ & \mathbf{F}_2\mathbf{y}_2 \geq \boldsymbol{h}_2 - \boldsymbol{E}_2\mathbf{x}_2^* \end{aligned} \tag{2.52}$$

Note that in (2.45) there are (***NC***+1) subproblems and each is an independent optimization with the number of constraints and decision variables no higher than a single OPF problem—denoted as ***O****(1)*. Thus the optimization complexity of the first-layer is of dimension (***NC***+1) × ***O****(1)*. However, there is only one subproblem in (2.52) because we

intend to control the system's *overall* risk level in both normal and contingency conditions. The size of problem (2.52) is extremely large when the system is large, and its optimization complexity is of dimension ***O(NC***+1*)*.

There are three cases that may occur when solving (2.52): 1) infeasible, under which a feasibility cut need to be added to the master in (2.51); 2) has optimal solution $\mathbf{y}_2^*$ but with $\alpha(\boldsymbol{x}_2^*) > \hat{u}^*$, where $\hat{u}^*$ is 0 at the first iteration and the optimal value in (2.51) at the following iterations, then $\hat{u}^*$ is an unrealistic estimate. In order to make $\hat{u}$ be more realistic, we need to send an optimality cut to the master (2.51); 3) has optimal solution $\mathbf{y}_2^*$ and with $\alpha(\boldsymbol{x}_2^*) \le \hat{u}^*$, then $\hat{u}^*$ is realistic. The algorithm stops and the current solution is optimal. The key is how to obtain the feasibility cut and optimality cut, which are discussed as follows.

Feasibility cut. First we need to ascertain if (2.52) is feasible or not. Since its size is large, it is not suitable to solve it directly. The inequality constraint in (2.52) is in fact expressions (2.37)-(2.40). Note that at given $\mathbf{x}_2^*$ in (2.52), i.e., given PL_l^{k*}, only one constraint will hold in (2.37)-(2.39). Let's define

$$\hat{S}ev_{l,k} = \max\{(PL_l^k / PL_{l,\max}^k + c_l)/(c_l - 1), (PL_l^k / PL_{l,\max}^k - c_l)/(1 - c_l), 0\}$$

$$l = 1, 2, ..., NL; k = 0, 1, 2, ..., NC \qquad (2.53)$$

Then the full expression of (2.52) becomes:

$$\text{Min} \sum_{k=1}^{NC} \sum_{l=1}^{NL} Sev_{l,k} \qquad (2.54)$$

Subject to

$$Sev_{l,k} \ge \hat{S}ev_{l,k}, \qquad \mathbf{z}_{l,k} \qquad (2.55)$$

$$\sum_{k=1}^{NC} Pr_k \sum_{l=1}^{NL} Sev_{l,k} \le K_R \times Risk_{max}, \qquad \mathbf{z}_1 \qquad (2.56)$$

$$l = 1, 2, ..., NL; k = 0, 1, 2, ..., NC$$

where $\mathbf{z_1}$ and $\mathbf{z}_{l,k}$ are the simplex multiplier vectors of constraints (2.55) and (2.56). It is proved in the Appendix that if there is:

$$\sum_{k=1}^{NC} Pr_k \sum_{l=1}^{NL} \hat{S}ev_{l,k} - K_R \times Risk_{max} \le 0 \qquad (2.57)$$

then problem (2.54)-(2.56) is optimal with solution $Sev^*_{l,k} = \{\hat{S}ev_{l,k}\}, \forall l,k$. Otherwise, the problem is infeasible and there exists an *extreme ray* for the dual to (2.54)-(2.56)

$$\begin{aligned} &\text{Max } K_R \times Risk_{max} z_1 + \sum_{k=1}^{NC} \sum_{l=1}^{NL} \hat{S}ev_{l,k} \mathbf{z}_{l,k} \\ &s.t. \quad Pr_k z_1 + \mathbf{z}_{l,k} \le 1 \\ &\qquad z_1 \le 0, \mathbf{z}_{l,k} \ge 0 \\ &\qquad l = 1, 2, ..., NL; k = 0, 1, 2, ..., NC \end{aligned} \qquad (2.58)$$

An extreme ray to (2.58), denoted as vector $\{\Delta \mathbf{z}_1, \Delta \mathbf{z}_{l,k}\}$ can be obtained by solving the following optimization (2.59):

$$\begin{aligned} &\text{Max } K_R \times Risk_{max} \Delta z_1 + \sum_{k=1}^{NC} \sum_{l=1}^{NL} \hat{S}ev_{l,k} \Delta \mathbf{z}_{l,k} \\ &s.t. \quad Pr_k \Delta z_1 + \Delta \mathbf{z}_{l,k} \le 0 \\ &\qquad -1 \le \Delta z_1 \le 0, 0 \le \Delta \mathbf{z}_{l,k} \le 1 \\ &\qquad l = 1, 2, ..., NL; k = 0, 1, 2, ..., NC \end{aligned} \qquad (2.59)$$

It is proved in the Appendix that problem (2.48) is optimal with solution { $\Delta z_1^* = -1$, $\Delta \mathbf{z}_{l,k}^* = Pr_k, \forall\, l,k$} and the optimal objective value is just the left hand side of (2.57) and is greater than zero here. Now, we can get the *feasibility cut* as shown in (2.60):

$$(\boldsymbol{h}_2^{effective} - \boldsymbol{E}_2^{effective}\mathbf{x}_2)^{\mathrm{T}} \Delta \mathbf{z}^* \geq 0 \tag{2.60}$$

where vector $\Delta \mathbf{z}^* = [-1, \boldsymbol{Pr}_k], \forall\, l,k$. $\boldsymbol{h}_2^{effective}$ and $\boldsymbol{E}_2^{effective}$ are the coefficients of the effective constraints regarding to the severity function. They are subsets of $\boldsymbol{h_2}$ and $\boldsymbol{E_2}$ in (2.52).

Optimality cut. If (2.52) is optimal, and thus its dual (2.58) is optimal but with the value of objective function $\alpha(\boldsymbol{x}_2^*) > \hat{u}$, an optimal cut need to be added to the master (2.51). It is shown in the Appendix that problem (2.58) is optimal with solution {$\mathbf{z}_1^*=0$, $\mathbf{z}_{l,k}^*= 1, \forall\, l,k$ }. Then, the *optimality cut* is

$$(\boldsymbol{h}_2^{effective} - \boldsymbol{E}_2^{effective}\mathbf{x}_2)^{\mathrm{T}} \mathbf{z}^* \leq \hat{u} \tag{2.61}$$

where vector $\mathbf{z}^* = [0, 1, \ldots, 1]$.

It is interesting to see that by using the approach above, we can solve all the optimization problems algebraically, rather than using simplex or another optimization method at the external layer. This greatly increases the computing speed of the RB-SCOPF.

2.4.5 Iterative Procedure

Based on the above analysis, we can obtain a two layer (or nested) Benders decomposition technique to solve the full RB-SCOPF. The iterative algorithm is as follows.

1) Start with an approximation of $\hat{u}^*$ which is a lower bound to $\hat{u}$.

2) Solve the master problem in the internal layer. The results are OPF schedule without transmission security constraints while ensuring the Benders cuts, if any, from the external loop are satisfied.

3) With the schedule in 2), check the circuit security violations in subproblems (2.45). If any violations occur, the feasibility cuts in (2.46) are added to the master, go to step 2). Else, no overload violations occurs (at both normal and post-contingency conditions) for the schedule. Go to step 4).

4) Obtain updated $\hat{u}^*$ by solving LP (2.51) given the scheduled result from 3).

5) Based on the schedule result from 3), check if the system's overall risk level is within limit. If not, problem (2.52) is infeasible. Generate a feasibility cut as in (2.60) and go to step 2). Else, go to step 6).

6) Solve problem (2.52), and obtain the objective function value $\alpha(\mathbf{x}_2^*)$. If $\alpha(\mathbf{x}_2^*) > \hat{u}^*$, then $\hat{u}^*$ is an unrealistic estimate of $\hat{u}$. Generate an optimality cut as in (2.61), go to step 2). Else, $\hat{u}^*$ is realistic, and the current solution is optimal. Stop.

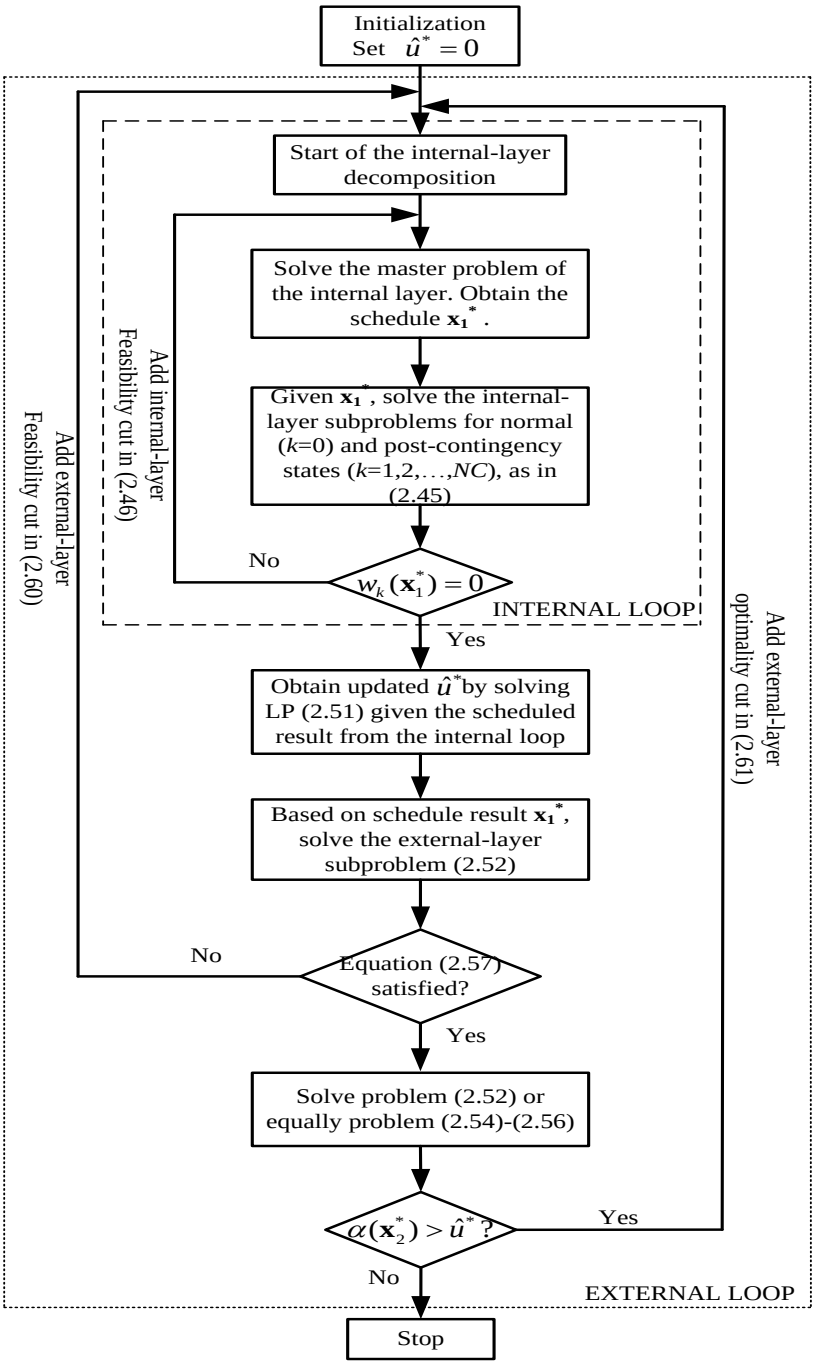

Fig. 2.6. Iteration procedure for RB-SCOPF using two-layer Benders decomposition

The above iteration procedure is shown in Fig. 2.6. It is important to note that SCOPF and RBOPF are both special cases of RB-SCOPF. The algorithm used in the first layer could be used to solve SCOPF, while the algorithm used in the second layer could solve RBOPF.

2.5 Numerical Results

In this section we present two representative numerical examples by the proposed approaches: a 9-bus test system [88] and the ISO New England real system. The former is a simple system that we chose to test the correctness of our algorithm. Since the system is small, we can solve the optimization problem as a whole by simultaneously imposing all post-contingency and risk constraints. The result is then used to compare with that obtained by our proposed two-layer decomposition approach. The latter is a real system from ISO New England, and we provide the results obtained from our software here along with a comparison of some security indices to identify the merits of RB-SCOPF over SCOPF.

2.5.1 The Nine-bus Test System

The diagram of the *nine-bus* test system is shown in Fig. 2.7. The line impedances are indicated in the diagram with per unit values. The loads at bus 5, 6, and 8 are 125 MW, 90 MW and 100 MW, respectively. For simplicity, we assume the generators only provide one-segment bidding prices, which are \$20, \$40 and \$80/MWh for generator 1, 2 and 3, respectively. The economic maximum outputs of these generators are 150, 200, and 150 MW, respectively. The parameters of the transmission lines and transformers, including the impedances, resistances and MW limits are shown in Table 2.1. Two N-1 contingencies are

considered, i.e., the outages of circuits 4-5 and 6-9. Assume their outage probabilities are both 0.01 at certain time *t*, thus the probability of normal state is 0.98.

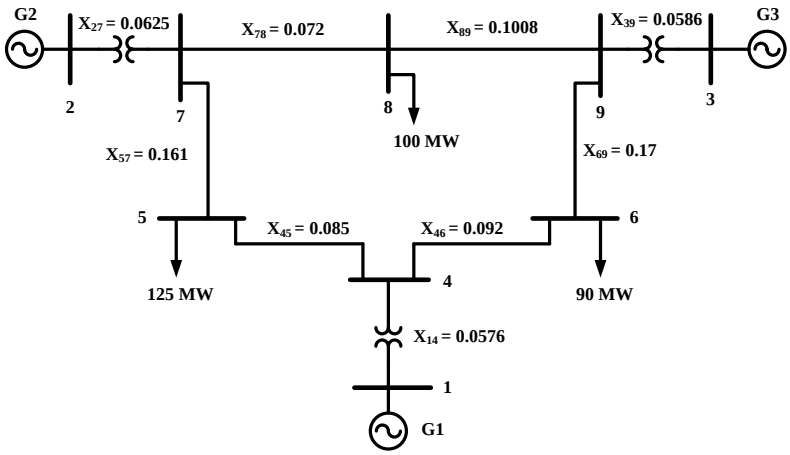

Fig. 2.7. The Nine-bus test system

We assume this is a lossless network while the loss is constant during the computation. In order to estimate the losses, a base case power flow is solved at first. The loss offset is -4.46 MW calculated against reference bus 1. The maximum risk R_{max} is set as the risk level for SCOPF, which is 0.9 in this example. We use the algorithm in section 2.4 to solve the RB-SCOPF. At first the HSM case (K_C=1, K_R = 0.5) is solved. To initialize the external loop optimization, we set the guess of $\hat{u}^*$ be -∞ at beginning. Then the algorithm comes to the internal loop with the estimated $\hat{u}^*$. A base case OPF (no contingency constraints) is run as master problem of the first-layer decomposition. At this operation point, line 6-4 will lead to violation at contingency 1, thus a feasibility cut is added to the master. Contingency 2 do not lead to violations. A new base-case operating point was then calculated and the results were sent to subproblems. After two iterations in the internal loop, all the violations are alleviated

then the results were sent to the external loop. Given the generator dispatch results from the internal loop, we first check the feasibility of risk. The risk subproblem is feasible, thus no feasibility cut is needed. Its optimal value is 1.4375, greater than the estimated $\hat{u}^*$ from the internal loop (which is -∞), thus an optimality cut is sent back, and the algorithm comes to the internal loop again. All the above cuts are added to the master. We get a newer estimate of $\hat{u}^*$ with value 1.4375. Then we come to the external loop and solve the risk subproblem again. The optimal function value is 1.4375, the same with the estimated $\hat{u}^*$. Thus the algorithm stops.

Since the system is small, we can solve the RB-SCOPF problem without decomposition. We found the result is the same with that obtained by the above approach, which identify the correctness of our proposed method. The RB-SCOPF result, including the HSM model, the ESM model (K_C =1.05, K_R = 0.75) and the HEM model (K_C =1.20, K_R = 0.5) are shown in Table 2.2 and Table 2.3. Table 2.4 lists the circuits with flow over 90 percent of their limits at both normal and post-contingencies for SCOPF, RBOPF and various models of RB-SCOPF. The following provides discussions about the results:

- Compared with SCOPF, RBOPF has less cost and less risk, but may cause high overloads for post-contingency states. For example, the flow on circuit 6-4 is 112.5% of its limit at contingency 1.
- HSM of RB-SCOPF is the most secure model but with the highest cost. Similar to SCOPF, it does not allow overload for post-contingency states, but its risk is only half.
- The cost of ESM model is close to SCOPF, but the risk is only 50 percent. It decreases the power flow of circuit 7-8 at normal state from 100% limit to 93.75%

limit, while it permits relatively small post-contingency overloads (5 percent) of circuit 6-4 at contingency 1.

Table 2.1 Parameters of the nine bus system

Circuits	1-4	2-7	9-3	5-4	6-4	7-5	9-6	7-8	8-9
Impedance (p.u.)	0.0576	0.0625	0.0586	0.085	0.092	0.161	0.17	0.072	0.1008
Resistance (p.u.)	0	0	0	0.01	0.017	0.032	0.039	0.0085	0.0119
MW limits (MW)	150	200	100	100	120	150	100	100	100

Table 2.2 Comparison of Risk and Cost for Nine Bus system

Constraints	SCOPF	RBOPF	RB-SCOPF		
			HSM (K_C=1, K_R = 0.5)	ESM (K_C =1.05, K_R = 0.5)	HEM (K_C =1.20, K_R = 0.5)
Risk	0.9	0.45	0.45	0.45	0.45
Cost ($)	11377.8	11172.5	11679.3	11476.6	11172.5

Table 2.3 Comparison of Generator Outputs

Options		G1 (WM)	G2 (WM)	G3 (WM)
SCOPF		136.46	161.60	21.40
RBOPF		146.76	142.88	29.82
RB-SCOPF	HSM	136.46	154.83	28.17
	ESM	143.06	148.14	28.26
	EESM	146.76	142.88	29.82

Table 2.4 Circuits with flow over 90% limit

Options		States of circuit flow over 90% limit
SCOPF		*100% limit, circuit 7-8 at normal state* *100% limit, circuit 6-4 at contingency 1*
RBOPF		*92.81% limit, circuit 7-8 at normal state* *112.5% limit, circuit 6-4 at contingency 1*
RB-SCOPF	HSM	*94.38% limit, circuit 7-8 at normal state* *100% limit, circuit 6-4 at contingency 1*
	ESM	*93.75% limit, circuit 7-8 at normal state* *105% limit, circuit 6-4 at contingency 1*
	HEM	*92.81%% limit, circuit 7-8 at normal state* *112.5% limit, circuit 6-4 at contingency 1*

The result of HEM model is the same as the result from RBOPF. This happens because RBOPF is a special case to RB-SCOPF with K_C large. In this example when K_C is greater than 1.125 the dispatch result will not change.

2.5.2 The ISO New England System

The original network data from ISO New England has 12,300 buses, 13,500 circuits and 1136 contingencies. After consolidating part of the zero impedance branches (ZBRs), the system has 2351 buses and 3189 circuits. We only consider the first 250 contingencies in this example. However, the conclusion should be the same if all the contingencies are considered. The generator bidding data we used are from a winter day in 2009. Wind turbine units are not included since they do not have bidding curves. The number of bidding units is almost 400.

For the RB-SCOPF problem in this case, there are 802,150 decision variables and 4,002,196 constraints. Solving the problem directly will cause unacceptable computing time and extreme PC memory requirements. The time required for solving is estimated. In our experiment, the base case problem could be solved in about 2 seconds. As from [89], if there are O(L) bit numbers, the linear programming algorithm will require O($n^{3.5}L$) arithmetic operations, where n is the number of decision variables and L is the number of bits for the input. Based on this conclusion, the time need to solve our problem directly will be about 1.8 years. However, it is more efficiency to compute the RB-SCOPF if our proposed approach is used.

Table 2.5 Iterations of the Algorithm

iter.	loop type	no. of cuts	time (s)
1-6	Internal	179 OPF feasibility cuts generated	522.45
7-29	External	23 risk feasibility cuts generated	3643.14
30-31	External	2 risk optimality cuts generated	300.74
32	Internal	No cut generated	< l
33	External	No cut generated	< 1

Table 2.6 Binding Contingencies at Successive Internal Iterations

iter.	binding contingencies
1	7,9,11,12,14,15,17,20,21,22,23,24,25,27,28,29,31,32,33,34,35,36,37,38,39,40,42,48,49,51,52,53,54,60,61,63,65,66,67,68,70,71,72,79,80,83,84,85,86,87,90,91,92,93,94,95,98,99,101,105,109,113,114,118,119,120,122,125,126,128,129,133,134,135,137,138,140,141,142,146,147,148,149,150,151,153,154,157,158,159,160,161,165,167,169,171,174,175,179,180,181,183,184,186,187,188,189,190,191,193,198,199,200,201,202,205,208,209,212,213,215,218,220,223,226,227,228,231,232,233,236,238,239,241,242,244,246,247,249,250
2	7,12,14,15,21,29,33,36,40,49,61,67,84,98,126,138,149,150,154,198,201,205,220,226,233
3	15,29,138,233
4	15,29,138,233
5	29,138
6	15,29,138

First we solve the HSM case (K_C=1, K_R = 0.5). The cost for the base case OPF is $571530. The base case dispatch result is then sent to subproblems to check if there are violations in the first-layer decomposition. Table 2.5 summarizes the procedure of iterations. The algorithm stops at 33 iterations. In the first 6 iterations, the algorithm runs in the internal loop. Totally 179 feasibility cuts are generated and sent back to the master. Table 2.6 lists the binding contingencies. During iteration 7-29, the algorithm runs in the external loop. The risk subproblem is infeasible thus one feasibility cut is generated every iteration. After 23 feasibility cuts are sent back to the master of the *second-layer*, the risk subproblem

becomes feasible. But the estimated $\alpha(\boldsymbol{x}_2^*)$ is greater than $\hat{u}^*$ in part D of section 2.4.4, so an optimality cut is generated. Two optimality cuts are sent to the master in iteration 30 and 31. Then the algorithm comes to the internal loop again. No violation occurs at this time, so the algorithm comes to the external loop. Neither feasibility cut nor optimality cut is generated. At this time, there is $|\alpha(\boldsymbol{x}_2^*)-\hat{u}^*|<\varepsilon$, where ε is the set error. The algorithm stops. Fig. 2.8 indicates the changes of operation cost and the estimated severity $\hat{u}^*$ in each step.

Table 2.7 Results for the ISO New England System

Constraints	SCOPF	RBOPF	RB-SCOPF		
			HSM (K_C=1, K_R = 0.5)	ESM (K_C =1.05, K_R = 0.5)	HEM (K_C =1.20, K_R = 0.5)
Risk	18.2690	9.1345	9.1345	9.1345	9.1345
Cost ($/*hr*)	684642.50	605407.32	728899.10	610611.54	605542.08
ASI	24.5466	24.0768	24.5458	24.0824	24.0848
CEI	850.02	80.14	254.83	197.42	219.65

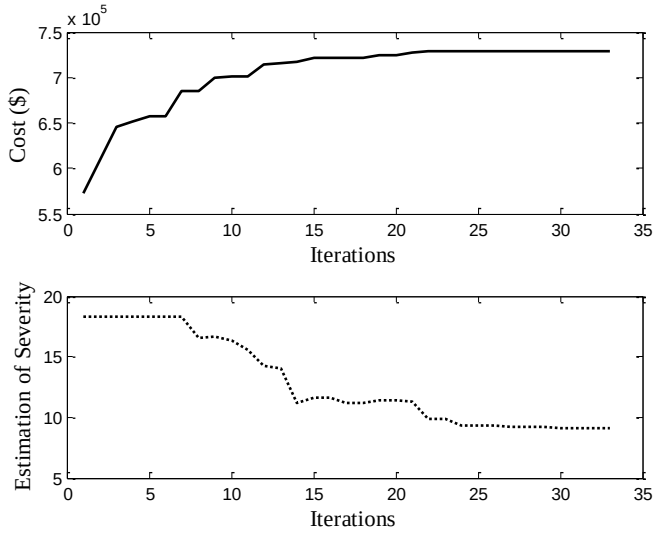

Fig. 2.8 The change of cost and estimated severity with iterations

The solving procedure for ESM (K_C =1.05, K_R = 0.5) and HEM (K_C =1.20, K_R = 0.5) is similar. Table 2.7 compares the results of SCOPF, RBOPF and various cases of RB-SCOPF for the ISO New England system. Two new indices, i.e. ASI (Angular Separation Index) and CEI (Cascading Expectation Index) are included in the table. Their meanings are shortly explained as follows.

Angular separation index is used to measure the stress of power flow in the system based on the fact that the risk of angular instability is higher if high angular separations exist over many circuits. The formulation is

$$ASI = \sum_{i=0}^{N} \left(Pr(E_i) Sev_{ASI}(E_i) \right) \tag{2.62}$$

where E_i expresses the ith event, $Pr(\bullet)$ is the probability of an event, and

$$Sev_{ASI}(E_i) = \sum_{j:\left|\theta_j\right| \geq 0.5} \left| \sin \theta_j \right| \tag{2.63}$$

where $Sev_{ASI}(\bullet)$ is the angular separation severity, θ_j is the angular separation of circuit j with power flow over 90 percent of its overload limit.

Table 2.8 Comparison of Computing Results for ISO-NE System

Options		Iterations to converge	No. of circuits with flow over 90% *TTL*	
			normal state	*contig.* states
SCOPF		7	33	8183
RBOPF		43	26	6411
RBSCOPF	HSM	33	28	6819
	ESM	49	22	5388
	EESM	26	23	5678

Cascading expectation index is a product of cascading overload probability and cascading overload severity. The overload probability of a circuit is a function of its ultimate power flow and the change of power flow during cascading trip. The overload severity is the number of tripped circuits in a cascading overload evaluation.

In Table 2.8 we control the risk level of RBOPF and RBSCOPF as half of SCOPF. The results show that the corresponding costs of RBOPF and RB-SCOPF are lower than SCOPF except the HSM model. And also, SCOPF has higher values on ASI and CEI, thus has worse long-time performance on security according to our proposed index.

Table 2.8 compares the results on the number of iterations and number of circuits with flow over 90 percent *TTL* at both normal and contingency states. It is indicated that the computing time of RBOPF and RB-SCOPF are 4-7 times than that of SCOPF. The number of severe loading (greater than 90% *TTL*) circuits is reduced in RBOPF and SCOPF model.

2.6 Conclusion

This chapter provides a new methodology to solve the preventive Risk-based security-constrained optimal power flow problems. A two-stage Benders Decomposition strategy was proposed. At the first stage, the algorithm iterates within the internal loop that has been decomposed into an unconstrained economic dispatch and separate post-contingency analysis with generation rescheduling to eliminate overload violations. At the second stage, the algorithm iterates in the external loop that is comprised of a "base-case" risk problem and risk violation check subproblems. To facilitate the decomposition procedure, a new expression of severity function is proposed.

The algorithm has been tested the ISO New England's real operational system. The results indicate that RB-SCOPF could improve the system's performance in terms of both security and costs compared with traditional SCOPF.

In order to implement the proposed algorithm, the future research might include the following topics:

- Apply the proposed method to solve corrective risk-based security-constrained optimal power flow.
- How to choose appropriate K_C and K_R so that desired tradeoff between the system security and the economics is obtained. This will require research on the sensitivity of the objective function to K_C and K_R.
- To show that a system with less loaded high stress lines and more loaded low stress lines is more secure than the system with more loaded high stress and less loaded low stress lines. This is to show that the dispatch outcomes based on RB-SCOPF will have higher steady state security margins.
- Consider the risk of wind fluctuation, which is to be embedded into the OPF model.

Appendix

A. Proof of conclusion for (2.57)

Proof: Recall that the KKT condition for LP max $\{c^T x : Ax \le b, x \ge 0\}$ is: there exists a vector $y \in \mathbf{R}$ such that the following constraints hold

$$0 \le \begin{bmatrix} b - Ax \\ x \end{bmatrix} \perp \begin{bmatrix} y \\ A^T y - c \end{bmatrix} \ge 0 \qquad (2.A.1)$$

where "$\perp$" means the two vectors are perpendicular.

For LP (2.54) ~ (2.56), define set

$$S = \left\{ \hat{S}ev_{l,kt} \right\}, \forall l = 1,2,...,NL \ \forall k = 0,1,2,...,NC . \tag{2.A.2}$$

a) If equation (2.57) holds, then *S* satisfies both equation (2.55) and equation (2.56). Consequently, *S* is a feasible solution set for LP (2.54)~ (2.56). In addition, it is obvious from (2.53) that $\hat{S}ev_{l,k} > 0$, $\forall l = 1,2,...,NL \ \forall k = 0,1,2,...,NC$. Plug in solution *S* into the KKT condition (A.1), we get that the LP problem is optimal with solution *S* only if there exists a vector $y = [y_{l,k}, y_{(lk+1)}]^T$ such that the following constraints hold:

$$0 \le \begin{bmatrix} \hat{S}ev_{l,k} - 1 \cdot \hat{S}ev_{l,k} \\ K_R \times Risk_{max} - \sum_{k=1}^{NC} Pr_k \sum_{l=1}^{NL} \hat{S}ev_{l,k} \\ \hat{S}ev_{l,k} \end{bmatrix} \perp \begin{bmatrix} y_{l,k} \\ y_{(lk+1)} \\ -y_{l,kt} + Pr_k \cdot y_{(lk+1)} + 1 \end{bmatrix} \ge 0 \tag{2.A.3}$$

It is not hard to find that $\left\{ y_{l,k} = 1,\ y_{(lk+1)} = 0 \right\}$ satisfies the above conditions, thus S is the optimal solution of LP (2.54) ~ (2.56).

b) If equation (2.57) does not hold, i.e. $K_R \times Risk_{max} - \sum_{k=1}^{NC} Pr_k \sum_{l=1}^{NL} Sev_{l,kt} \le 0$, then (A.3) does not hold. The KKT conditions are not satisfied. So LP (2.54) ~ (2.56) is not optimal. It is easy to see that this problem cannot be unbounded. Thus it is infeasible, and has an extreme ray for its dual in (2.58).

B. Proof of the optimal solution of (2.59)

In (2.59), there are:

$$\Delta \mathbf{z}_{l,k} \le -Pr_k \Delta \mathbf{z}_1, \forall k,l \tag{2.A.4}$$

The objective function

$$
\begin{aligned}
f &= K_R \times Risk_{max} \Delta \mathbf{z}_1 + \sum_{k=1}^{NC} \sum_{l=1}^{NL} \hat{S}ev_{l,k} \Delta \mathbf{z}_{l,k} \\
&\le K_R \times Risk_{max} \Delta \mathbf{z}_1 - \sum_{k=1}^{NC} Pr_k \sum_{l=1}^{NL} \hat{S}ev_{l,k} \ \Delta \mathbf{z}_1 \\
&= (K_R \times Risk_{max} - \sum_{k=1}^{NC} Pr_k \sum_{l=1}^{NL} \hat{S}ev_{l,k} \ ) \Delta \mathbf{z}_1
\end{aligned}
\tag{2.A.5}
$$

Since

$$
K_R \times Risk_{max} - \sum_{k=1}^{NC} Pr_k \sum_{l=1}^{NL} \hat{S}ev_{l,k} \ < 0 \tag{2.A.6}
$$

the objective function reach its maximum value

$$
f^* = \sum_{k=1}^{NC} Pr_k \sum_{l=1}^{NL} \hat{S}ev_{l,k} \ - K_R \times Risk_{max} \tag{2.A.7}
$$

when$\{ \Delta \mathbf{z}_1^* = -1, \ \Delta \mathbf{z}_{l,k}^* = Pr_k \, , \forall \, l,k \}$.

C. Proof of the optimal solution of (2.58)

If (2.58) is optimal, equation (2.57) holds. Since $\mathbf{z}_1 \le 0$, in (2.58) there is

$$
\mathbf{z}_{l,k} \le 1 - Pr_k \mathrm{z}_1 \tag{2.A.8}
$$

The objective function

$$
\begin{aligned}
f &= K_R \times Risk_{max} \mathrm{z}_1 + \sum_{k=1}^{NC} \sum_{l=1}^{NL} \hat{S}ev_{l,k} \mathbf{z}_{l,k} \\
&\le K_R \times Risk_{max} \mathrm{z}_1 + \sum_{k=1}^{NC} \sum_{l=1}^{NL} \hat{S}ev_{l,k} (1 - Pr_k \mathrm{z}_1) \\
&= (K_R \times Risk_{max} - \sum_{k=1}^{NC} Pr_k \sum_{l=1}^{NL} \hat{S}ev_{l,k}) \mathrm{z}_1 + \sum_{k=1}^{NC} \sum_{l=1}^{NL} \hat{S}ev_{l,k} \\
&\le \sum_{k=1}^{NC} \sum_{l=1}^{NL} \hat{S}ev_{l,k}
\end{aligned}
\tag{2.A.9}
$$

The equality holds when $\{\mathbf{z}_1^*=0, \mathbf{z}_{l,k}^*= 1, \forall \, l,k \}$.

CHAPTER 3. SOLVING CORRECTIVE RISK-BASED SECURITY-CONSTRAINED OPF WITH LAGRANGIAN RELAXATION AND BENDERS DECOMPOSITION

3.1 Introduction

The risk-based security-constrained optimal power flow (RB-SCOPF) [90] is an extension to the currently widely-used SCOPF model ([91]-[93]) in an effort to enhance both *security* and *economics* of bulk power systems. It considers, in addition to classic constraints in both normal state and predefined "N-1" contingency states, the risk constraints related with both single circuits (type I risk constraints) and the whole system (type II risk constraints). The objective of RB-SCOPF is to maximize the surplus of the real-time market. In the case of fixed, inelastic demand, this objective is equivalent to minimizing the offer-based generation costs at normal state without violating the pre-defined N-1 security criteria and the required risk level of the entire system. Similar to SCOPF model, the RB-SCOPF has been formulated under two models: *preventive* and *corrective*, referred to as PRB-SCOPF and CRB-SCOPF, respectively. Their major difference lies in that the control variables are allowed to adjust during a short time interval after the contingency occurs in the latter. In this chapter we focus on how to solve the CRB-SCOPF. Similar to PRB-SCOPF, the following two characteristics of CRB-SCOPF make the solving procedure difficult:

- Combinatorial nature — the risk constraint is a function of state variables in both normal and all the contingency states, since we intend to control the *system*'s overall risk level. The state-coupling (type II) risk constraints could be relaxed in

the objective function to solve the de-coupled problem.

- High dimensionality — the CRB-SCOPF model simultaneously imposes all post-contingency constraints. If the system is large and many contingencies are considered, it would cause prohibitive CPU time and memory requirements to solve the problem directly.

In addition, the CRB-SCOPF has a different feature over PRB-SCOPF that we have to use LP algorithm to compute the subproblems, while for PRB-SCOPF the subproblems could be solved algebraically, as we did in Chapter 2. Hence, to compute CRB-SCOPF is more difficult than to compute PRB-SCOPF. To handle the above difficulties, we present an effective approach to solve CRB-SCOPF problem. The Lagrangain relaxation (LR) algorithm ([94], [95]) is applied to the original problem to relax complicating (or linking) constraints to the objective function. Based on this dual relaxation, the original large-scale optimization problem, which consist of both complicating variables and complicating constraints, could be decomposed into a tractable subproblem that consists only of the former. The relaxed subproblem, called the Lagrangian dual problem (DP), could be solved by the Benders decomposition (BD) approach. The master problem in DP is a 'base-case' economic dispatch problem associated with corresponding type I risk constraints; and the subproblems are independent contingency analysis with generation rescheduling to eliminate constraint violations. The procedure is shown in Fig. 3.1.

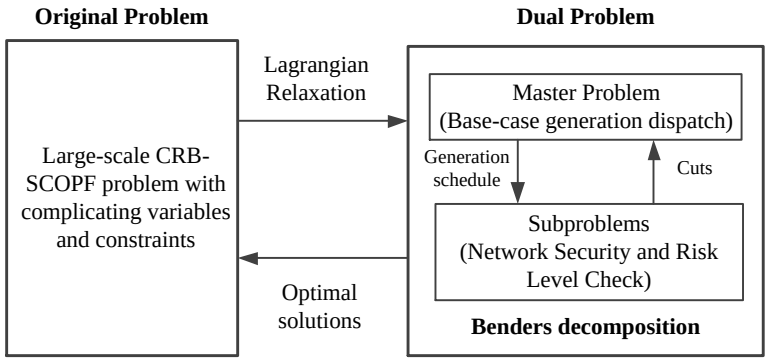

Fig. 3.1. Decomposition structure of the CRB-SCOPF problem

3.2 Lagrangian relaxation decomposition method

3.2.1 Introduction

The Lagrangian relaxation (LR) is a widely used technique to solving optimization problems with complex constraints and special structures. General form of LR decomposition problem (**Primal Problem**, **P**) is as follows:

$$\begin{aligned} \min_{x} \quad & f(x) \\ s.t. \quad & a(x) = 0 \\ & b(x) \le 0 \\ & c(x) = 0 \qquad \lambda \\ & d(x) \le 0 \qquad \mu \end{aligned} \tag{3.1}$$

where $f(x) \in \mathbb{R}$ is the objective function, four constraints $a(x) \in \mathbb{R}^{n_a}$, $b(x) \in \mathbb{R}^{n_b}$, $c(x) \in \mathbb{R}^{n_c}$ and $d(x) \in \mathbb{R}^{n_d}$. n_a, n_b, n_c, and n_d are respectively the size of the constraints. *c(x)* and *d(x)* are complicating constraints, i.e., constraints if been relaxed, the problem (1) will be easy to solve. λ and μ are the Lagrangian multiplier of *c(x)* and *d(x)*.

The **Lagrangian function** (**LF**) is defined as [96]:

$$L(x,\lambda,\mu) = f(x) + \lambda^T c(x) + \mu^T d(x) \tag{3.2}$$

where complicating constraints *c(x)* and *d(x)* have been moved to the objective function with associated multipliers. Under regularity and convexity assumptions, the resulting **Dual Function** (**DF**) is defined as:

$$\begin{aligned} \phi(\lambda,\mu) = \min_{x} \quad & L(x,\lambda,\mu) = f(x) + \lambda^T c(x) + \mu^T d(x) \\ s.t. \quad & a(x) = 0 \\ & b(x) \le 0 \end{aligned} \tag{3.3}$$

In general, the dual function is concave and non-differentiable [96]. The **Dual Problem** (**DP**) is then defined as:

$$\begin{aligned} \max_{\lambda,\mu} \quad & \phi(\lambda,\mu) \\ s.t. \quad & \mu \ge 0 \\ & \lambda \ unconstrained \end{aligned} \tag{3.4}$$

The above LR decomposition procedure is quite attractive if the dual function (3) is easy to solve with given λ^* and μ^*. In this case, the problem to be solved is called the **relaxed primal problem** (**RPP**) for given λ^* and μ^*, as follows:

$$\begin{aligned} \min_{x} \quad & L(x,\lambda^*,\mu^*) = f(x) + \lambda^{*T} c(x) + \mu^{*T} d(x) \\ s.t. \quad & a(x) = 0 \\ & b(x) \le 0 \end{aligned} \tag{3.5}$$

Based on the above analysis, we can obtain the general algorithm of LR method to solve problem (3.1):

a) Guess an initial value of λ^0 and μ^0.

b) Let $\lambda^{old} = \lambda^0$ and $\mu^{old} = \mu^0$, solve (3.5).

c) Update λ and μ based on the result in b), get λ^{new} and μ^{new}. General updating method includes *Subgradient* and *Cutting Plane Method*.

d) If $\left\| \begin{bmatrix} \lambda^{new} \\ \mu^{new} \end{bmatrix} - \begin{bmatrix} \lambda^{old} \\ \mu^{old} \end{bmatrix} \right\| \le \varepsilon$,stop. Else, go to b).

In what follows we will discuss the relationship between the primal problem and the dual problem. Because in the dual function (DF) the constraints $c(x) = 0$ and $d(x) \le 0$ have been eliminated from the primal problem (P), the optimal solution obtained from the Lagrangian dual problem (DP) may not be feasible to the primal problem. In such case, the Lagrangian relaxation technique is still attractive because it provides the lower bound of the primal problem, as the following theorems [96]:

Theorem 1 (Weak Duality Theorem)**:** Suppose the optimal solution to the primal problem [**P**] is $\boldsymbol{x}^*$, and the optimal objective value of **P** denotes as $f(\boldsymbol{x}^*)$. For any $\lambda, \mu \ge 0$, there exists: $\phi(\lambda, \mu) \le f(x^*)$.

Theorem 2: The dual function $\phi(\lambda, \mu)$ is a concave function.

Suppose $\boldsymbol{x}^*$ is the minimizer or the primal problem, and (λ^*, μ^*) is the maximizer for the dual problem. Reference [95] proved that under convexity assumptions, there exists

$$f(x^*) = \phi(\lambda^*, \mu^*) \tag{3.6}$$

For nonconvex case, the optimal objective value of the dual problem provides a lower bound to the primal problem as the above weak duality theorem says. The difference of the optimal objective function values between the primal and dual problems is called the **duality gap**. In most of engineering and science problems, the duality gap is relatively small.

A simple example with linear programing is provided to demonstrate the procedure of the LR decomposition method.

For the LP problem (3.7)

$$\begin{aligned} \min \quad & x_1 + 2x_2 \\ s.t, \quad & x_1 \le 1 \\ & -x_1 \le 0 \\ & -x_1 - x_2 + 2 \le 0 \qquad \lambda_1 \\ & -x_2 \le 0 \qquad \lambda_2 \end{aligned} \tag{3.7}$$

there are four constraints. We want to relax the last two constraints, and λ_1 and λ_2 are the Lagrangian multipliers for them. It is easy to obtain that the optimal solution is $x_1^* = x_2^* = 1$, the optimal objective function value is 3.

The *dual function* is:

$$\begin{aligned} \phi(\lambda_1, \lambda_2) = \min \quad & x_1 + 2x_2 + \lambda_1(-x_1 - x_2 + 2) + \lambda_2(-x_2) \\ s.t. \quad & x_1 \le 1 \\ & -x_1 \le 0 \end{aligned} \tag{3.8}$$

or equally

$$\begin{aligned} \phi(\lambda_1, \lambda_2) = \min \quad & (1-\lambda_1)x_1 + (2-\lambda_1-\lambda_2)x_2 + 2\lambda_1 \\ s.t. \quad & x_1 \le 1 \\ & -x_1 \le 0 \end{aligned} \tag{3.9}$$

From (3.9) we can see that there is no constrains for x_2. For any given λ_1^* and λ_2^*, the objective function is always $-\infty$! This will make the LR method fail. However, from the KKT condition we have

$$\frac{\partial L}{\partial x_2} = 2 - \lambda_1 - \lambda_2 = 0 \tag{3.10}$$

where $L = (1-\lambda_1)x_1 + (2-\lambda_1-\lambda_2)x_2 + 2\lambda_1$.

If (3.10) is considered, then the *dual problem* becomes:

$$\begin{aligned} \max_{\lambda_1,\lambda_2} \quad & \phi(\lambda_1,\lambda_2) = \begin{cases} (1-\lambda_1)+2\lambda_1 & \text{if } 1-\lambda_1 \le 0 \\ 0+2\lambda_1 & \text{if } 1-\lambda_1 \ge 0 \end{cases} \\ s.t. \quad & \lambda_1 \ge 0 \\ & \lambda_2 \ge 0 \\ & 2-\lambda_1-\lambda_2 = 0 \end{aligned} \tag{3.11}$$

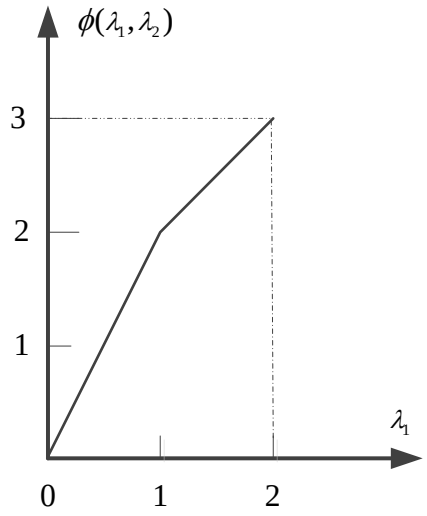

Fig 3.2. The expression of dual problem

From Fig. 3.2, we can see that the problem (3.11) is optimal when $\lambda_1 = 2$ and $\lambda_2 = 0$. The optimal objective value is 3. The corresponding optimal solutions $x_1^* = x_2^* = 1$. It is obvious that the solution obtained from LR method is the same with the results solved directly from the primal problem.

3.2.2 Application of LR in solving CRB-SCOPF

As an efficient technology, Lagrangian relaxation has been used successfully in many power system cases to relax the complicating constraints. For example, reference [97] proposed a framework to carry out the multi-area coordinated optimal power flow problem, in which the whole system is decomposed into independent optimal dispatch areas by LR. Reference [98] applies LR to the optimal restoration problem of distribution systems after a blackout occurs. Reference [99] uses LR approach to solve the dynamic multi-period economic dispatch problem for large-scale power systems. In [100], LR is applied to decompose the long-term security-constrained unit commitment (SCUC) into successive short term SCUC problems. The major difficulty of applying LR approach lies in the multiplier updating procedure. In general, there are four methods to update the Lagrangian multiplier: Subgradient method, Cutting Plane method, bundle method and dynamically constrained cutting plane method [95], [101]. In this chapter, the cutting plane algorithm is adopted since it provides good results according to our test. On the other hand, since the reference [86] was published, Benders decomposition has been used as an effective tool to solve various CSCOPF and other related problems such as power transmission network design, unit commitment, ATC calculation and optimal reactive power planning, etc. [102] - [106]. The major concern of applying Benders is that the algorithm may not converge to either a global or a local optimal solution if the feasible region is not convex [95], [86]. In this chapter, the results are obtained based on DC power flow model, thus the convexity is guaranteed. The proposed approach converges successfully with decent performance.

3.3 Description of CRB-SCOPF Model

The CRB-SCOPF problem can be formulated in compact form as follows:

$$\underset{x_0,\ldots,x_{NC},u_0}{\text{Min}} \quad f_0(\boldsymbol{x_0}, \boldsymbol{u_0}) \tag{3.12}$$

$$s.t. \quad \boldsymbol{g}_k(\boldsymbol{x}_k, \boldsymbol{u}_0) = 0, \quad k = 0, \ldots, NC \tag{3.13}$$

$$\boldsymbol{h}_0(\boldsymbol{x}_0, \boldsymbol{u}_0) \le \boldsymbol{h}_0^{max} \tag{3.14}$$

$$\boldsymbol{h}_k(\boldsymbol{x}_k, \boldsymbol{u}_k) \le K_C \times \boldsymbol{h}_k^{max}, k = 1, \ldots, NC \tag{3.15}$$

$$\left|\boldsymbol{u}_0 - \boldsymbol{u}_k\right| \le \Delta \boldsymbol{u}_k, \quad k = 1, \ldots, NC \tag{3.16}$$

$$0 \le Risk(\boldsymbol{g_1}, \ldots, \boldsymbol{g_{NC}}) \le K_R \bullet Risk_{\max} \tag{3.17}$$

where f_0 is the objective function, vector $\boldsymbol{x}$ represents the state variables (i.e., real and imaginary part of bus voltages), vector $\boldsymbol{u}$ represents control variables (such as the voltage and active power on generators, transformer ratios, phase shifter angle, etc.), k represents the system configuration (k = 0 corresponds to the normal state of the system, while k = 1, 2, …, NC corresponds to the post-contingency states), NC represents the total number of contingencies, g_k (resp. h_k) is the set of equality (resp. inequality) constraints for the kth configuration of the system, $\boldsymbol{h}_k^{max}$ represents the limit of the inequality constraints at state k, $\Delta \boldsymbol{u}_k$ represents the vector of maximal allowed variation of control variables between the normal state and the kth post-contingency state, $Risk(\bullet)$ represents the system's overall risk level, $Risk_{max}$ is the system's maximal allowed risk level, K_C and K_R are coordination factors used to impose control over a tradeoff between security and economy.

The objective in (3.12) intends to minimize the system's costs at the normal state. Constraints (3.13)-(3.15) impose the feasibility of the system at pre-contingency and post-contingency states. Equality constraints (3.13) are power flow balance equations, while the inequality constraints (3.14) and (3.15) denote the operational and physical limits of the system. Constraint (3.17) requires that the system's overall risk level be within a pre-defined value, which can be set by using the SCOPF result as a benchmark. We deal with the risk constraint (3.17) by the method similar in Chapter 2. Similar to the classic SCOPF model, the inequalities (3.16) are "linking" constraints between the normal and post-contingency states, aimed at allowing adjustment of the control variables after the contingency occurs.

It can be shown that the traditional CSCOPF is just a special case of the CRB-SCOPF model, only by imposing $K_C = 1$ and $K_R = +\infty$.

3.4 Mathematical Framework to Solve CRB-SCOPF

3.4.1 CRB-SCOPF Formulation

As discussed in section 3.3, the objective of CRB-SCOPF is to determine a real-time generator schedule for minimizing the system's operating cost without violating the prevailing constraints. Hence, the objective function, as a detailed form of (3.12), is formulated as:

$$\text{Min} \sum_{i=1}^{NG} c_{i0} P_{i,0} \tag{3.18}$$

where NG is the total number of generators, NL is the total number of circuits, c_{i0} is the generation cost of unit i, $P_{i,0}$ is the generation output of unit i at normal state.

Generation constraints include the system power balance for normal and post-contingency states (3.19) and the operating reserve requirements at normal state (3.20),

$$\sum_{i=1}^{NG} P_{i,k} = \sum_{i=1}^{ND} PD_{i,k} + P_{Loss,k}, \quad k = 0,1,...,NC \tag{3.19}$$

$$\sum_{i=1}^{NG} R_{O,i} \geq Rev \tag{3.20}$$

where $P_{i,k}$ is the generation output of unit i at kth state, $PD_{i,k}$ is the demand at load bus i at kth state, $P_{Loss,k}$ is the system's loss at kth state, ND is the total load bus number, $R_{O,i}$ is the operating reserve of unit i, and Rev is the system reserve requirement. Equation (3.19) corresponds to (3.13) in section 3.3.

Real power generation limit (3.21),

$$P_{i,k}^{\min} \leq P_{i,k} \leq P_{i,k}^{\max}, \quad k = 0,1,...,NC; i = 1,2,...,NG \tag{3.21}$$

where $P_{i,k}^{\min}$ ($P_{i,k}^{\max}$) is the lower (upper) limit of real power generate of unit i at state k.

In real-time CRB-SCOPF problem, we check DC network security constraints during operation as (3.22) and (3.23) (AC network constraints will be examined further in a subsequent chapter).

$$-PL_{l,0}^{\max} \leq PL_{l,0} \leq PL_{l,0}^{\max}, \quad l = 1,2,...,NL \tag{3.22}$$

$$-K_C \bullet PL_{l,k}^{\max} \leq PL_{l,k} \leq K_C \bullet PL_{l,k}^{\max}, \; l = 1,2,...,NL; \; k = 1,2,...,NC \tag{3.23}$$

where $PL_{l,0}$ ($PL_{l,k}$) is the real power flow on circuit l at normal (kth post-contingency) state, $PL_{l,0}^{\max}$ ($PL_{l,k}^{\max}$) is the maximum transmission limit of circuit l at normal (kth post-contingency)

state, NL is the total number of system circuits. The expressions of $PL_{l,0}$ and $PL_{l,k}$ are shown in equations (3.35) and (3.36) of chapter 2. Equations (3.22) and (3.23) correspond to (3.14) and (3.15), respectively.

In (3.23) there is a factor K_C to relax the post-contingency circuit limits. Similar to chapter 2, three different operational models for CRB-SCOPF are proposed, according to what value K_C is imposed: highly secure model (HSM), economic-secure model (ESM), and highly economic model (HEM), where K_C was chosen as 1, 1.05 and 1.20, respectively. We do not allow circuit overflows at normal state, thus there is no multipliers on the limits in (3.22).

Generator output corrective limits at post-contingency,

$$P_{i,0} - P_{i,k} \le \Delta P_k, \;\; k = 1, 2, ..., NC \tag{3.24}$$

$$P_{i,k} - P_{i,0} \le \Delta P_k, \;\; k = 1, 2, ..., NC \tag{3.25}$$

where ΔP_k is the allowed variation of generation outputs between normal and the kth post-contingency state. Equation (3.24) and (3.25) corresponds to (3.16) in section 3.3.

The risk constraints, by using the equivalent transmission as shown in equation (3.31) of chapter 2 and letting c_l = 0.9, could be formulated as (3.26)-(3.29):

$$Sev_{l,k} \ge 0, \;\; l = 1, 2, ..., NL; k = 0, 1, 2, ..., NC \tag{3.26}$$

$$Sev_{l,k} \ge 10 \times (PL_{l,k} / PL_{l,k}^{\max} - 0.9), \; l = 1, 2, ..., NL; k = 0, 1, 2, ..., NC \tag{3.27}$$

$$Sev_{l,k} \ge 10 \times (-PL_{l,k} / PL_{l,k}^{\max} - 0.9), \; l = 1, 2, ..., NL; k = 0, 1, 2, ..., NC \tag{3.28}$$

$$\sum_{k=1}^{NC} Pr_k \sum_{l=1}^{NL} Sev_{l,k} \le K_R \times Risk_{max} \tag{3.29}$$

where $Sev_{l,k}$ is the severity of circuit l at the kth post-contingency, $Risk_{max}$ is set as the risk level of SCOPF. Equations (3.26) – (3.29) corresponds to (3.17) in section 3.3.

Constraints (3.26)-(3.27) are associated with single circuit (type I risk constraints), while constraint (3.29) is associated with the whole system (type II risk constraints). Constraint (3.29) is the complicating constraint that links the normal and all the post-contingency states.

3.4.2 Lagrangian Relaxation

The problem CRB-SCOPF (3.18)-(3.29) is with both complicating variables (equations (3.24)-(3.25)) and complicating constraint (equation (3.29)). Largrangian relaxation technique is applied for the solution of (3.18)-(3.29). The coupling constraint (3.29) is relaxed and embedded into the objective function by using a non-negative Lagrangian multiplier (λ). Then the original problem (3.18)-(3.29) could be formulated in terms of Largrangian dual function as shown in (3.30) subjecting to constraints (3.19)-(3.28),

$$\begin{aligned} & LR(\lambda) \\ & = \text{Min}[\sum_{i=1}^{NG} c_{i0} P_{i,0} + \lambda(\sum_{k=1}^{NC} Pr_k \sum_{l=1}^{NL} Sev_{l,k} - K_R \times Risk_{max})] \\ & = -\lambda K_R \times Risk_{max} + \text{Min}[\sum_{i=1}^{NG} c_{i0} P_{i,0} + \lambda \sum_{k=1}^{NC} Pr_k \sum_{l=1}^{NL} Sev_{l,k}] \end{aligned} \tag{3.30}$$

which is a concave function [95].

The relaxation of coupling constraint (3.29) makes the problem to be solved includes only

complicating variables, thus transforms the primal problem into an easier-to-solve dual problem. It can be shown that the optimal value of the Lagrangian relaxation problem (denoted as *LRV*) should always be less than or equal to that of the primal problem (denoted as *PV*) for two reasons: 1) the feasible region of the Lagrangian relaxation problem encompasses that of the primal problem, and 2) for any non-negative Lagrangian multiplier λ, the objective function value of the Lagrangian relaxation problem (3.18) is always smaller than that of the primal problem (3.30) if inequality (3.29) is satisfied. This means, the *LRV* is always a lower bound to *PV*. We need to get the largest lower bound over all the possible Lagrangian multipliers, as shown in (3.31),

$$DV = \underset{\lambda \geq 0}{\text{Max}} \; LR(\lambda) \tag{3.31}$$

which is called the Lagrangian dual problem, *DV* denotes its optimal value subjective to constraint $\lambda \geq 0$.

Our aim is to solve the dual problem quickly through an iterative fashion. The algorithm for solving the dual problem proceeds as follows.

1) Initialization. Set the iteration number v = 1. Initialize the Lagrangian dual variable $\lambda^{(v)} = \lambda^0$. The λ^0 is chosen such that the solution of dual problem given λ^0 is a feasible solution to the primal problem, i.e. if we solve (3.30) under λ^0 and substitute the solution to the primal problem, formulation (3.19)-(3.29) should be satisfied. Set the initial lower bound $LB^{(v-1)} = -\infty$.
2) Solve the relaxed primal problem, i.e. formulation (3.30) subjecting to constraints (3.19)-(3.28) and get the minimizer (denote as $\boldsymbol{x}^{(v)}$) and the objective function value

at the minizer (denote as $LRV^{(v)}$). Update the lower bound to *PV*, i.e., $LB^{(v-1)} \leftarrow LRV^{(v)}$ if $LRV^{(v)} > LB^{(v-1)}$.

3) Update the multipliers using any of the commonly used methods stated in the introduction. For different problems, these methods can converge to the optimal solution with various speeds. We need to choose a proper method depending on what problem to solve. If possible, update also the upper bound of the objective function.

4) Check the convergence of the algorithm. If the relative difference of multiplier vectors between two successive iterations is lower than a pre-specified threshold, i.e. $\left\|\lambda^{(v+1)} - \lambda^{(v)}\right\| / \left\|\lambda^{(v)}\right\| \leq \varepsilon$, the algorithm stops. Otherwise set v+1 ← v and go to step 1).

Some widely used methods in step 3) such as subgradient method (SG) and cutting plane method (CP) have been applied successfully in many cases. However, the two algorithms differ in many ways, like the assumptions, the convergence speeds, and the search directions. Their formulations and features are compared as follows.

Subgradient Method: The subgradient method solves the Lagrangian dual problem heuristically. It is an iterative approach in which the Lagrangian multipliers are adjusted to find the best (or nearly the best) lower bound. The general procedure at iteration v is

$$\lambda^{(v+1)} = \max(0, \lambda^{(v)} + \xi^{(v)} \cdot g^{(v)}) \tag{3.32}$$

$$\xi^{(v)} = \frac{\mu \cdot (LRV^{*} - LRV^{(v)})}{\left\|g^{(v)}\right\|^2} \tag{3.33}$$

where $\xi^{(v)}$ is the step size, LRV^* is the estimated upper bound of Lagrangian relaxed function, μ is the convergence factor with value between 0 and 2, and $g^{(v)}$ is the subgradient of Lagrangian function (3.30) at $\lambda^{(v)}$, as shown in formulation (3.34)

$$g^{(v)} = \frac{\partial LR(\lambda)}{\partial \lambda} = (\sum_{k=1}^{NC} Pr_k \sum_{l=1}^{NL} Sev_{l,k}^{(v)}) - K_R \times Risk_{max} \tag{3.34}$$

where $Sev_{l,k}^{(v)}$ is the solution of decision variables at *k*th iteration.

The SG method is simple to implement and with small computational burden. However, its convergence speed is slow due to the oscillating feature as a consequence of the non-differentiability of the dual function [95]. Besides, in order to apply the rule specified in (3.33) it is require to know LRV^* as a priori, which is hard to obtain for large-scale CRB-SCOPF problem.

Cutting Plane method: In each iteration of cutting plane method, the multiplier is updated by solving the following linear programming problem

$$\begin{aligned} &\text{Max} \quad z \\ &s.t. \quad z \le LRV^{(k)} + u \cdot g^{(k)}, \\ &\qquad u \ge 0, \qquad k = 1, 2, ..., v \end{aligned} \tag{3.35}$$

where *u* is a scalar, $g^{(k)}$ is the same as in (3.34), *z* is an unconstrained decision variable that estimates the currently best objective function value.

The linear programming (3.35) is a relaxed dual problem that approximates the actual dual problem with the iteration grows. The number of constraints increases with the number of iterations, thus may cause high computational burden if the size of multiplier vector is large. However, we only relax one constraint in the CRB-SCOPF problem. Hence only one Lagrangian multiplier is needed. The LP (3.35) could be solved very fast with current technologies even if the iteration number is high. In the numerical example part of this chapter, the cutting plane method is applied to update multipliers.

Another important issue in the algorithm to solve the dual problem comes from step 2). If the system is small, the Lagrangian dual problem could be solved as a whole with fast algorithm. For large systems, however, the Lagrangian dual problem is a large-scale optimization problem with liking variables. Benders decomposition will be used to solve the dual problem, as shown in what follows.

3.4.3 Benders decomposition to solve the dual subproblem

To solve the Lagrangian dual problem directly will cause prohibitive CPU computing time and memories if the system is large and many contingencies are considered. The Benders decomposition is an efficient method to solve the DP, which contains linking variables between normal state and contingency states. In Benders approach, the original DP, i.e. formulation (3.30) with constraints (3.19)-(3.28), is decomposed into a master problem and a successive of slave subproblems that interact iteratively.

Without the loss of generality, the DP is expressed here in compact form as shown in (3.36)-(3.41), where the first term (as a constant for given λ) in (3.30) is not included in the objective function:

$$\text{Min } c_0^T x_0 + d_0^T y_0 + \sum_{k=1}^{NC} d_k^T y_k \tag{3.36}$$

$$s.t.\ A_0 x_0 \geq b_0 \tag{3.37}$$

$$E_0 x_0 + F_0 y_0 \geq r_0 \tag{3.38}$$

$$A_k x_k \geq b_k \tag{3.39}$$

$$E_k x_k + F_k y_k \geq r_k \tag{3.40}$$

$$|x_0 - x_k| \leq \Delta_k \tag{3.41}$$

For all $k = 1, 2, \ldots, NC$

where x_0 and x_k (y_0 and y_k) denote the state &control variables (the severity decision variables) at normal and the kth contingency state, respectively. c_0 is vector of the generation cost coefficient, vector d_k is shown in (3.42)

$$d_k = \gamma \times \begin{bmatrix} Sev_{1,k} \\ Sev_{2,k} \\ \vdots \\ Sev_{NL,k} \end{bmatrix}^T, \text{ for all } k = 0, 1, \ldots, NC \tag{3.42}$$

and the inequality (3.37) denotes constraint (3.19)-(3.23) when k = 0, where the equality (3.19) is transferred to two inequality constraints; equation (3.39) denotes constraints (3.19), & (3.21)-(3.23) when $k \geq 1$; equation (3.38) (or (3.40))denotes the risk constraints (3.26)-(3.28) when $k = 0$ (or $k \geq 1$); equation (3.41) denotes the coupling constraints (3.24)-(3.25).

Based on the above formulations, the master problem is formulated as (3.43), which is a base-case OPF problem associated with the type I risk constraints at normal state:

$$\begin{aligned} &\text{Min } \; c_0^{\,T} x_0 + d_0^T y_0 + \sum_{k=1}^{NC} \hat{\mu}_k \\ &s.t. \quad A_0 x_0 \geq b_0 \\ &\qquad E_0 x_0 + F_0 y_0 \geq r_0 \\ &\quad \textit{and Benders cuts from subproblems} \end{aligned} \tag{3.43}$$

where $\hat{\mu}_k$ (k = 1,…, NC) represents the kth optimistic estimate of $d_k^T y_k$. It is an unconstrained decision variable in the master.

The kth subproblem (k = 1, 2,…, NC) is

$$\xi_k = \text{Min } \; d_k^T y_k \tag{3.44}$$

$$s.t. \quad A_k x_k \geq b_k \tag{3.45}$$

$$E_k x_k + F_k y_k \geq r_k \tag{3.46}$$

$$\left| x_0^* - x_k \right| \leq \Delta_k \tag{3.47}$$

where x_0^* is the optimal solution of x_0 from (3.43).

First we need to check the feasibility of optimization problem (3.44)-(3.47). Note that the range of y_k is [0, +∞), which means we could always find large enough y_k to satisfy inequality (3.46). Thus, constraint (3.46) could be eliminated in the feasibility-check procedure. We formulate the following subproblem to check the feasibility of (3.44)-(3.47)

$$
\begin{aligned}
w_k(x_0^*) = \text{Min}\ \ & \mathbf{1}^T \cdot \boldsymbol{s}_1 + \mathbf{1}^T \cdot \boldsymbol{s}_2 \\
s.t.\quad & A_k x_k + \boldsymbol{s}_1 \geq b_k && \pi_{k1} \\
& \left| x_0^* - x_k \right| - \boldsymbol{s}_2 \leq \Delta_k && \pi_{k\Delta}
\end{aligned} \tag{3.48}
$$

where **1** is the vector of ones, $\boldsymbol{s_1} \geq \mathbf{0}$ and $\boldsymbol{s_2} \geq \mathbf{0}$ are vectors of slack variables used to check the violation of constraints. π_{k1} and $\pi_{k\Delta}$ are the associated Lagrangian multipliers of corresponding inequalities. From problem (3.42), we can conclude that the problem (3.44)-(3.47) is feasible if $w_k(x_0^*) = 0$, and infeasible if $w_k(x_0^*) > 0$.

A feasibility cut as shown in (3.49) needs to be added to the master if problem (3.44)-(3.47) is infeasible

$$w_k(x_0^*) + \pi_{k\Delta}(x_0 - x_0^*) \leq 0 \tag{3.49}$$

Otherwise, if problem (3.44)-(3.47) has optimal solution (x_k^*, y_k^*) but with $\xi_k > \hat{\mu}_k^*$, where $\hat{\mu}_k^*$ is the optimal solution of $\hat{\mu}_k$ in (3.43), then $\hat{\mu}_k^*$ is an unrealistic estimate. We need to send back an optimality cut to the master problem such that $\hat{\mu}_k$ is more realistic. The optimality cut is shown in (3.50)

$$w_k(x_0^*) + \pi_{k\Delta}(x_0 - x_0^*) \leq \hat{\mu}_k \tag{3.50}$$

Finally, if problem (3.44)-(3.47) has optimal solution with the objective function value $\xi_k > \hat{\mu}_k^*$, then no Benders cut is generated. The algorithm stops, and the current solution (x_k^* , y_k^*) is the optimal solution to the original problem.

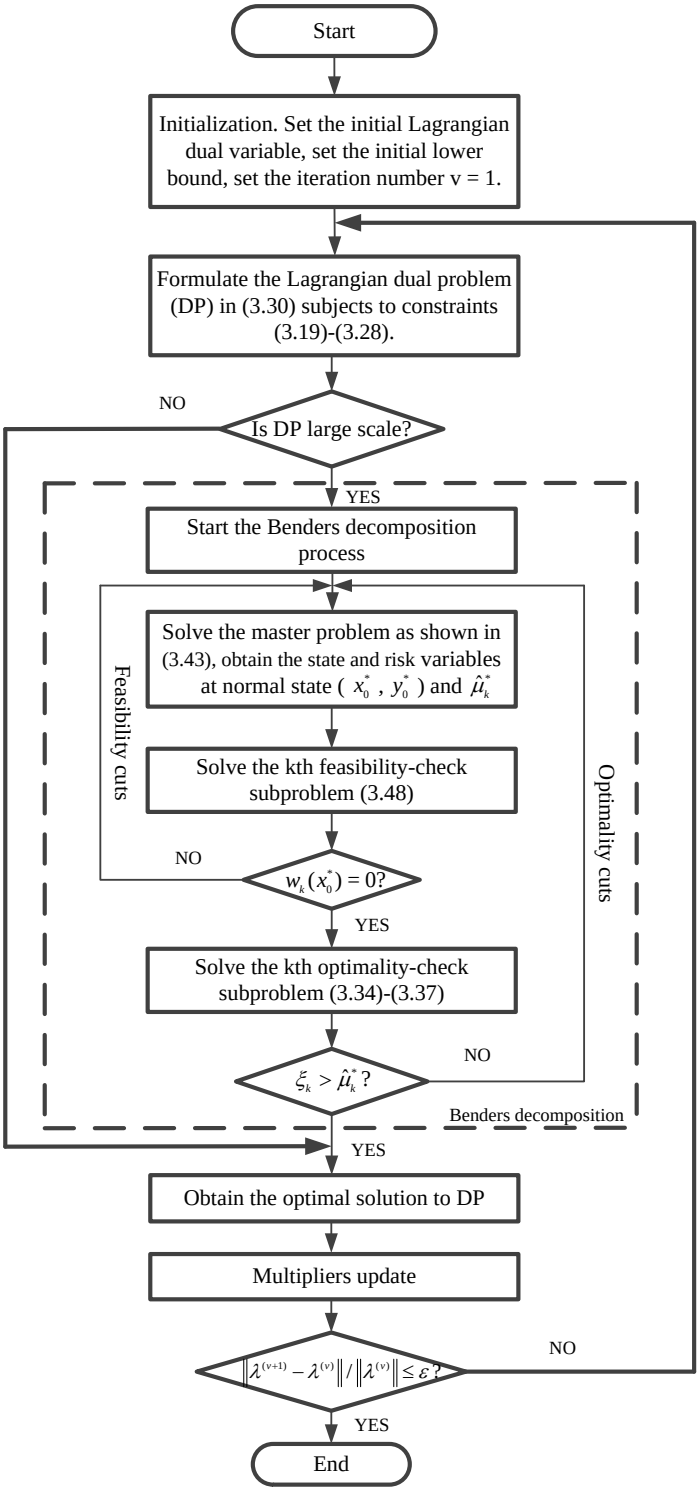

Fig. 3.3. Iterative procedure for CRB-SCOPF using Lagrangian relaxation and Benders decomposition

3.4.4 Iterative Procedure

Based on the above analysis, we can get an iterative approach to solve CRB-SCOPF problem, as shown in Fig. 3.3. If the size of the system is small, we can solve the Lagrangian dual problem directly by LP (for DC power flow) or NLP (for AC power flow) algorithms without using Benders decomposition. This is because Benders decomposition may spend rather a long time to iterate between the master and the subproblems, especially when the solution is close to optimal. However, if the system is large and many contingencies are considered, it will cause prohibitive time to solve the dual problem as a whole. Benders decomposition is more efficient and recommended to use at this time.

The Benders decomposition algorithm terminates when no Benders cuts are generated after solving the feasibility-check and optimality-check subproblems. The Lagrangian relaxation algorithm terminates when the multiplier difference between two consecutive iterations is below a pre-specified threshold.

3.5 Illustrative Examples

The proposed algorithm to solve CRB-SCOPF problem was tested on two representative numerical examples: the IEEE 30-bus system and the ISO New England bulk system. The former is a small system that only Lagrangian relaxation algorithm is used. The dual problem was solved by LP algorithms directly. The latter is ISO New England's real power system. Benders decomposition is applied to improve efficiency.

The generation costs and risk level are compared between CRB-SCOPF and CSCOPF, for the purpose of demonstrate the benefits of the former in terms of both *economy* and *security*.

However, the computational burden of CRB-SCOPF is higher than CSCOPF.

The results reported here are tested using MATLAB R2010a and CPLEX 12.1, on a 3.16GHz Intel Core 2 CPU and 4Gb RAM PC.

3.5.1 The IEEE 30-bus system

The IEEE 30 bus system is from [60], and its single line diagram is shown in Fig. 3.4. The system is composed of 30 buses, 41 branches, 6 thermal units and 20 loads. To better apply the proposed algorithm, some changes are made to the original data as follows: the transmission limits of circuit 2-6, 12-13, 23-24 are modified to 20MW, 40MW, and 7.47MW, respectively; the transmission limits of circuits 6-8 and 21-22 are reduced to 90% of the original ones. Besides, the generation costs of original data are with quadratic form. We use 3-segament piecewise linear curve to approximate the quadratic cost curve in this example. Let P_{min} and P_{max} denote the minimal and maximum outputs of a generator, respectively. Then the intervals of the 3-segements are [P_{min}, (P_{max} - P_{min}) / 3], [(P_{max} - P_{min}) / 3, 2×(P_{max} - P_{min}) / 3], and [2×(P_{max} - P_{min}) / 3, P_{max}], respectively. Plotted figure indicates that the error between the original quadratic curve and the approximated linear curve is small.

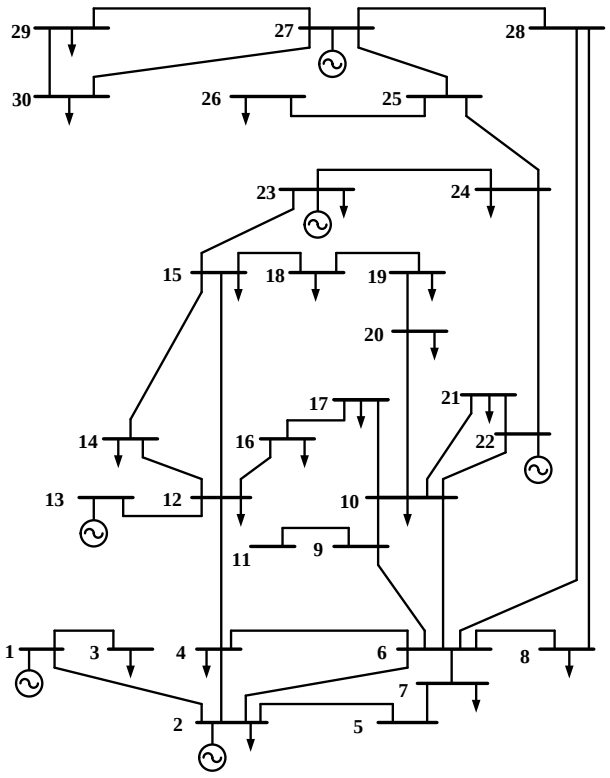

Fig. 3.4 Single line diagram of the IEEE 30-bus system

We assume that the system is lossless, and bus 1 is the reference bus. In general there are 36 N-1 post-contingencies be defined, i.e. every circuit could be lost thus contribute to a contingency except for those lines whose outage may lead to islanding. One fact lies in that the probabilities of the contingencies are related with the length of the line — the longer the line is, the higher probability the outage may happen. However, the line lengths are not available in the data, so we use the impedance data to replace them. We set the probability for the benchmark impedance, i.e. the average impedance of all the circuits, to be 0.002. The probabilities for the 36 contingencies are calculated by 0.002 times the ratio of the circuit impedance to the benchmark impedance.

As regards to the coupling constraints between the normal and post-contingency states, we assume that every generator is able to reschedule ±7% of its active power physical range following the loss of a circuit. Based on these assumptions, the CSCOPF is solved at first for the system. The minimum generation cost is $116207.5 without violating the *N*-1 contingency criteria. The risk of the system, as an index computed form the CSCOPF result, is 0.115. If we set the parameter $K_R = 0.5$, then the risk index for the CRB-SCOPF should be 0.575, which means we set the risk level of CRB-SCOPF be a half to CSCOPF.

Table 3.1 Evolution of the LR Algorithm Using a Cutting Plane Multiplier Updating Method for Various Cases

approach	iter.	λ	$LR(\lambda)$	Gen. costs	time (s)
HSM	1	60000.0	125837.7	127977.9	1.9817
	2	0	116230.1	116207.5	
	3	10594.9	119410.6	117982.9	
	4	58909.8	125874.9	121352.7	
	5	58926.9	125876.1	125867.1	
ESM	1	60000.0	101544.2	103608.7	2.0595
	2	0	101984.2	101957.5	
	3	1154.3	102846.8	102544.5	
	4	3719.2	103485.3	103603.3	
	5	3701.8	103484.7	103134.1	
	6	3711.2	103485.4	103351.0	
	7	3713.2	103485.6	103475.1	
HEM	1	60000.0	100458.2	102240.1	2.4289
	2	0	100368.2	100331.6	
	3	1003.6	101270.3	100820.5	
	4	3065.8	102122.2	102197.6	
	5	2980.1	102120.1	101410.3	
	6	2997.6	102123.9	101893.9	
	7	3000.1	102124.1	102110.4	
CSCOPF	-	-	-	116207.5	0.2071

The CRB-SCOPF problem was solved using Lagrangian relaxation algorithm. Set initial Lagrangian multiplier $\lambda_0 = 6 \times 10^4$. The cutting plane method was used for multiplier updating. For the HSM, ESM and EESM cases, the LR algorithm terminated after 5, 7, and

7 iterations, respectively. The evolutions of Lagrangian multiplier λ, dual function $LR(\lambda)$, and generation costs with iterations, and the CPU computing time with iterations for various cases are shown in Table 3.1. As a comparison, the generation costs and CPU time for CSCOPF are also listed in the Table. The risks and generation costs for CSCOPF and various cases of CRB-SCOPF are demonstrated in Table 3.2.

Table 3.2 Comparison of Risk and Generation Costs for the IEEE 30-Bus System

Constraints	CSCOPF	CRB-SCOPF		
		HSM (K_C=1, K_R = 0.5)	ESM (K_C =1.05, K_R = 0.5)	HEM (K_C =1.20, K_R = 0.5)
Risk	0.1150	0.0575	0.0575	0.0575
Cost ($)	116207.5	125867.1	103475.1	102110.4

Table 3.3 summarizes the circuits with flow over 90% of corresponding transmission limits. At normal state, the power flows on two circuits are over 90% limit: circuit 12-13 with 100% limit, and circuit 21-22 with 91.83% limit. However, the CRB-SCOPF dispatch result will lead only one circuit, i.e. circuit 21-22, with power flow over 90% limit. The transmission congestion on circuit 12-13 has been eliminated. At contingency states, CSCOPF will result in 58 circuits, while CRB-SCOPF will only cause 19, 21, 21 circuits for HHS, ESM and HEM models respectively, be over 90% transmission limits. The number of highly-loaded circuits for CRB-SCOPF has decreased significantly compared to CSCOPF. Nevertheless, there are 4 circuits be over 100% limit for ESM at contingency states: 1.0106 limits of circuit 21-22 at 7th contingency, 1.05 limits of circuit 2-6 at 16th contingency, 1.05 limits of circuit 23-24 at 30th contingency, and 1.05 limits of circuit 25-27 at 36th contingency. Similarly, 4 circuits be over 100% limit for EESM are: 1.0133 limits of circuit

21-22 at 7th contingency, 1.1013 limits of circuit 2-6 at 16th contingency, 1.2 limits of circuit 23-24 at 30th contingency, and 1.2 limits of circuit 25-27 at 36th contingency.

Table 3.3 Summaries of Circuits with Flow Over 90% Limits for Various Cases

approach		no. of circuits with flow over 90% *limit*		
		normal state		*contig*. states
CSCOPF		2	*circuit 12-13, 100% limit* *circuit 21-22, 91.83% limit*	58
CRB-SCOPF	HSM	1	*circuit 21-22, 91.21% limit*	18
	ESM	1	*circuit 21-22, 90.73% limit*	21
	HEM	1	*circuit 21-22, 91.10% limit*	21

Based on the above results and analysis, some comments are presented as follows to describe the features of CRB-SCOPF:

- The CRB-SCOPF is an improved real-time dispatch tool than the traditional CSCOPF model. It has very good merits, such as allowing the system operators to make a tradeoff between system security and economy, imposing the circuit power flows distributed more evenly, releasing the system's transmission stress at normal state, etc. However, the computational burden of CRB-SCOPF is higher than that of CSCOPF.
- We do not allow circuit overflows at normal state in various CRB-SCOPF models. Only a certain level overflows is allowed at contingency states, i.e. we allow 5% overflow for ESM, and 20% overflow for HEM. Note that the probability for a contingency to happen is very low, i.e. most of the time the system will remain at ordinary state. Thus it is very attractive to explore the application of ESM and HEM

model in real-time use, since they will bring significant improvements in economic efficiency.

- The HSM is the most secure but most costly model, thus may lead to a relatively conservative operation status. Compared to CSCOPF model, it will always be less risky nevertheless less economic. Hence we suggest the HSM model be used only when there is high requirement on system's security, such as heavy load, extreme weather conditions, or in the time when important public activities may be hold, etc.

3.5.2 The ISO New England bulk System

We obtain the raw data from ISO New England. The original network data consist of 12,300 buses, 13,500 circuits and 1136 contingencies. In this example, only the first 250 contingencies are considered to demonstrate the algorithm to solve CRB-SCOPF. However, the conclusion to be obtained should be the same if all the contingencies are considered. The bidding data of generation units we used are from a winter day in 2009 within the New England area. Wind turbine units are not included since they currently do not have to provide bidding curves within ISO New England electricity market. The total number of bidding units is close to 400.

Table 3.4 Summaries of CSCOPF Results for ISO New England Bulk System

no. of Iterations	no. of Benders cuts generated	costs ($) on base-case	costs ($) on CSCOPF	CPU time (s)
32	244	571530.3	616172.1	1855.6

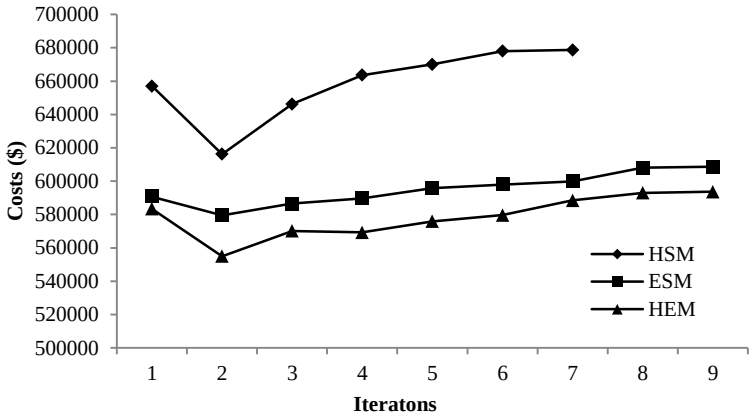

Fig.3.5. The evolution of generation costs with the Lagrangian relaxation iterations for HSM, ESM, and HEM

Table 3.5 CPU Time for Various Models

Model	HSM	ESM	HEM
CPU time	5.2 hours	6.7 hours	6.9 hours

At first we solve the CSCOPF model for ISO New England system. Note that CSCOPF is a special case of CRB-SCOPF in (3.1)-(3.6). We could use the Benders decomposition algorithm proposed in section III to solve CSCOPF by imposing the Lagrangian multiplier $\lambda = 0$. The CSCOPF problem has 322,456 decision variables and 2,246,041constraints based on DC power flow model. We assume that the generators could be rescheduled within ±5% of their active power physical ranges at post-contingencies. The Benders decomposition algorithm for CSCOPF will iterates between a base-case economic dispatch and separate post-contingency analysis with generation rescheduling. The summary of CSCOPF algorithm is shown in Table IV. Based on the results, we can compute the risk of the system under CSCOPF model is $Risk_{CSCOPF}$ = 18.24, which is used as the benchmark risk level for CRB-SCOPF. If we set K_R = 0.5, the maximum allowed risk value for CRB-SCOPF will be 9.12, which is a half to that of CSCOPF.

The CRB-SCOPF model in this case consists of 990,395 decision variables and 5,347,798 constraints. We use Lagrangian relaxation and Benders decomposition as shown in section 3.3 to solve the large-scale programming. The evolution of generation costs with Lagrangian relaxation iterations for various models are shown in Fig. 3.5. For HSM model, the algorithm terminates at the fifth iteration by satisfying the convergence condition as shown in Fig. 3.3. Similarly, the ESM and HHSM models converge both at 9 iterations. The CPU time for various models is demonstrated in Table 3.5. The most computational part of the algorithm comes from using Benders decomposition to solve the LR dual problems. For a given Lagrangian multiplier λ, the BD algorithm iterates between a master problem and a bunch of subproblems. The initial multiplier is set as λ = 100000. The first iteration in BD corresponds to an economic dispatch problem associated with corresponding type I risk constraints. At the resulting base-case operating point, contingency analysis was then carried out. Totally there are 31 contingencies lead to infeasibilities and 219 contingencies lead to feasibilities but with optimal objective value larger than $\hat{\mu}_k$ (k = 1,…, NC) , i.e. the kth optimistic estimate of $d_k^T y_k$ in(37). Thus 31 feasibility cuts and 219 optimality cuts are generated and returned to the master problem. A new master problem is solved again and the result is sent to the subproblems. This process terminates until reaching the stopping condition after 28 iterations. Hence we obtain the optimal solution of Lagrangian dual problem for the initial λ. Based on the result, a new multiplier is calculated by using cutting plane method. The new dual problem is solved again. The algorithm stops until the multiplier difference between two successive iterations is lower than a pre-specified threshold.

Table 3.6 Comparison of Risk and Generation Costs for the ISO New England Bulk System

Constraints	CSCOPF	CRB-SCOPF		
		HSM (K_C=1, K_R = 0.5)	ESM (K_C =1.05, K_R = 0.5)	HEM (K_C =1.20, K_R = 0.5)
Risk	18.24	9.12	9.12	9.12
Cost ($)	616172.1	678654.3	608672.2	593676.6

Table 3.7 Number of Circuits with Flow Over 90% Limits in Various Cases Based on ISO New England Bulk System

approach		no. of circuits with flow over 90% *limit*	
		normal state	*contingency* states
CSCOPF		30	7201
CRB-SCOPF	HSM	21	5876
	ESM	19	5019
	EESM	18	4963

We compared the generation costs and the system's risk value for CSCOPF and various cases of CRB-SCOPF in TABLE 3.6. The numbers of circuits with flow over 90% limits in both normal and contingency states are shown in Table 3.7, classified by different approaches. From these results we could conclude that the bunch of CRB-SCOPF models is an efficient tool to manage the system's risk while providing controls over a tradeoff between the economy and security of the system.

3.6 Conclusion

A mathematical framework to solve the corrective risk-based SCOPF model, which can take into account the system's corrective capabilities after contingency has occurred, has been presented in this chapter. The original problem is with both combinatorial nature and high dimensionality, i.e. has both linking constraints and linking variables, and thus is very

difficult to be solved directly for large systems. The Lagraingian relaxation approach is applied to relax the linking constraints. The relaxed problem, called Lagrangian dual problem, contains only linking variables. We use Benders decomposition method to solve the dual problem. The algorithm allows iterations between a master problem, which consists of a base-case economic dispatch problem and the associated type I risk constraints, and a bunch of subproblems, which include feasibility-check and optimal-check procedure to eliminate the violating constraints. Based on the optimal solution of dual problem, an efficient cutting plane method is applied to update the Lagrangian multipliers.

The algorithm has been tested on IEEE 30-bus system and the ISO New England's bulk power system. The results indicate that CRB-SCOPF could manage the system risk while providing controls over the tradeoff between security and economy.

Future research on the application of the algorithm may include finding efficient techniques to solve the CRB-SCOPF problem with AC network constraints. To improve the computing efficiency, we can assume that the circuits with power flow below 45% percent of limits at normal state will never lead to overload severity at contingency states. Since the number of highly loaded circuits in real systems is small, this kind of assumption may greatly reduce the scale of optimization.

CHAPTER 4. ONLINE RISK-BASED SECURITY-CONSTRAINED ECONOMIC DISPATCH IN POWER SYSTEM AND MARKET OPERATION

4.1 Introduction

Economic Dispatch (ED) is one of the most important tasks in the operation of power system. The objective of ED problem is to identify an hourly unit dispatch schedule that minimizes the generation costs based on existing unit commitment (UC) results. To ensure the operational security, a so-called "N-1" criterion [61], [107] has generally been applied in the ED procedure of today's independent system operator (ISO) managed electricity markets, thus extending the ED to Security-Constrained Economic Dispatch (SCED). The SCED model allows the system be able to withstand the loss of a single component failure for all pre-defined possible contingency scenarios. In the past decades, the SCED approach has well-served the power industry to achieve economic operation with high security levels. However, this deterministic approach, without considering contingency probabilities, has a fundamental weakness in that the system security cannot be quantified. Under the SCED model, the power system could be either secure — if there are no violations of criteria, or insecure otherwise. The SCED cannot measure how secure the system is, or how insecure the system is. Hence, risk, a quantification of system health, is used as a constraint in the security-constrained economic dispatch [108]. The corresponding optimization problem is called Risk-based SCED (RB-SCED), which has the following characteristics: 1) It treats the post-contingencies with different occurring likelihoods, depending on the facility's operational condition and weather condition in that area. This could avoid the occurring of unnecessarily low-risk, thus excessively high-cost operational conditions caused by SCED.

2) It intends to effectively manage both the *system* security level as well as security associated with individual circuit flows. The strength is that the overall system stress level can be controlled while simultaneously ensuring risk of post-contingency flows on individual circuits does not become excessive. 3) It is inherently a "balance-to-center" approach — by constraining the flow on highly-loaded circuits, it makes the distribution of flow on the system more even.

Risk based approach is an emerging new direction that is studied and beginning to be used in power system planning [2][3], maintenance [4][5] and online operation [6][7]. A risk-limiting dispatch under smart-grid environment was proposed in [8]. The formulation of risk, as well as several kinds of severity functions, was described in [36]. It was shown in [71] that the short-term contingency probability could be calculated based on information of weather, geography, voltage class, and historical data, and a statistic regression method for real-time contingency probability assessment was developed.

To realize the application on real-time operation, the RB-SCED algorithm must be solved within a time scale of several minutes. To this end, we propose an efficient computation strategy by using Lagrangian relaxation and Benders decomposition. The simultaneous feasibility test (SFT) [52] is performed to further improve the computing efficiency.

4.2 Contribution of this Chapter

RB-SCED is a special form of RB-SCOPF. In this chapter, we focus on how to realize the RB-SCED algorithm in the industry. We only consider the preventive RB-SCED model, in accordance to the fact that all the ISOs in the USA are currently using preventive SCED for their real-time electricity market. In this chapter, we will develop the model and the

computational framework for preventive RB-SCED, and present the results based on the ISO New England electricity market and power system.

In chapter 2 and chapter 3, we have developed the computational strategies to compute PRB-SCOPF and CRB-SCOPF, and tested them on the ISO-NE system. However, we just adopted a simplified network model in these chapters, as shown in the following:

- The network was simplified as pure nodes and branches, while in real-world power system more complicated network model is used.
- We used DC power flow to check if there exists overloading at post-contingency states. However, the industry adopts a better approach, called the contingency screening (CS) process, to check post-contingency violations: at first DC power flow is used to do fast CS, then the post-contingency states are ranked based on their severities, finally a certain number (like ten) of most severe post-contingency states are chosen to be analyzed using AC power flow. By this way, more precise result could be guaranteed.
- Constant loss model was used in chapter 2 and chapter 3. However, the industry is modeling system loss with more complicated models. This chapter will introduce and use these models.
- There is need to make topology analysis for the work. For example, the industry software should be able to deal with islanding conditions. In addition, there exists large amount of zero-impedance branches (ZBRs) in the original data. The commercial software should be able to eliminate ZBRs and reorder the nodes.

To deal with the above issues, we embed the proposed RB-SCED algorithm into commercial software TARA (Transmission Adequacy & Reliability Assessment), which has

been applied in ISO-NE and is able to model the system with more realistic tools.

Another important issue deserves to be considered: in Chapter 3, we have developed a computational strategy to compute CRB-SCOPF by using Lagrangian relaxation and Benders decomposition. The question is if this method could be applied to solve preventive RB-SCED. The answer is positive. In fact, there are some interesting features if we apply the strategy in Chapter 3 to solve preventive RB-SCED. Recall that in Chapter 3 we have to solve individual LPs for each subproblem, but we can solve the subproblems of preventive RB-SCED algebraically, as will be shown in section 4.3 and 4.4. In this Chapter, we will use Lagrangian relaxation and Benders decomposition to solve PRB-SCED, rather than the method proposed in Chapter 2, for the following considerations:

- It will be easier for ISO-NE to upgrade to CRB-SCED in the future.
- It is beneficial to have another approach to solve PRB-SCOPF.
- As shown in section 2.4.4, the risk-subproblem simultaneously considers all the post-contingency states, thus the sizes of matrix $\boldsymbol{E_2}$ and $\boldsymbol{F_2}$ in (2.52) of Chapter 2 are very large. The data stored in disk may need more time to be read, thus the computational efficiency is decreased.

4.3 The RB-SCED Formulation

The formulation of preventive RB-SCED is similar to the one in Chapter 2, but we make a few improvements here to adapt to the industry software. The RB-SCED problem is formulated as in equation (4.1) – (4.6). Compare to Chapter 2, the following changes are made:

- Equation (4.3) is added to denote the inequality constraints of the system at normal

state, such as the upper and lower limits of unit outputs.

- The effect of phase angle regulator (PAR) is considered, thus the form of power flow equations is changed, see (4.4) and (4.5).
- New severity function has been used, as shown in Fig. 2.4 of Chapter 2. The expression of the severity function, as well as the equivalent LP transformation, is shown in the Appendix of this Chapter.

$$\text{Min } \{ f(\underline{P}_0) \} \tag{4.1}$$

Subject to:

$$h(\underline{P}_0) = 0 \tag{4.2}$$

$$q(\underline{P}_0) \le 0 \tag{4.3}$$

$$-\underline{g}_{\max} \le g_l^0(\underline{P}_0, \underline{PAR}_0) \le \underline{g}_{\max} \tag{4.4}$$

$$-K_C \underline{g'}_{\max} \le g_l^k(\underline{P}_0, \underline{PAR}_0) \le K_C \underline{g'}_{\max}, \; k = 1, 2, \ldots, NC \tag{4.5}$$

$$0 \le Risk(g_l^1, g_l^2, ..., g_l^{NC}) \le K_R Risk_{\max} \tag{4.6}$$

where $\underline{P}_0$ is the vector of generation output at normal state, $\underline{PAR}_0$ is the vector of phase angle regulator, NC is the number of contingencies. K_C and K_R are coordination factors used to impose control over a tradeoff between security and economy. Equation (4.1) minimizes system production costs $s(\underline{P}_0)$. Equation (4.2) is the power balance equation. Equation (4.3) is the inequality constraints at normal state, including the unit output limits, phase angle regulator limits, and system spinning and operating reserve requirements. Equation (4.4) is the circuit loading constraints under normal condition, and (4.5) are circuit loading

constraints at each of the *NC* post-contingency states. Equation (4.6) is the system overall risk constraint, which is a function of circuit flows at post-contingency states. We do not consider the circuit overload risk at normal state.

The circuit load flow in (4.4) and (4.5) could be formulated as follows

$$g_l^k = \sum_{i=1}^{ND} sf_{i,l}^k \bullet (P_i - D_i) + \sum_{j=1}^{NP} sp_{j.l}^k \bullet PAR_j \quad \forall l = 1,2,...,NL, \forall k = 0,1,2,...,NC \qquad (4.7)$$

,

Where *ND* is the number of nodes, *NP* is the number of PARs, *NL* is the number of circuits. h_l^k is the flow on *l*th circuit at contingency *k*, and *k* = 0 represents the normal state. $sf_{i,l}^k$ is the power shift factor of the *i*th node to *l*th circuit under state *k*, and $sp_{j.l}^k$ is the shift factor of the *j*th PAR to *l*th circuit under state *k*. P_i and D_i represent the unit real power output and demand at *i*th node, respectively.

The risk constraint (4.6), if we utilize the equivalent LP optimization for the severity function as shown in Fig. 2.4 of Chapter 2, could be formulated as follows

$$\sum_{k=1}^{NC} Pr_k \sum_{l=1}^{NL} Sev_l^k \le K_R \times Risk_{max}, \quad Sev_l^k \text{ subject to constraints (4.A.7)-(4.A.14) .} \qquad (4.8)$$

where Pr_k is the probability of state *k*. Equation (4.8) is the system overall risk constraints.

4.4 Computational Strategy to Solve RB-SCED

As discussed in Section 4.2, we use the computational strategy in Chapter 3 to solve the preventive RB-SCED. Equation (4.8) is a complicated constraint that linking decision variable at both normal and contingency states. At the first state, we apply the Lagrangian relaxation to relax (4.8) into the objective function, which is called the outer level of the algorithm. At the second stage, Benders decomposition was applied to solve the Lagrangian relaxation problem, which is called the inner level.

4.4.1 The outer level: Lagrangian relaxation

The Lagrangian relaxation to the original problem (4.1)-(4.6) is shown as follows

$$L(\lambda_R) = \text{Min}\left\{ f(\underline{P}_0) + \lambda_R \left(\sum_{k=1}^{NC} Pr_k \sum_{l=1}^{NL} Sev_l^k - K_R \times Risk_{max}\right)\right\} \tag{4.9}$$

Subject to

Constraints (4.2)-(4.5) and (4.A.7)-(4.A.14) .

where λ_R is the Lagrangian multiplier associated with constraint (4.6).

The subgradient method, as introduced in Section 3.4.2, is applied to update the Lagrangian multiplier λ_R. The algorithm for the outer level is the same in Chapter 3. We do not elaborate it here, and just provide the procedure as below:

Outer level algorithm: Lagrangian relaxation

1: Input: μ , LRV^*, K_C, K_R and $Risk_{max}$.

2: Set $v = 0$. Given an initial guess to multiplier $\lambda_R^{\,0}$.

3: **while** $\left|\lambda_R^{(v+1)} - \lambda_R^{(v)}\right| > \varepsilon$, **do**

4: Solve LR dual problem, with the algorithm from inner level.

5: v ← v+1.

6: $g^{(v+1)} \leftarrow g^{(v)}$.

7: $\lambda_R^{(v+1)} \leftarrow \lambda_R^{(v)}$.

8: **end while**

4.4.2 The inner level: Benders decomposition

The inner level algorithm is different from that in Chapter 3, thus we elaborate it in this section. The problem described in (4.9) associated with the corresponding constraints is a large scale LP problem. The Benders decomposition (BD) algorithm, which iterates between a master problem and a bunch of subproblems, is applied to solve the LP. For given solution results from the master, the *k*th subproblem may have 3 kinds of solutions: infeasible, optimal but with objective function value lower than a bound and optimal with objective function value greater than the bound. For the first case, we need to add a feasibility cut to the master. In our implementation, we use simultaneous feasibility test (SFT) procedure to generate transmission security constraints, which is inherently a faster way to generate Benders feasibility cut for large system. For the second case, we need to generate optimality cut and send it to the master. For the third case, no cut is generated.

The *k*th (k =1, 2, …, NC) subproblem at post-contingency state is

$$\text{Min } \lambda_R \Pr_k \sum_{l=1}^{NL} Sev_l^k \tag{4.10}$$

Subject to:

$$g_l^k = \sum_{i=1}^{ND} sf_{i,l}^k \bullet (P_i^* - D_i) + \sum_{j=1}^{NP} sp_{j.l}^k \bullet PAR_j^* \tag{4.11}$$

$$g_l^k \le g_{l\max}^k \tag{4.12}$$

and constraints (4.A.8)-(4.A.14).

where P_i^* and PAR_j^* are solution from the master problem.

In order to get the Benders cut, we need to write down the Lagrangian relaxation of the subproblem. Let ζ_l^k denotes the multiplier of (4.11), π_l^k denotes the multiplier of (4.12), $\delta_{l,i}^k$ (i =1, 2, …, 7) denote the multiplier of constraints (4.A.8)-(4.A.14), respectively. Then the Lagrangian relaxation of problem (4.10) subject to (4.11), (4.12) and (4.A.8)-(4.A.14) is shown in (4.13).

$$\begin{aligned} LR_k = {} & \lambda_R \Pr_k \sum_{l=1}^{NL} Sev_l^k - \sum_{l=1}^{NL} \zeta_l^k [g_l^k - \sum_{i=1}^{ND} sf_{i,l}^k \bullet (P_i^* - D_i) + \sum_{j=1}^{NP} sp_{j.l}^k \bullet PAR_j^*] + \sum_{l=1}^{NL} \pi_l^k (g_l^k - g_{l\max}^k) \\ & + \sum_{l=1}^{NL} \delta_{l,1}^k (Sev_l^k + a_{4l} g_l^k + a_{5l}) + \sum_{l=1}^{NL} \delta_{l,2}^k (Sev_l^k + a_{2l} g_l^k + a_{3l}) + \sum_{l=1}^{NL} \delta_{l,3}^k (Sev_l^k + a_{1l} g_l^k + 9) + \sum_{l=1}^{NL} \delta_{l,4}^k Sev_l^k \\ & + \sum_{l=1}^{NL} \delta_{l,5}^k (Sev_l^k - a_{1l} g_l^k + 9) + \sum_{l=1}^{NL} \delta_{l,6}^k (Sev_l^k - a_{2l} g_l^k + a_{3l}) + \sum_{l=1}^{NL} \delta_{l,7}^k (Sev_l^k - a_{4l} g_l^k + a_{5l}) \end{aligned} \tag{4.13}$$

We apply KKT condition on (4.13) and obtain

$$\frac{\partial LR_k}{\partial g_l^k} = -\zeta_l^k + \pi_l^k + a_{4l}\delta_{l,1}^k + a_{2l}\delta_{l,2}^k + a_{1l}\delta_{l,3}^k - a_{1l}\delta_{l,5}^k - a_{2l}\delta_{l,6}^k - a_{4l}\delta_{l,7}^k = 0 \qquad (4.14)$$

$$\frac{\partial LR_k}{\partial Sev_l^k} = \lambda_R \Pr_k + \delta_{l,1}^k + \delta_{l,2}^k + \delta_{l,3}^k + \delta_{l,4}^k + \delta_{l,5}^k + \delta_{l,6}^k + \delta_{l,7}^k = 0 \qquad (4.15)$$

There are 9 unknown variables in (4.14) and (4.15). To get the Benders cut, we need to know the values of all the variables. If the optimization problem (4.10) subject to (4.11)-(4.12) and (4.A.8)-(4.A.14) is feasible, which could be guaranteed by SFT constraints, (4.12) should always be satisfied. Hence

$$\pi_l^k = 0 \text{ , for all the feasible subproblems} \qquad (4.16)$$

In (4.11), if P_i^* and PAR_j^* are obtained from the master, then h_l^k could be calculated. Substitute the h_l^k into (4.A.8)-(4.A.14), only one of the seven constraints is effective. Thus, only one of the $\delta_{l,i}^k$ (i =1, 2, …, 7) will be non-zero. Define $\bar{Sev}_l^k$ be the maximum right-hand side value of (4.A.8)-(4.A.14) for given h_l^k, we get

$$\delta_{l,i}^k = \begin{cases} -\lambda_R \Pr_k, & \text{if } \bar{Sev}_l^k \text{ corresponds to the } i\text{th equation} \\ 0, & \text{otherwise} \end{cases} \qquad i = 1, 2, \ldots, 7 \qquad (4.17)$$

Substitute (4.17) into (4.14), we obtain the value of ζ_l^k, whose expression is omitted here. Thus, all the variables in (4.14) and (4.15) have been solved. We can write the optimality cut as shown in (4.18)

$$\alpha_k \geq \lambda_R \Pr_k \sum_{l=1}^{NL} Sev_l^k + \sum_{i=1}^{ND} \frac{\partial LR_k}{\partial P_i} \cdot (P_i - P_i^*) + \sum_{j=1}^{NP} \frac{\partial LR_k}{\partial PAR_j} \cdot (PAR_j - PAR_j^*) \tag{4.18}$$

where α_k ($k = 1, 2, \ldots, NC$) are variables introduced in the master problem, and

$$\frac{\partial LR_k}{\partial P_i} = \sum_{l=1}^{NL} \zeta_l^k sf_{i,l}^k \tag{4.19}$$

$$\frac{\partial LR_k}{\partial PAR_j} = \sum_{l=1}^{NL} \zeta_l^k sp_{j.l}^k \tag{4.20}$$

Note that from the above approach we have obtained the Benders cuts algebraically, without solving the optimization problem (4.18) subjects to (4.20) and (4.A.8)-(4.A.14). This has greatly improved the computational efficiency of RB-SCED.

The master problem, includes the SFT constraints and the optimality cuts form the subproblem, could be written in the following LP

$$\begin{aligned} \text{Min} \quad & f(\underline{P}_0) + \sum_k \alpha_k \\ s.t. \quad & h(\underline{P}_0) = 0 \\ & q(\underline{P}_0) \leq 0 \\ & SFT \text{ constraints} \\ & \textit{Optimality cuts in } (4.18) \end{aligned} \tag{4.21}$$

The algorithm of the inner level is outlined as below

Inner level algorithm: Benders decomposition

1: Define: iteration no. v, the set of SFT constraints Sv, the set of optimality cut constraints Ov. Set initial conditions: $v = 0$, $S0 = \emptyset$, and $O0 = \emptyset$, where $\emptyset$ is empty set.

2: while ($Sv \neq \emptyset$ and $Ov \neq \emptyset$ and $v \neq 0$) do

3: v ← v+1.

4: Solve master problem (21), obtain the dispatch P* and PAR*.

5: for (k = 1 to NC) do

6: Solve the kth subproblem.

7: if (infeasible) do

8: Sv ← SFT constraints.

9: else if (optimal but $\alpha_k < \lambda_R \Pr_k \sum_{l=1}^{NL} Sev_l^k$) do

10: Ov ← Optimal cut constraint (18)

11: else do

12: $Sv = \emptyset$ and $Ov = \emptyset$.

13: end if

14: end for

15: end while

The procedure for the comprehensive algorithm is shown in Fig. 4. 1.

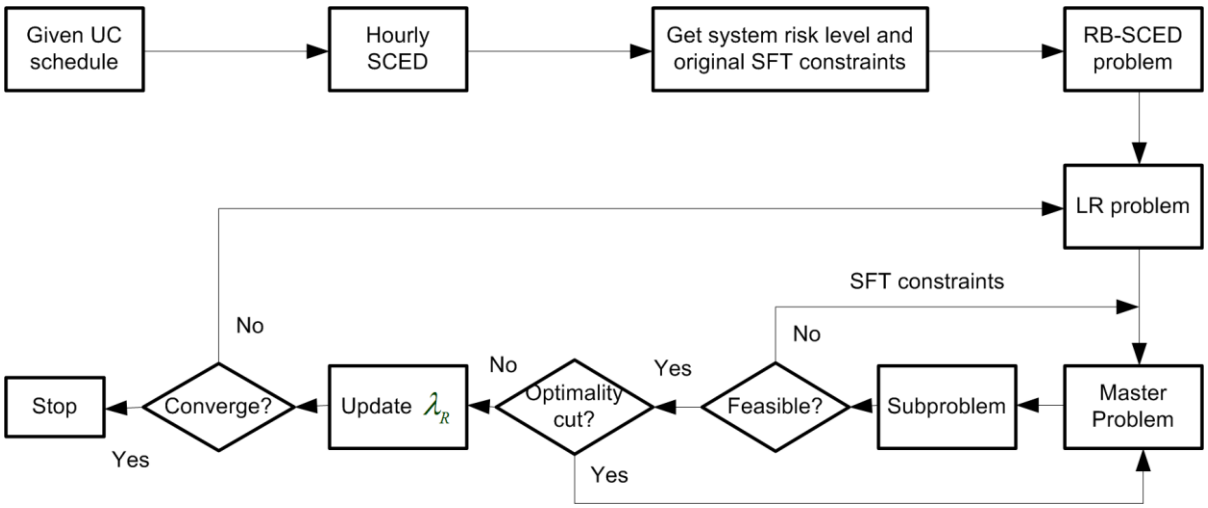

Fig. 4.1. Flowchart of RB-SCED algorithm

4.5 Illustrative Example

The proposed RB-SCED approach was tested on the ISO New England (ISO-NE) bulk system. The system network data include 308 generating units, 546 loads, 2804 LMP locations, 12765 nodes and 33 PAR branches. In particular, we select one specific hour data of generators' biding curves, reserve offers, nodal loads, and system reserve requirements, including 10 minute spinning reserve, 10 minute non-spinning reserve, and 30 minute reserve. The total generation capacity in the hour is 30062.4 MW and the forecasted load is 18576.1 MW.

Other parameters are set as follows: we set c_1 equals to 5 and c_2 equals to 25 according to the ISO-NE's network data. The condition of convergence for LR algorithm is set as ε = 0.01, where ε is the average change rate of lambda at two successive iterations.

The proposed two-level algorithm by combining using Lagrangian Relaxation and Benders decomposition is tested in GAMS. The linear programming is solved with CPLEX 12.1 on a PC laptop with Inter Core 2Duo 2.50 GHZ CPU and 3GB memory. The average

computation time for the approach is 20 minutes.

We compare the result of SCED and RB-SCED in the following 3 ways: a) The difference of generation costs between SCED and RB-SCED; b) the costs of RB-SCED for different operation modes of HSM, ESM and HEM; c) the sensitivity of the cost to different risk level.

Our test of the algorithm based on the ISO-NE system has provided 3 different results: a) we found that for some specific hours the algorithm fails on ISO-NE data; b) we will provide the test result of RB-SCED algorithm on a single hour; b) we provide result of RB-SCED for successive 24 hours.

4.5.1 Failure of the algorithm for some specific hours

The network data is from the EMS of ISO-NE control room on the first hour of June 16, 2010. At first we run the SCED for this specific hour. The result shows that there are totally 7 lines be over 90% thermal limits. One of the lines is at base case, with power flow b -180.9 MW on it while the thermal rating of the line at normal state is 192 MW. The loading rate is -94.2%. The other 6 lines comes from post-contingency states, with the loading rates be 103.9%, 110.3%, 100.4%, -96.6%, 100.4% and -96.9%, respectively.

We found that the cost does not change with the LR iterations when the value of lambda changes. This means that the outer level algorithm, whose function is to adjust the risk level of the system, has been failed. The reason is analyzed as follows. At base-case, only bus *THAMES_115_9997* has different shift factor on line *Line_MONTVLLE_1120-1*. The value of the shift factor is -0.9995, while the shift factor of other buses to the line in the system is 0.0005. The bus *THAMES_115_9997* corresponds to unit *UN.THAMES 115 THAM*, which

has identical EcoMax and EcoMin. This means, we cannot change the output of this unit to adjust the flow on line *Line_MONTVLLE_1120-1*. The procedure is indicated in Fig. 4.2.

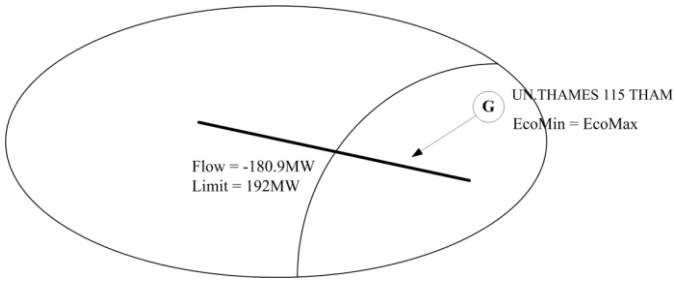

Fig. 4.2. Failure to adjust the output of unit with EcoMin = EcoMax

The reason for the failure the number of lines be over 90% limit at base-case and contingency cases are two small. If there are more units can be dispatched to change flow on a highly- loaded line, the probability of failure will decrease. This also means, the benefits of RB-SCOPF is more pronounced when there is often significant congestion on a system.

4.5.2 The Application of RB-SCED on a single hour

The network data is from the EMS of ISO-NE control room on the tenth hour of June 16, 2010. Totally there are 5 LR iterations at the outer level and 41 Benders iterations at the outer level. The algorithm takes about 20 minutes. The evolution of Lambda_R is shown in Table 4.1. The change of upper and lower bounds of Benders iterations on the last time of LR algorithm is shown in Fig. 4.3.

The comparison of SCED and different modes of RB-SCED are shown in Table 4.2. Compared to the traditional SCED, the RB-SCED will have lower risk level. The HSM mode has the highest mode, while the ESM and HEM modes have lower cost than the

SCED. The value of cost is negative is because the ISO-NE allows demand side bidding in the electricity market.

Table 4.1 Lagrangian Multiplier Evolution

LR iterations	Value of Lambda
LRI1	100000.0
LRI2	158956.7
LRI3	145091.7
LRI4	132941.3
LRI5	130976.5

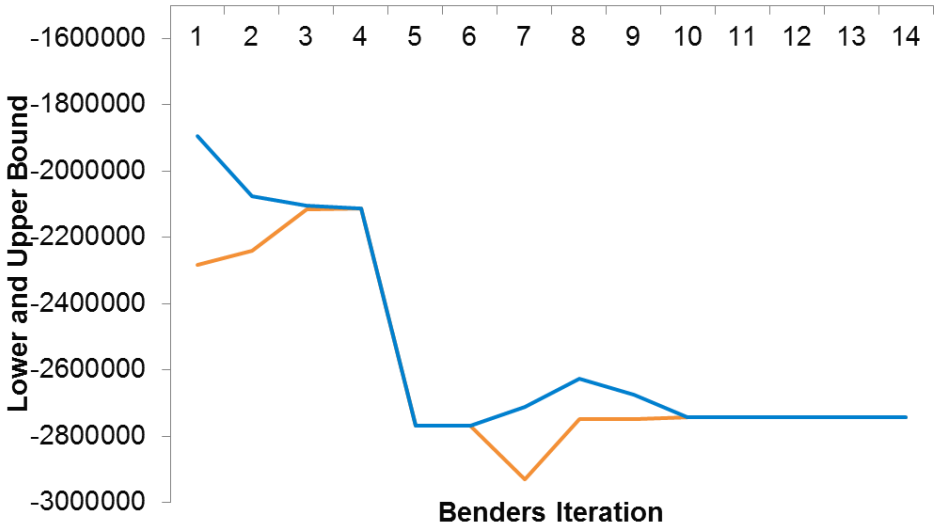

Fig. 4.3. Iterations of Benders decomposition

Table 4.2 Compare the Results of SCED and RB-SCED on a Single Hour

		Risk	Cost
SCED		1.98	-3495859.052
RB-SCED	HSM	1.03	-3675941.175
	ESM	1.03	-3386471.231
	HEM	1.03	-3301268.053

4.5.3 The Application of RB-SCED on successive 10 hours

The network data is from the EMS of ISO-NE control room on the first 10 hours of June 16, 2010. The result of the algorithm on successive 10 hours based on ISO-NE system is shown in Table 4.3. Since the algorithm fails at hour 1, the corresponding values are blank in the table. We present the result of HSM mode for RB-SCED only in this part.

Table 4.3 Compare the Results of SCED and RB-SCED on Successive 10 Hours

Hours	Cost ($)		Risk	
	SCED	RB-SCED	SCED	RB-SCED
1	-2551732		0.403533	
2	-2583216	-2942251	0.903533	0.522676
3	-2534003	-2899433	0.703533	0.403841
4	-2575826	-2799534	1.203533	0.733808
5	-2534559	-2758140	0.903533	0.505793
6	-2436926	-2690770	0.603533	0.303807
7	-2638981	-3083830	1.103533	0.680352
8	-3040819	-3169676	1.403579	0.848846
9	-3284619	-3433705	1.403604	0.713021
10	-3495859	-3675941	1.983549	1.048818

4.6 Conclusion

A new real-time dispatch model, called risk-based security constrained economic dispatch that takes account both the N-1 post-contingency security criteria and the risk level of the system, is proposed in this paper. The operational decision made by this model could reach a higher security level. By combining the advantages of RBED and SCED on security control, the RB-SCED could realize a better tradeoff between the security and the economy of the system, based on the real operational condition. However, the computation of RB-SCED is more complicated than that of SCED. We proposed a two level decomposition

algorithm to solve the model. At the outer level, Lagrangian relaxation is applied to relax the risk constraint into the objective function. At the inner level, Benders decomposition is used to solve the LR sub-problem. To further improve the computational efficiency, simultaneous feasibility test (SFT) is applied to generate the shift factors of the overloading circuits. The test result based on ISO-NE bulk system indicates that the RB-SCED has lower risk and lower costs than traditional SCED.

Some interesting directions are open for the future research. First, to encourage the ISOs to replace the current SCED with new RB-SCED, we should demonstrate more benefits the RB-SCED may have. For example, the security assessment study, on both static security and dynamic security, should be enforced to compare the performance of the two different dispatch tools. The assessment results are useful for ISO's decision on adopting the risk-based approach. Second, as a new market clearing tool, the RB-SCED will determine a new LMP mechanism for the market participants. The new LMP should include an additional risk component, which should be investigated further. Finally, it is useful to make a sensitivity analysis of the model between the objective function and the constraint parameters, like K_C and K_R. This would helpful in determine how much cost reduction will be obtained if we transfer to RB-SCED.

Appendix

In Section 2.3.3 of Chapter 2, Fig. 2.4 shows a piece-wise linear function. To simplify the expression, define a bunch of variables

$$a_{1l} = 10 / P_{LTE,l} \tag{4.A.1}$$

$$a_{2l} = (c_1 - 1)/(P_{STE,l} - P_{LTE,l}) \tag{4.A.2}$$

$$a_{3l} = (c_1 P_{LTE,l} - P_{STE,l})/(P_{STE,l} - P_{LTE,l}) \tag{4.A.3}$$

$$a_{4l} = (c_2 - c_1)/(P_{DAL,l} - P_{STE,l}) \tag{4.A.4}$$

$$a_{5l} = (c_2 P_{STE,l} - c_1 P_{DAL,l})/(P_{DAL,l} - P_{STE,l}) \tag{4.A.5}$$

all of which are constants for the *l*th circuit.

The expression of the severity function is then

$$Sev_l^k = \begin{cases} -a_{4l} g_l^k - a_{5l}, & -P_{DAL,l} \le g_l^k < -P_{STE,l} \\ -a_{2l} g_l^k - a_{3l}, & -P_{STE,l} \le g_l^k < -P_{LTE,l} \\ -a_{1l} g_l^k - 9, & -P_{LTE,l} \le g_l^k < -0.9P_{LTE,l} \\ 0, & -0.9P_{LTE,l} \le g_l^k < 0.9P_{LTE,l} \\ a_{1l} g_l^k - 9, & 0.9P_{LTE,l} \le g_l^k < P_{LTE,l} \\ a_{2l} g_l^k - a_{3l}, & P_{LTE,l} \le g_l^k \le P_{STE,l} \\ a_{4l} g_l^k - a_{5l}, & P_{STE,l} \le g_l^k < P_{DAL,l} \end{cases} \tag{4.A.6}$$

In order to involve this piece-wise linear function into an optimization problem, an applicable way is to introduce 7 integer variables, each one of which represents a 0-1 state indicating if P_l is located in the corresponding area. However, this may greatly increase the computational complexity of the original problem. Thus, an applicable way is to transfer the deterministic expression in (4.A.6) into an optimization problem as shown in (4.A.7)-(4.A.14)

$$\text{Min } Sev_l^k \tag{4.A.7}$$

Subject to

$$Sev_l^k \geq -a_{4l} g_l^k - a_{5l} \tag{4.A.8}$$

$$Sev_l^k \geq -a_{2l} g_l^k - a_{3l} \tag{4.A.9}$$

$$Sev_l^k \geq -a_{1l} g_l^k - 9 \tag{4.A.10}$$

$$Sev_l^k \geq 0 \tag{4.A.11}$$

$$Sev_l^k \geq a_{1l} g_l^k - 9 \tag{4.A.12}$$

$$Sev_l^k \geq a_{2l} g_l^k - a_{3l} \tag{4.A.13}$$

$$Sev_l^k \geq a_{4l} g_l^k - a_{5l} \tag{4.A.14}$$

Note that this transformation requires that the function to be convex, which could to satisfied by equation (2.15) and (2.16) in Section 2.3.3, Chapter 2.

CHAPTER 5. RISK AND "N-1" CRITERIA COORDINATION FOR REAL-TIME OPERATIONS

5.1 Introduction

Risk assessment (RA) has been widely used in other industries such as nuclear, aerospace, oil, food, public health, information technology and financial engineering. It is an emerging new approach for economy-security decision-making. Most previous work focuses on Risk-based Security Assessment (RBSA) [32], [67], [109]. Most control center operators continue to use the "N-1" principle alone because it is simple to implement and to understand, and our tools have not evolved to enable observation of its weaknesses. We have developed a risk-based security-constrained optimal power flow (RB-SCOPF) for real-time risk assessment and control. The RB-SCOPF enforces three types of flow-related constraints: normal state deterministic flow limits, contingency state deterministic flow limits (the "N-1" criteria), and contingency state system risk, which depends only on contingency states but not the normal state. Each constraint group is scaled by a single parameter setting allowing tradeoffs between deterministic constraints and system risk. Reference [68] illustrates long-term benefits to economy and to system risk of operating under the RB-SCOPF relative to SCOPF. In this chapter, we show how cost and risk change in RB-SCOPF and SCOPF, using coordination parameters in RB-SCOPF to effect tradeoffs between system risk and N-1 criteria, and thereby characterize conditions under which RB-SCOPF outperforms SCOPF. In Section 5.2, we compare the SCOPF and RB-SCOPF models and describe the method used for the coordination. Section 5.3 presents study results, and Section 5.4 concludes.

5.2 Risk and "N-1" Criteria Coordination

In our work, risk is a probabilistic index designed to reflect the overall stress of the system's operating condition. It extends from the notion of risk as an expected severity, i.e., the summation over possible contingency states of each state's *probability* multiplied by its severity. In previous RBSA work, risk indices are calculated for severity capturing overload, cascading overload, low voltage and voltage instability. Here, we consider only the risk of post-contingency circuit overloading in the RB-SCOPF model, consistent with real-time dispatching in electricity markets. Although the risk calculation is based on thermal loading only, studies have shown that its use enhances post-contingency voltage, angle and cascading performance. The system's overall risk can be expressed as formulation (2.25).

The SCOPF and RB-SCOPF models have been elaborated in previous chapters. To better illustrate the topic in this chapter, we summarize them in Table 5.1, where $f(\underline{P_0})$ is the sum of generation cost, equality constraints $\underline{h}(\underline{P_0}) = \underline{0}$ are power flow balance equations, $\underline{g}_{\min} \leq \underline{g}(\underline{P_0}) \leq \underline{g}_{\max}$ represent constraints on circuit flows and bus injection limits, and $\underline{g}_k(\underline{P_0}) \leq \underline{g}'_{max}$ are N-1 contingency constraints. In the RB-SCOPF model, a parameter K_C ($K_C \geq 1$) is used to scale the emergency thermal limit $\underline{g}'_{max}$, to facilitate tradeoffs between post-contingency overloading, system risk reduction, and improved economic objective. Use of K_C is consistent with the concept of adaptive emergency transmission rates (ATR) [73], which has been applied in the real-time operation of ISO New England. $Risk_{max}$ is the maximum allowed system risk, and K_R ($K_R \leq 1$) is a parameter to control the system's overall risk level.

Table 5.1 Formulation of Security-constrained OPF Models

Model A: SCOPF	Model B: RB-SCOPF
$\text{Min}\{f(\underline{P}_0)\}$ Subject to $\underline{h}(\underline{P}_0)=\underline{0}$ $\underline{g}_{\min} \le \underline{g}(\underline{P}_0) \le \underline{g}_{\max}$ $\underline{g'}_{\min} \le \underline{g}_k(\underline{P}_0) \le \underline{g'}_{\max}, k=1,...,NC$	$\text{Min}\{f(\underline{P}_0)\}$ Subject to $\underline{h}(\underline{P}_0)=\underline{0}$ $\underline{g}_{\min} \le \underline{g}(\underline{P}_0) \le \underline{g}_{\max}$ $K_C\underline{g'}_{\min} \le \underline{g}_k(\underline{P}_0) \le K_C\underline{g'}_{\max}, k=1,...,NC$ $0 \le Risk(\underline{g}_1(P_0),...\underline{g}_{NC}(P_0)) \le K_R Risk_{\max}$

In RB-SCOPF, it is the coordination between K_R and K_C that enables control over tradeoffs between individual circuit risk, system risk, and economy. In what follows, we illustrate the significance of K_R and K_C selections. We accomplish this by studying the dependence of objective function $f(\underline{P}_0)$ with K_R and K_C. The procedure for performing this utilizes sensitivities (shadow prices) of $f(\underline{P}_0)$ to K_R or K_C within an interval of the parameter, bounded by "breakpoints," for which sensitivity analysis is valid. Breakpoints are identified when the shadow price changes significantly, according to the following binary search tree algorithm:

1) Select the K_R range [K_R^{min}, K_R^{max}]. Solve the LP problem at K_R^{min} and K_R^{max}; save the objective functions and the shadow prices of the risk constraint.
2) Solve the LP at $K_R^{(1)} = (K_R^{min} + K_R^{max})/2$. This is used as the parent node of the tree. It divides the tree into 2 parts: the left subtree with K_R range [K_R^{min}, $K_R^{(1)}$] and the right subtreee with [$K_R^{(1)}$, K_R^{max}].
3) If the objective at $K_R^{(1)}$ equals to the objective at K_R^{min} (K_R^{max}), discard the left (right) subtree. Otherwise, let $K_R^{(2)} = (K_R^{min} + K_R^{(1)})/2$ and $(K_R^{(1)} + K_R^{max})/2$, and identify two new parent nodes. Continue the procedure in 1).
4) The algorithm stops if the differences in objectives for all parent and child nodes

are within a predefined vale ε. The breakpoints are the K_R values at the "leaf" nodes.

5.3 Numerical Illustration on IEEE 30-bus system

The IEEE 30 bus system is used to illustrate the Table I models. The system has 30 buses, 41 branches, 6 thermal units and 20 loads. We define 36 N-1 post-contingencies by assuming that every circuit could be lost and contribute to a contingency. The probability of a contingency is proportional to its line impedance, which is assumed to reflect line length.

Table 5.2 illustrates the breakpoints when K_C equals 1.05. Based on the breakpoint information we draw the cost-risk relationship curve. Similarly, we draw the curves for other values of K_C, as shown in Fig. 5.1. This is called the K_R-K_C coordination diagram, which demonstrates the coordination between costs, risk and "N-1 criteria." Two observations regarding this diagram follow. (1) Since SCOPF is a special case of RB-SCOPF, and since we choose $Risk_{max}$ equal to the risk associated with the operating condition computed by the SCOPF, the operating condition for SCOPF corresponds to the point (K_R, K_C) = (1, 1) in the diagram, a useful reference point. (2) The problem may become infeasible if we decrease K_R. This is shown in Fig. 5.1, as the region where $K_R \leq$ 0.13 when K_C = 1. The 3-D plot of K_C-K_R coordination is shown in Fig. 5.2.

Table 5.2 "Breakpoints" When Kc is 1.05

K_R	1	0.82	0.46	0.28	0.12	0.025	0.006
$\lambda(\times 10^4)$	0.4	10.3	49.1	58.6	102.5	139.3	145.2

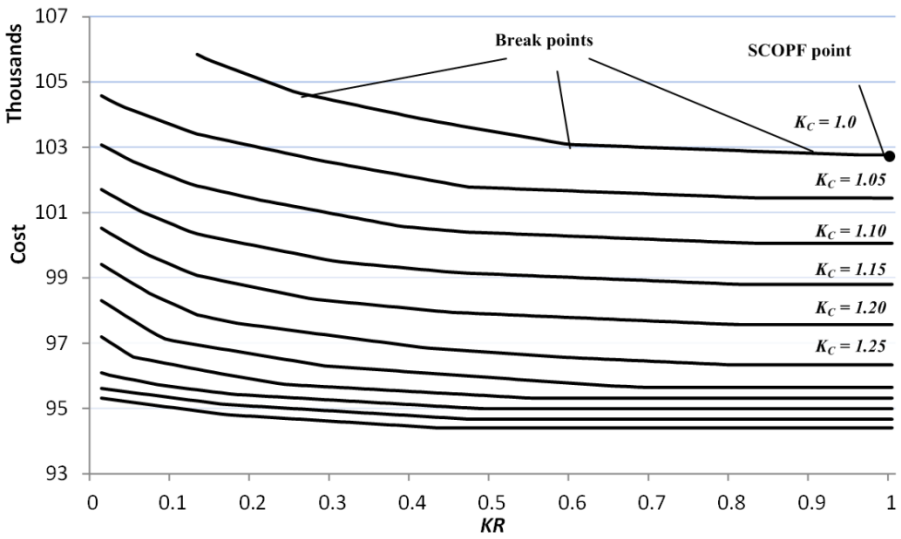

Fig. 5.1. The change of costs with system risk for fixed K_C (K_C equals to 1.00, 1.05, 1.10, 1.15, 1.20, 1.25, 1.30, 1.35, 1.40, 1.45, and 1.50, respectively, from top line to bottom line)

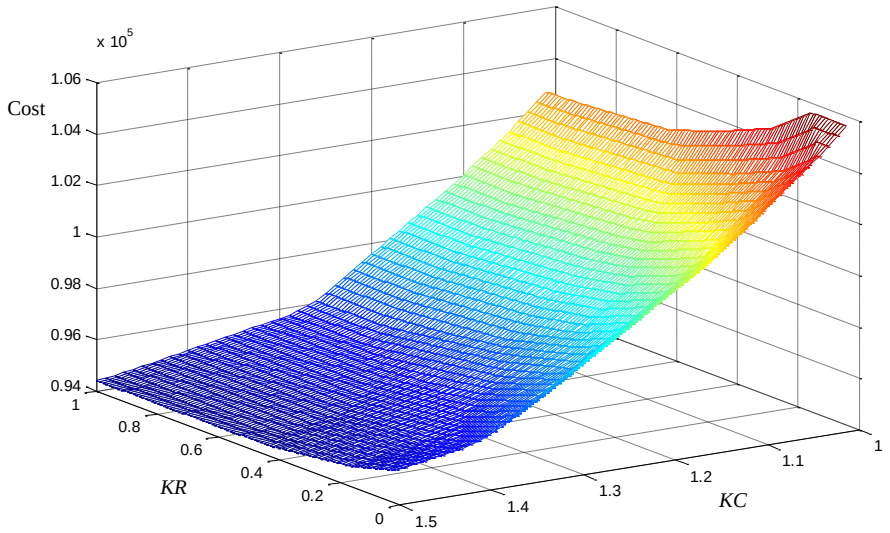

Fig. 5.2 3-D Plot of K_C-K_R coordination

It can be seen in Fig. 5.1 that the traditional SCOPF does not determine the best operating condition — neither is it the point with lowest cost nor is it the point with lowest risk. There

are points available in the diagram that are better than the point determined by SCOPF in terms of system risk and economics. By choosing proper KR and KC according to real-time conditions, the system may gain significant economic benefits while improving the security level, effects that will bear considerable benefit over time. For example, one may choose the "high security" operating point, say (KR, KC) = (0.6, 1), under conditions when high system security is required, such as heavy load and severe weather. Similarly, one may choose a "high economy" operating point, say (KR, KC) = (0.5, 1.2), if the system stress is low. Although a certain number and level of post-contingency overloading can be allowed under many different types of conditions, the use of "high economy" mode is most attractive under two specific types of conditions: 1) when post-contingency overloads occur only for what are perceived to be unlikely contingencies; 2) when corrective actions are available to rapidly reduce post-contingency flow on an overloaded circuit. The degree of allowable post-contingency overloading can be controlled through choice of KC, which can be identified based on the concept of ATR in three ways: 1) choose KC as the ATRs computed at selected flowgates; 2) choose KC as minimum ATR of all lines; 3) use different KC for several different line groups, where the grouping is done geographically and/or by voltage levels.

5.4 Conclusion

Three contributions are made in this chapter. First, it extends the traditional deterministic SCOPF to RB-SCOPF and provides a visualization diagram, called K_R-K_C coordination diagram, for decision-support that enables efficient security-economy tradeoff analysis. Second, it proposes an efficient algorithm to find "breakpoints" in the K_R-K_C coordination

diagram. Third, it shows how system risk and post-contingency overload levels on individual circuits can be coordinated to enhance both economy and security of a power system in real-time operations, and it identifies types of conditions for which high-security and high-economy modes would be best suited. Use of RB-SCOPF results in improved long-term power system performance, for both economics and security; this chapter provides additional insight on its use to facilitate its eventual adoption by industry.

CHAPTER 6. RISK-BASED LOCATIONAL MARGINAL PRICING AND CONGESTION MANAGEMENT

6.1 Introduction

The Locational Marginal Pricing (LMP) is a market-pricing approach used to determine optimal generation unit dispatches as well as locational energy and transmission congestion prices. It is defined as the cost of supplying an increment of load at the system or location. The LMP mechanism has been implemented in large number of electricity markets worldwide, such as ISO-New England, New York ISO, PJM, California ISO, Midwest ISO, New Zealand, etc. [110]-[114].

Traditionally, the LMP is derived from security-constrained economic dispatch model. The LMP formulation can be decomposed into three components: marginal energy price, marginal loss price, and marginal congestion price [115]-[118]. In reference [119], a risk-based security-constrained economic dispatch (RB-SCED) model has been developed for the purpose of quantifying/controlling the system's overall risk level. Compare to SCED, RB-SCED enforces three types of flow-related constraints: normal state deterministic flow limits, contingency state deterministic flow limits (the "N-1" criteria) — both appears in SCED, and contingency state system risk — appears in RB-SCED only. Thus, the LMP derived from RB-SCED should contain an additional component called marginal risk price, and the traditional LMP is extended to risk-based LMP (RLMP). The risk component is a price signal to reflect the system's overall security level. In this paper, we will examine the features of RLMP and compare its differences with LMP.

In the current electricity market, all congestion management systems are using linear programming (LP) techniques in market clearing process [79]. This is achieved by DC idealization of power flow equations. Thus, the DCOPF model is used in this paper. In previous literatures, the calculation of loss component in DCOPF-based LMP remains a challenging task [79], [120]. To avoid the complicated issue related with loss modeling and emphasize the main point to be presented, the loss price is ignored in this paper.

The rest of this chapter is organized as follows. Section 6.2 describes the traditional LMP model. Section 6.3 presents the definition and formulation of risk-based LMP. Section 6.4 discusses the features of RLMP through a six-bus system. Section 6.5 concludes.

6.2 Traditional LMP model

Traditionally, LMPs are calculated based on the security constrained economic dispatch (SCED) in day-ahead and real-time electricity market. The objective of SCED is to maximize social surplus while meeting the system load balance operational constraints. The so-called "N-1" criteria, which require no transmission constraints violation under all pre-defined contingencies, must be satisfied in SCED model. In most cases of real-time market there is absence of price-sensitive demand, under which the maximizing of social surplus is equivalent to minimizing production costs. Without loss of generality, we will use this form of objective function in the model. The SCED is an OPF problem considering security transmission constraints at both normal and post-contingency states and, under the above assumptions, can be formulated as follows

$$\text{Min} \quad \sum_{i=1}^{NG} c_i \times P_i \tag{6.1}$$

Subject to:

$$\sum_{i=1}^{NG} P_i - \sum_{i=1}^{NG} D_i - Loss = 0, \tag{6.2}$$

$$\sum_{i=1}^{NG} GSF_{l-i}^{0}(P_i - D_i) \le Limit_l^0, \text{ for } l \in \{all\ lines\}, \tag{6.3}$$

$$P_i^{\min} \le P_i \le P_i^{\max}, \tag{6.4}$$

$$h_l^k = \sum_{i=1}^{NG} GSF_{l-i}^{k}(P_i - D_i), \quad \text{for } l \in \{all\ lines\}, k \in \{all\ contingencies\}, \tag{6.5}$$

$$h_l^k \le Limit_l^k, \text{ for } l \in \{all\ lines\}, k \in \{all\ contingencies\}. \tag{6.6}$$

where equation (6.1) is the objective function, (6.2) is the power balance constraint, (6.3) is the transmission limit at normal state, (6.4) is the generation output limits, (6.5) is the circuit flows at post-contingency states, and (6.6) is the post-contingency flow limits. All the parameters in (6.1) – (6.6) and in the rest of this chapter are defined in the Appendix of this chapter. Define λ_1, $\mu_{1l}^0 \ge 0$, $\gamma_{1i}^{\max} \ge 0$ and $\gamma_{1i}^{\min} \ge 0$, η_{1l}^k, $\mu_{1l}^k \ge 0$ be the Lagrangian multipliers of constraints (6.2), (6.3), (6.4), (6.5), and (6.6), respectively. The LMP is defined as a change in production cost due to an increment of load at the location. By this definition, the LMP at bus *i* can be obtain as the partial derivative of the Lagrangian of (6.1)-(6.6)

$$\begin{aligned}\psi_1 = &\sum_{i=1}^{NG} c_i \times P_i - \lambda_1 (\sum_{i=1}^{NG} (P_i - D_i) - Loss) \\ &+ \sum_{l=1}^{NL} \mu_{1l}^0 [\sum_{i=1}^{NG} GSF_{l-i}^0 (P_i - D_i) - Limit_l^0] \\ &+ \sum_{i=1}^{NG} \gamma_{1i}^{\max} (P_i - P_i^{\max}) + \sum_{i=1}^{NG} \gamma_{1i}^{\min} (-P_i + P_i^{\min}) \\ &- \sum_{k=1}^{NC} \sum_{l=1}^{NL} \eta_{1l}^k [h_l^k - \sum_{i=1}^{NG} GSF_{l-i}^k (P_i - D_i)] \\ &+ \sum_{k=1}^{NC} \sum_{l=1}^{NL} \mu_{1l}^k (h_l^k - Limit_l^k)\end{aligned} \tag{6.7}$$

At the optimal point, the Karush–Kuhn–Tucker (KKT) conditions must be satisfied, as shown in (6.8)-(6.9)

$$\frac{\partial \psi_1}{\partial P_i} = c_i - \lambda_1 + \frac{\partial Loss}{\partial P_i} \lambda_1 + \sum_{l=1}^{NL} \mu_{1l}^0 GSF_{l-i}^0 + \gamma_{1i}^{\max} - \gamma_{1i}^{\min} + \sum_{k=1}^{NC} \sum_{l=1}^{NL} \eta_{1l}^k GSF_{l-i}^k = 0, \forall i \tag{6.8}$$

$$\frac{\partial \psi_1}{\partial h_l^k} = -\eta_{1l}^k + \mu_{1l}^k = 0, \forall k, l \tag{6.9}$$

Then the LMP at bus i can be calculated in (6.10), by taking into account that $(\partial Loss / \partial D_i) = -(\partial Loss / \partial P_i)$ and the equality in (6.9):

$$LMP_i = \frac{\partial \psi_1}{\partial D_i} = \lambda_1 - \frac{\partial Loss}{\partial P_i} \lambda_1 - (\sum_{l=1}^{NL} \mu_{1l}^0 GSF_{l-i}^0 + \sum_{k=1}^{NC} \sum_{l=1}^{NL} \mu_{1l}^k GSF_{l-i}^k) \tag{6.10}$$

From (6.10), the LMP can be decomposed into three components: marginal energy price, marginal loss price and marginal congestion price, where

$$LMP_i^{Energy} = \lambda_1 \tag{6.11}$$

$$LMP_i^{Loss} = -\frac{\partial Loss}{\partial P_i} \lambda_1 \tag{6.12}$$

$$LMP_i^{Congestion} = -(\sum_{l=1}^{NL} \mu_{1l}^0 GSF_{l-i}^0 + \sum_{k=1}^{NC}\sum_{l=1}^{NL} \mu_{1l}^k GSF_{l-i}^k) \quad (6.13)$$

The actual solution of LMP calculation based on the above SCED model, especially the LMP loss modeling, remains a challenging task [115]-[117]. In the discussion of this work, the loss price is ignored to avoid complicated issues related to loss calculation, such as the choice of loss distribution factors and the modeling of distributed-slack reference [126]-[127].

6.3 Definition and Calculation of Risk-based LMP

6.3.1 Modeling of Overload Risk

In our work, risk is a probabilistic index designed to reflect the overall stress of the system's operating condition. It extends from the notion of risk as an expected severity, i.e., the summation over possible contingency states of each state's *probability* multiplied by its severity. The system's overall risk can be expressed as formulation (2.25).

As described in previous chapters, the overload severity of a post-contingency circuit is proportional to the circuit's power flow as a percentage of the circuit's rating (*PR*): the higher the *PR* is, the more severe the loading condition is. The severity function is the same as in section 2.3.3. To simplify the expression, only the positive part of the severity function is adopted here, as shown in Fig. 6.1.

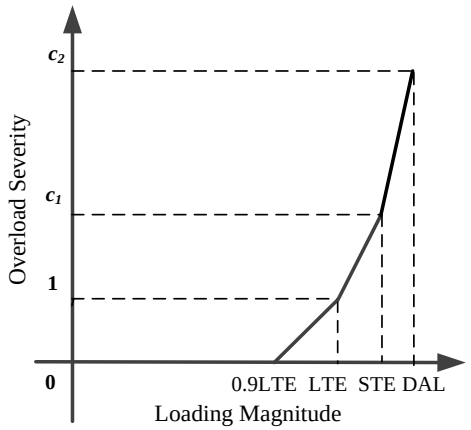

Fig. 6.1. Overload severity function

The expression of piece-wise linear function in Fig. 6.1 is

$$Sev_l^k = \begin{cases} 0, & 0 \le h_l^k < 0.9P_{LTE,l} \\ a_{1l}h_l^k - 9, & 0.9P_{LTE,l} \le h_l^k < P_{LTE,l} \\ a_{2l}h_l^k - a_{3l}, & P_{LTE,l} \le h_l^k \le P_{STE,l} \\ a_{4l}h_l^k - a_{5l}, & P_{STE,l} \le h_l^k < P_{DAL,l} \end{cases} \tag{6.14}$$

where a_{1l}, a_{2l}, a_{3l}, a_{4l} and a_{5l} are defined in chapter 2. In order to involve this piece-wise linear function into an optimization problem, transfer the deterministic formulation (6.14) into optimization form (6.15)-(6.19)

$$\text{Min } Sev_l^k \tag{6.15}$$

Subject to

$$Sev_l^k \ge 0, \tag{6.16}$$

$$Sev_l^k \ge a_{1l}h_l^k - 9, \tag{6.17}$$

$$Sev_l^k \ge a_{2l}h_l^k - a_{3l}, \tag{6.18}$$

$$Sev_l^k \ge a_{4l}h_l^k - a_{5l}. \tag{6.19}$$

6.3.2 Risk-based LMP decomposition

The RB-SCED can be formulated as

$$\text{Min} \quad \sum_{i=1}^{NG} c_i \times P_i \tag{6.20}$$

Subject to:

$$\sum_{i=1}^{NG} P_i - \sum_{i=1}^{NG} D_i - Loss = 0, \tag{6.21}$$

$$\sum_{i=1}^{NG} GSF_{l-i}^{0}(P_i - D_i) \le Limit_l^0, \ for\ l \in \{all\ lines\}, \tag{6.22}$$

$$P_i^{\min} \le P_i \le P_i^{\max}, \tag{6.23}$$

$$h_l^k = \sum_{i=1}^{NG} GSF_{l-i}^{k}(P_i - D_i), \quad for\ l \in \{all\ lines\}, k \in \{all\ contingencies\}, \tag{6.24}$$

$$h_l^k \le K_C \times Limit_l^k, \ for\ l \in \{all\ lines\}, k \in \{all\ contingencies\}, \tag{6.25}$$

$$Sev_l^k \ge 0, \tag{6.26}$$

$$Sev_l^k \ge a_{1l} h_l^k - 9, \tag{6.27}$$

$$Sev_l^k \ge a_{2l} h_l^k - a_{3l}, \tag{6.28}$$

$$Sev_l^k \ge a_{4l} h_l^k - a_{5l}, \tag{6.29}$$

$$\sum_{k=1}^{NC} Pr_k \sum_{l=1}^{NL} Sev_l^k \le K_R \times Risk_{max} \tag{6.30}$$

where equation (6.20) - (6.24) are the same with the ones in section 6.2, a parameter K_C is multiplied to the transmission limit in (6.25), (6.26)-(6.30) are risk constraints corresponding to individual circuits, and (6.30) is the risk constraint related to the whole

system. Define λ_2, $\mu_{2l}^0 \geq 0$, $\gamma_{2i}^{\max} \geq 0$ and $\gamma_{2i}^{\min} \geq 0$, η_{2l}^k, $\mu_{2l}^k \geq 0$, $\delta_{l,1}^k \geq 0$, $\delta_{l,2}^k \geq 0$, $\delta_{l,3}^k \geq 0$, $\delta_{l,4}^k \geq 0$, and $\tau \geq 0$ be the Lagrangian multipliers of constraints (6.21) - (6.30), respectively.

The risk-based LMP, according to the RB-SCED model, can be calculated as the partial derivative of the Lagrangian of (6.20)-(6.30)

$$\begin{aligned}
\psi_2 = & \sum_{i=1}^{NG} c_i \times P_i - \lambda_2 (\sum_{i=1}^{NG} (P_i - D_i) - Loss) \\
& + \sum_{l=1}^{NL} \mu_{2l}^0 [\sum_{i=1}^{NG} GSF_{l-i}^0 (P_i - D_i) - Limit_l^0] \\
& + \sum_{i=1}^{NG} \gamma_{2i}^{\max} (P_i - P_i^{\max}) + \sum_{i=1}^{NG} \gamma_{2i}^{\min} (-P_i + P_i^{\min}) \\
& - \sum_{k=1}^{NC} \sum_{l=1}^{NL} \eta_{2l}^k [h_l^k - \sum_{i=1}^{NG} GSF_{l-i}^k (P_i - D_i)] \\
& + \sum_{k=1}^{NC} \sum_{l=1}^{NL} \mu_{2l}^k (h_l^k - K_C \times Limit_l^k) - \sum_{k=1}^{NC} \sum_{l=1}^{NL} \delta_{l,1}^k Sev_l^k \\
& - \sum_{k=1}^{NC} \sum_{l=1}^{NL} \delta_{l,2}^k (Sev_l^k - a_{1l} h_l^k + 9) - \sum_{k=1}^{NC} \sum_{l=1}^{NL} \delta_{l,3}^k (Sev_l^k - a_{2l} h_l^k + a_{3l}) \\
& - \sum_{k=1}^{NC} \sum_{l=1}^{NL} \delta_{l,4}^k (Sev_l^k - a_{4l} h_l^k + a_{5l}) \\
& + \tau (\sum_{k=1}^{NC} Pr_k \sum_{l=1}^{NL} Sev_l^k - K_R \times Risk_{max})
\end{aligned} \tag{6.31}$$

At the optimal point, the KKT conditions must be satisfied, as shown in (6.32)-(6.33)

$$\frac{\partial \psi_2}{\partial h_l^k} = -\eta_{2l}^k + \mu_{2l}^k + \delta_{l,2}^k a_{1l} + \delta_{l,3}^k a_{2l} + \delta_{l,4}^k a_{4l} = 0, \forall k, l \tag{6.32}$$

$$\frac{\partial \psi_2}{\partial Sev_l^k} = -\delta_{l,1}^k - \delta_{l,2}^k - \delta_{l,3}^k - \delta_{l,4}^k + \tau \cdot Pr_k = 0, \ \forall k, l \tag{6.33}$$

The risk-based LMP at bus *i* can be calculated as:

$$\begin{aligned}
RLMP_i &= \frac{\partial \psi_2}{\partial D_i} \\
&= \lambda_2 - \frac{\partial Loss}{\partial P_i} \lambda_2 - (\sum_{l=1}^{NL} \mu_{2l}^0 GSF_{l-i}^0 + \sum_{k=1}^{NC} \sum_{l=1}^{NL} \eta_{2l}^k GSF_{l-i}^k)
\end{aligned} \tag{6.34}$$

At optimal solution, the values of post-contingency flows h_l^k are known. If no flows are at the corner points, i.e., points (0.9LTE, 0), (LTE, 1), and (STE, c_1) in Fig. 6.1, then only one of the four constraints is effective in (6.27)-(6.30), depending on what interval the optimal value of $(h_l^k)^*$ is within. Therefore, only one of the Lagrangian multipliers $\delta_{l,i}^k$ (i = 1, 2, 3, 4) will be non-zero. Define four segments in Fig. 6.1: segment 1 be (0, 0.9$P_{LTE,l}$), segment 2 be (0.9$P_{LTE,l}$, $P_{LTE,l}$), segment 3 be ($P_{LTE,l}$, $P_{STE,l}$), and segment 4 be ($P_{STE,l}$, $P_{DAL,l}$). Then, from equation (6.33) we have

$$\delta_{l,i}^k = \begin{cases} \tau Pr_k, \ if \ (h_l^k)^* \ in \ the \ i\text{th} \ segment \\ 0, \ otherwise \end{cases}, i = 1,2,3,4. \tag{6.35}$$

Define parameter

$$r_l^k = \begin{cases} 0, if \ (h_l^k)^* \ in \ segment \ 1 \\ a_{1l}, if \ (h_l^k)^* \ in \ segment \ 2 \\ a_{2l}, if \ (h_l^k)^* \ in \ segment \ 3 \\ a_{4l}, if \ (h_l^k)^* \ in \ segment \ 4 \end{cases} \tag{6.36}$$

Substitute (6.35) and (6.36) into (6.32), we have

$$\eta_{2l}^k = \mu_{2l}^k + r_l^k Pr_k \tau \tag{6.37}$$

Substitute (6.37) into (6.34), we obtain the expression of risk-based LMP (RLMP)

$$\begin{aligned} RLMP_i = \lambda_2 - \frac{\partial Loss}{\partial P_i}\lambda_2 - (\sum_{l=1}^{NL} \mu_{2l}^0 GSF_{l-i}^0 + \sum_{k=1}^{NC}\sum_{l=1}^{NL} \mu_{2l}^k GSF_{l-i}^k) \\ - \sum_{k=1}^{NC}\sum_{l=1}^{NL} r_l^k Pr_k GSF_{l-i}^k \tau \end{aligned} \tag{6.38}$$

From (6.38), the Risk-based LMP can be decomposed into four components: marginal energy price, marginal loss price, marginal congestion price and marginal risk price,

$$RLMP_i = RLMP_i^{Energy} + RLMP_i^{Loss} + RLMP_i^{Congestion} + RLMP_i^{Risk} \tag{6.39}$$

$$RLMP_i^{Energy} = \lambda_2 \tag{6.40}$$

$$RLMP_i^{Loss} = -\frac{\partial Loss}{\partial P_i}\lambda_2 \tag{6.41}$$

$$RLMP_i^{Congestion} = -(\sum_{l=1}^{NL}\mu_{2l}^0 GSF_{l-i}^0 + \sum_{k=1}^{NC}\sum_{l=1}^{NL}\mu_{2l}^k GSF_{l-i}^k) \tag{6.42}$$

$$RLMP_i^{Risk}\Big|_{S_1} = -\sum_{k=1}^{NC}\sum_{l=1}^{NL} r_l^k Pr_k GSF_{l-i}^k \tau \tag{6.43}$$

Equation (6.38) provides a new formulation for LMP calculations, where the energy, loss, congestion, and risk components are shown in equations (6.40)-(6.42), respectively. In what follows we will see that the forms of the energy, loss, and congestion components will remain the same no matter the post-contingency flow h_l^k is at corner points or not, but the form of the risk component will change. Thus, we use a subscript S_1, which has been defined in the nomenclature, in (6.43) to demonstrate the risk component at set S_1.

If the optimal value of post-contingency flow $(h_l^k)^*$ is on one of the corner points, two of the four constraints will be binding in (6.27)-(6.30). The KKT conditions in (6.32) and (6.33), and the original form of RLMP in (6.34) will remain the same, but the form of RLMP components will change. If $(h_l^k)^*$ is on corner point (0.9LTE, 0), both constraint (6.27) and (6.28) are binding, and constraints (6.29) and (6.30) are unbinding. Thus $\delta_{l,1}^k$ and $\delta_{l,2}^k$ are nonzero, while $\delta_{l,3}^k$ and $\delta_{l,4}^k$ equal to zero. From (6.32) and (6.33), we have

$$\eta_{2l}^k = \mu_{2l}^k + \delta_{l,2}^k a_{1l} \tag{6.44}$$

Substitute (6.44) into (6.34), we obtain the form of RLMP at corner point (0.9LTE, 0). The energy, loss, and congestion components are the same as in (6.40)-(6.42), except the

risk component, whose form has to be changed as in (6.45):

$$RLMP_i^{Risk}\Big|_{S_2} = -a_{1l} GSF_{l-i}^k \delta_{l,2}^k, \quad if\ (h_l^k)^*\ at\ point\ (0.9LTE, 0). \tag{6.45}$$

Similarly, if $(h_l^k)^*$ is on corner point (LTE, 1), the risk component is shown in (6.46):

$$RLMP_i^{Risk}\Big|_{S_3} = -[\tau Pr_k a_{2l} + \delta_{l,2}^k (a_{1l} - a_{2l})] GSF_{l-i}^k, \quad if\ (h_l^k)^*\ at\ point\ (LTE, 1). \tag{6.46}$$

If $(h_l^k)^*$ is on corner point (STE, c_1), the risk component is shown in (6.47):

$$RLMP_i^{Risk}\Big|_{S_4} == -[\tau Pr_k a_{4l} + \delta_{l,3}^k (a_{2l} - a_{4l})] GSF_{l-i}^k, \quad if\ (h_l^k)^*\ at\ point (STE, c_1). \tag{6.47}$$

Then the formulation of RLMP is

$$RLMP_i^{Risk} = RLMP_i^{Risk}\Big|_{S_1} + RLMP_i^{Risk}\Big|_{S_2} + RLMP_i^{Risk}\Big|_{S_3} + RLMP_i^{Risk}\Big|_{S_4} \tag{6.48}$$

Compared with traditional LMP, the Risk-based LMP has two changes: 1) Since a multiplier $K_C \geq 1$ is multiplied to the post-contingency transmission limit, the Lagrangian multipliers associated with these constraints are changed. Thus the congestion part of risk-based LMP is different. This is shown in (6.13) and (6.42), where μ_{2l}^k is different with μ_{1l}^k. 2) An additional component, risk, is added to the traditional LMP. The risk component in (6.43), (6.45)-(6.47) is a price signal to reflect the system's overall security level. In the next section, we will discuss more features about the risk component, and examine how risk-based LMP will change the social surplus and market benefits.

6.4 Features of Risk-based LMP

In this section, a six-bus example [57] is presented to demonstrate the features of risk-based LMP. The single line system diagram is shown in Fig. 6.2. There are 6 buses, 11 transmission lines, 3 generators, and 3 loads in the system. All the line impedances are shown in the diagram with the per unit values. The loads at buses D, E, and F are 70, 70, and 160 MW. The original generation cost curves at bus A, B, and C are

$$Cost(P_A) = 5.33\times10^{-3}P_A^2 + 11.669\times P_A + 213 \quad (6.49)$$

$$Cost(P_B) = 8.89\times10^{-3}P_B^2 + 10.333\times P_B + 200 \quad (6.50)$$

$$Cost(P_C) = 7.41\times10^{-3}P_C^2 + 10.833\times P_C + 240 \quad (6.51)$$

respectively. In order to adapt to the linear programming procedure, we equally divide the generation output interval [P_{min}, P_{max}] into 3 parts, and use 3-segment linear curves to approximate the quadratic cost curve. The economic maximum (economic minimum) of generator A, B and C is 200 MW (50 MW), 150 MW (37.5 MW), and 180 MW (45 MW), respectively. The load at bus D, E, and F is 70 MW, 70 MW, and 160 MW, respectively. Line B-D and C-E are the limiting elements, with LTE, SET and DAL values shown in Table 6.1. All the other lines are assumed to have unlimited transmission capacities. Parameter c_1 and c_2 in Fig. 6.1 is set to 3 and 10, respectively. Eleven "N-1" post-contingencies are defined in this example, i.e., each transmission line can be lost thus lead to a contingency. The probabilities of those contingencies are assumed to be identically 0.002 for the purpose of focusing on the effects of severity function only. In reality, the probability

of post-contingencies depends on the line length, voltage level, and loading and weather conditions, thus more accurate risk values can be obtained if we use more complicated probability models.

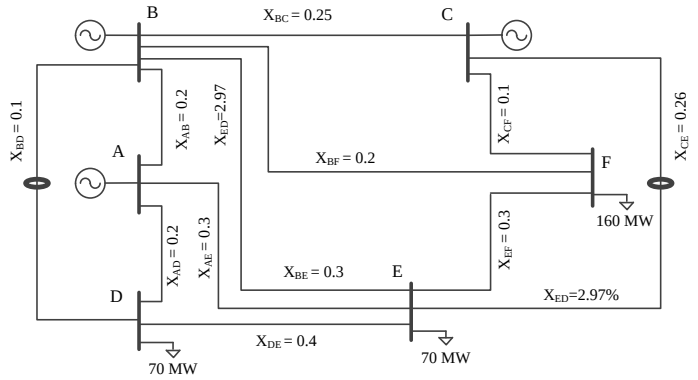

Fig. 6.2. Six-bus system diagram

Table 6.1 Thermal Limits on Line B-D and C-E

	LTE (MW)	STE (MW)	DAL (MW)
Line B-D	58	66	85
Line C-E	31	35	46

The calculation of loss component remains a challenging task in DCOPF-based LMP. In the following discussions, we ignore the loss price to avoid complicated issues related with marginal loss modeling and emphasis the main point to be presented. Hence, in the above SCED and RB-SCED models, the *Loss* is assumed to be equals to 0. The shift factors are calculated with bus A as the slack reference. Since we assume the system loss is 0, the result does not depend on the choice of reference bus.

The coordination of K_R and K_C can leads to different operation conditions. Similar to previous chapters, three operation models are defined for RB-SCED:

- High Security Mode (HSM), for all operation conditions when $K_R \leq 1$ and $K_C = 1$.

- Economy-Security Mode (ESM), for all operation conditions when $K_R \leq 1$ and K_C be slightly larger than 1, e.g., K_C =1.05.
- High Economy Mode (HEM), for all operation conditions when $K_R \leq 1$ and K_C be obviously larger than 1, e.g., K_C =1.20.

Table 6.2 shows the dispatch results for SCED, HSM (K_C =1, K_R = 0.9), ESM (K_C =1.05, K_R = 0.9) and HEM (K_C =1.2, K_R = 1). The system risk levels for them are 0,012, 0.0108, 0.0108, and 0.012, respectively. The operation costs for them are $4376.52, $4381.63, $4371.03, and $4352.09, respectively. The HSM do not allow post-contingency violations and has lower risk level, thus has higher security nevertheless higher cost than SCED. The ESM and HEM have lower (or at most equal) risk and lower costs than SCED. From (6.49) – (6.51) there exists relations between generation costs: Generation A > Generation C > Generation B, as shown in Fig. 6.3. The ESM and HEM are prompted to dispatch more MWs on cheaper units. The post-contingency flows of SCED, HSM, ESM and HEM are shown in Table 6.3 - Table 6.6.

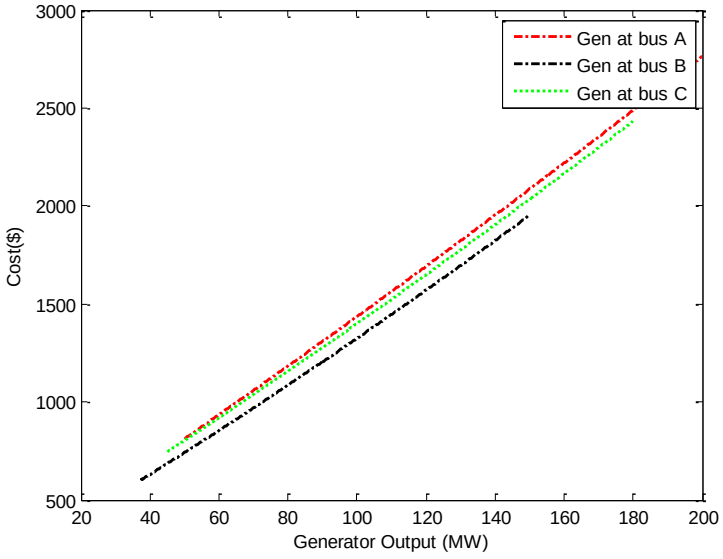

Fig. 6.3. Generation costs at bus A, B, and C

Table 6.2 Generation Outputs at Different Operation Conditions

	SCED	HSM (K_C =1.0; K_R =0.9)	ESM (K_C =1.05; K_R =0.9)	HEM (K_C =1.2; K_R =1)
Gen. at bus A (MW)	192.90	195.80	191.31	180.46
Gen. at bus B (MW)	66.00	65.64	71.56	82.41
Gen. at bus C (MW)	48.97	46.43	45.00	45.00

Table 6.3 Post-contingency Flows for SCED

Conting. No.	**Outage Line**	**Post-conting. flow at line B-F (MW)**	**Post-conting. flow at line C-E (MW)**
Conting. #1	A-B	-19.39	-5.90
Conting. #2	A-D	66.00	-1.45
Conting. #3	A-E	5.00	13.18
Conting. #4	B-C	18.97	-7.88
Conting. #5	B-D	0.00	3.16
Conting. #6	B-E	21.32	6.32
Conting. #7	B-F	26.48	-10.24
Conting. #8	C-E	15.40	0.00
Conting. #9	C-F	13.85	35.00
Conting. #10	D-E	7.38	3.27
Conting. #11	E-F	10.94	-8.77

Table 6.4 Post-contingency Flows for HSM (KC=1; KR=0.9)

Conting. No.	**Outage Line**	**Post-conting. flow at line B-F (MW)**	**Post-conting. flow at line C-E (MW)**
Conting. #1	A-B	-20.76	-6.80
Conting. #2	A-D	66.00	-2.24
Conting. #3	A-E	4.19	12.59
Conting. #4	B-C	18.45	-8.95
Conting. #5	B-D	0.00	2.31
Conting. #6	B-E	20.68	5.58
Conting. #7	B-F	25.92	-11.10
Conting. #8	C-E	14.60	0.00
Conting. #9	C-F	13.21	33.80
Conting. #10	D-E	6.59	2.55
Conting. #11	E-F	10.21	-9.67

Table 6.5 Post-contingency Flows for ESM (KC=1.05; KR=0.9)

Conting. No.	**Outage Line**	**Post-conting. flow at line B-F (MW)**	**Post-conting. flow at line C-E (MW)**
Conting. #1	A-B	-17.92	-6.59
Conting. #2	A-D	66.43	-2.23
Conting. #3	A-E	5.87	12.38
Conting. #4	B-C	20.11	-9.30
Conting. #5	B-D	0.00	2.48
Conting. #6	B-E	22.40	5.69
Conting. #7	B-F	27.58	-11.27
Conting. #8	C-E	16.13	0.00
Conting. #9	C-F	14.76	33.48
Conting. #10	D-E	8.06	2.52
Conting. #11	E-F	11.78	-9.65

Table 6.6 Post-contingency Flows for HEM (KC=1.2; KR=1)

Conting. No.	**Outage Line**	**Post-conting. flow at line B-F (MW)**	**Post-conting. flow at line C-E (MW)**
Conting. #1	A-B	-11.53	-5.31
Conting. #2	A-D	67.20	-1.43
Conting. #3	A-E	9.65	12.58
Conting. #4	B-C	23.59	-8.85
Conting. #5	B-D	0.00	3.64
Conting. #6	B-E	26.10	6.65
Conting. #7	B-F	31.08	-10.72
Conting. #8	C-E	19.64	0.00
Conting. #9	C-F	18.14	34.12
Conting. #10	D-E	11.46	3.19
Conting. #11	E-F	15.27	-8.71

In what follows, we will discuss the features of RLMP according to three questions based on the dispatch result of six-bus system.

Question 1: What's the meaning of the risk component?

Traditional LMPs are determined from the result of SCED. LMP may differ at different locations due to transmission congestion and system losses. The RLMPs are determined from risk-based SCED, and differ at different locations due to transmission

congestion, system losses, and risk limiting. In RLMP, the risk component is a price signal to reflect the system's overall security level.

Table 6.7 compares the LMPs for SCED and RLMPs for various cases of RB-SCED based on the six-bus system. In SCED model, high LMPs are located at bus D ($34.58) and bus E ($16.95). This is because they are connected to congestion lines B-D and C-E and cheap energy cannot be delivered to them when there is 1MW load increase at them due to congestion. This can be verified from the LMP congestion component, where Bus D and E have nontrivial positive values. The LMP energy component equals to $13.53, which is marginal cost at reference bus. LMP congestion component is negative at bus B and C. This means if we transfer 1 MW power from them to the reference bus, counter flows will be generated at line B-D and C-E, thus relieve the congestions on them.

In the HSM with K_C =1 and K_R =0.9, the RLMPs at bus D and E are smaller than LMPs. Since no post-contingency flow is allowed to be greater than STE, there may still be congestions on line B-D and C-E, and the RLMP congestion component is nonzero at non-reference bus. However, the RLMP congestion components are less than the LMP congestion components at bus D and E, and greater at bus B and C. This is because the RB-SCED model enforces constraints on highly-loaded lines and the post-contingency flows on non-highly loaded lines may decrease. The RLMP risk component, as shown in Table 6.7, is used to price the system risk of moving energy from one bus to the reference bus.

In ESM and HEM of Table 6.7, the congestion component equals to zero at all buses since we allow the post-contingency flows being larger than STE ($K_C > 1$), degree of the flow violation is controlled by the risk constraint. Compared to the LMPs, RLMP values at each bus are closer and without large deviations between buses.

Table 6.7 Results of LMP and RLMP

Model	Bus Name	(R)LMP	(R)LMP Energy	(R)LMP Loss	(R)LMP Congestion	RLMP Risk
SCED	A	13.53	13.53	0	0.00	-
	B	11.33	13.53	0	-2.20	-
	C	11.83	13.53	0	-1.70	-
	D	34.58	13.53	0	21.04	-
	E	16.95	13.53	0	3.41	-
	F	13.73	13.53	0	0.20	-
HSM (K_C =1; K_R =0.9)	A	13.53	13.53	0	0.00	0.00
	B	12.11	13.53	0	-1.80	0.37
	C	14.99	13.53	0	0.26	1.19
	D	33.13	13.53	0	19.48	0.11
	E	15.51	13.53	0	2.70	-0.73
	F	14.30	13.53	0	0.14	0.62
ESM (K_C=1.05; K_R =0.9)	A	13.53	13.53	0	0	0.00
	B	14.66	13.53	0	0	1.13
	C	17.13	13.53	0	0	3.60
	D	13.87	13.53	0	0	0.33
	E	11.35	13.53	0	0	-2.19
	F	15.41	13.53	0	0	1.87
HEM (K_C =1.2; K_R =1)	A	13.53	13.53	0	0	0.00
	B	14.32	13.53	0	0	0.79
	C	16.04	13.53	0	0	2.51
	D	13.77	13.53	0	0	0.23
	E	12.01	13.53	0	0	-1.53
	F	14.84	13.53	0	0	1.30

Question 2: Which generators/loads would likely see higher (or lower) prices?

Risk is neither good nor bad but is a direct measure of the extent to which there are differences in the cost of generation that cannot be equalized because of system risk requirements. The risk component in RLMP is used to price the overall risk of system. Generally, load pays risk price and generation is paid risk price. From Table 6.7, marginal risk prices can be positive or negative with respect to the reference bus. A positive marginal risk price means increasing the load at a bus would increase the system's risk level, and a

negative marginal risk price means increasing the load at a bus would decrease the system's risk level. Similarly, if an increase in generation at a bus results in an increase of system risk, then the marginal risk component of RLMP at that bus will be negative.

In (49), the risk component of RLMP is a combination of probabilities, shift factors, and the Lagrangian multiplier of the risk constraint. Bus E has negative marginal risk value. In Table III, the energy component is the same for LMP and RLMP. If a bus is at the source (sink) of a congested line, the congestion component will increase (decrease) from LMP to RLMP. This observations lead to the following criteria of determining which buses will see higher (or lower) prices:

- A bus will see higher price (than LMP) if it is at the source of a congestion line and the risk component is positive;
- A bus will see lower price (than LMP) if it is at the sink of a congestion line and the risk component is negative.
- Other buses may see either higher or lower price, depending on the calculating result.

In general, the RLMP mechanism has the effect of decreasing prices at buses with high LMPs and increasing prices at buses with low LMPs, thus makes smaller difference among buses.

Question 3: How does the choice of K_R and K_C affect the RLMP?

In the RB-SCED model, the choice of K_R and K_C affects the production costs and the generation dispatches. Reference [119] discussed some criteria on how to select appropriate K_R and K_C values. The general idea is to adopt high security model when the system operation condition is under stress and/or the weather condition is severe, and adopt

economy-security model or high economy model when the system operation condition is less stressful and no severe weather is foreseen. In today's ISO-based electricity market, the calculation of LMP is a post-dispatch process. Thus, the choice of K_R and K_C is an important procedure to determine appropriate system operation conditions based on the real-time information and should be finished before the calculation of RLMP.

Fig. 6.4 and Fig. 6.5 show how RLMP changes with K_R at each bus when K_C equals 1 and 1.05, respectively. Bus A has the same RLMP values with K_R changes and thus is not indicated in the figures. One may plot RLMP-K_R relation figures for other K_C values. The simulation result shows that the RB-SCED problem becomes infeasible when $K_R \leq 0.83$ for both cases. The step changes in the LMP and RLMP curves are due to the binding of new constraints in SCED and RB-SCED models.

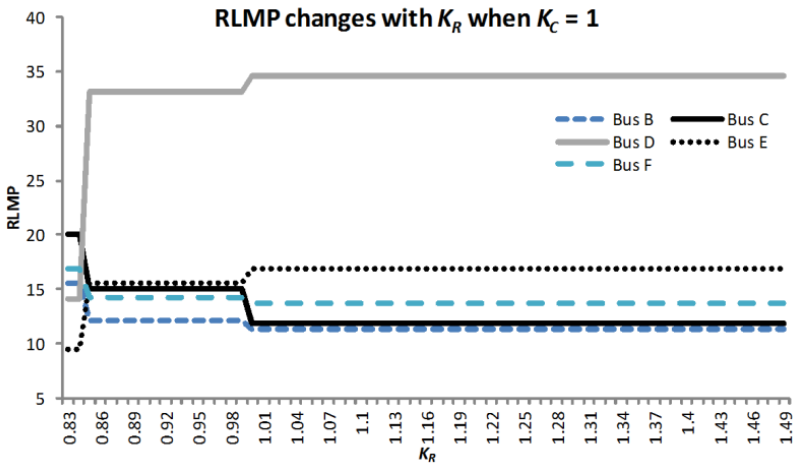

Fig. 6.4. RLMP changes with K_R at each bus when K_C = 1

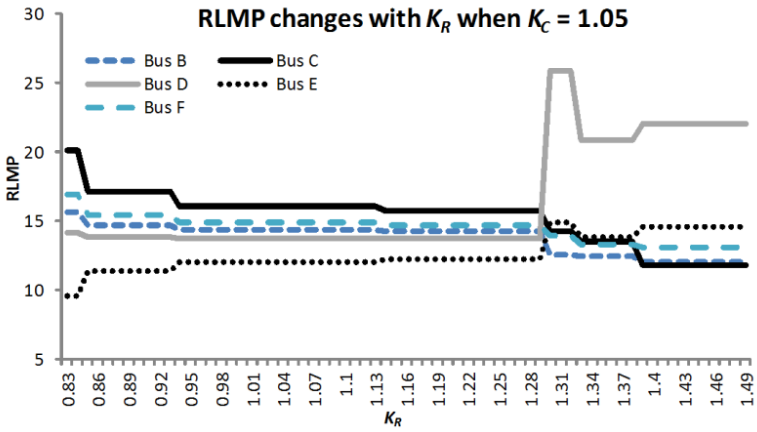

Fig. 6.5. RLMP changes with K_R at each bus when K_C = 1.05

6.5 Conclusion

Locational Marginal Pricing has been widely used in today's ISO-based electricity markets [121]-[122]. The successful application of LMP is enhanced by recent research on distributed-slack based LMP, reference bus independent LMP, ACOPF based LMP, and continuous LMP, etc. [123]-[129]. However, all of those researches are deterministic approach. In this chapter, we developed the Risk-based LMP based on risk-based SCED model proposed in previous chapters. Traditional LMP is composed of three components: marginal energy, marginal loss and marginal congestion. The RLMP includes an additional component, called risk component, besides the three components. The risk component is a price signal to reflect the system's overall security level. In this chapter, we have researched the features of RLMP on a six-bus system.

NOMENCLATURE

N	Number of buses
NG	Number of generators

NC	Number of contingencies
NL	Number of lines
l	The lth circuit
k	The kth post-contingency
c_i	Generation bid price
P_i	Generator output level
D_i	Nodal loads
$Loss$	System physical loss
GSF_{l-i}^{0}	Generation shift factor to line l from bus i at normal state
GSF_{l-i}^{k}	Generation shift factor to line l from bus i at post-contingency state
$Limit_l^0$	Transmission limit of line l at normal state
$Limit_l^k$	Transmission limit of line l at post-contingency state
h_l^k	The power flow on line l at kth post-contingency
LMP_i	Locational marginal pricing at bus i
$RLMP_i$	Risk-based locational marginal pricing at bus i
K_C	Parameter to control circuit overloading level
K_R	Parameter to control system risk level
$P_{LTE,l}$	Long time emergency rating of circuit l
$P_{STE,l}$	Short time emergency rating of circuit l
$P_{DAL,l}$	Drastic action limit rating of circuit l
Sev_l^k	Overload severity of circuit l at kth contingency
S_1	Set that the optimal post-contingency flows are not at corner points
S_2	Set that the optimal post-contingency flows are at corner point (0.9LTE, 0)
S_3	Set that the optimal post-contingency flows are at corner point (LTE, 1)
S_4	Set that the optimal post-contingency flows are at corner point (STE, c_1)

CHAPTER 7. VOLTAGE INSTABILITY PERFORMANCE OF RB-SCOPF

7.1 Introduction

In the previous chapters, we have demonstrated that operating conditions obtained from RB-SCOPF were more secure (less risky) than those obtained from SCOPF, where the assessment is based on a risk index that reflects line loading. This raises the question of whether the RB-SCOPF operating condition is more stable than the SCOPF-operating condition for other system problems. In this chapter, we compare the voltage stability performance of operating conditions obtained from RB-SCOPF and SCOPF, respectively, using a steady-state voltage instability index. We will model, for both the RB-SCOPF and the SCOPF operating conditions, a fictitious synchronous condenser (SC) with very wide reactive limits (e.g., ±1000 MVARs) at one reactive-weak extra-high voltage (e.g., 345 or 500 kV) bus in the system. We use the SC to vary the voltage from its nominal value to a very low value, identifying the bus reactive injection necessary from the SC to hold the given voltage. We identify the voltage instability point to be where additional negative reactive injection (corresponding to additional reactive load) no longer results in a solution.

7.2 Q-V curve in voltage instability analysis

During the past decades, voltage collapse phenomena have received widely researches around the world and are proved in a large number of power systems as a major reason for system insecurity [130]-[136]. The mechanism of voltage collapse is complicated and is still under research with more in-depth description and modeling [137]-[145]. This chapter will not deal with the dynamic aspects of voltage collapse but rather focus on static aspects, i.e.,

the determination of system's power transfer capacity by calculating the P-V or Q-V curves. Since the purpose of this chapter is to compare the voltage instability performances between SCOPF and RB-SCOPF under different active power dispatches, we focus mainly on Q-V curve analysis.

The Q-V curve describes the relationship between the reactive power and the voltage variations at a given bus. A standard power flow program can be used to produce Q-V curve by adding a fictitious generator at the bus of concern with zero active power and recording how its reactive output Q varies with its voltage V. This continuation method provides the loadability limit with respect to reactive power increase at a single bus. The Q-V relationship demonstrates the sensitivity of bus voltages with respect to reactive power injections or absorptions: if Q-V sensitivity is positive for every bus, the system is voltage stable; if Q-V sensitivity is negative for at least one bus, the system is voltage stable. This is because the existing control systems, including transformer taps, generator VARs, etc., are designed based on the assumption that compensating VARs (Q) will increase voltage (V), and vice versa.

Fig. 7.1 shows the Q-V curve corresponding to a stable situation. The vertical axis depicts the reactive MVAR output of the fictitious generator, and the horizontal axis depicts the respective voltage to sustain the output. In Fig. 7.1, the base point is the system's operating point, with the fictitious generator output being zero. As the voltage decreases, the reactive power consumption of the generator increases, which equivalently represents an increase in MVAR load. Thus, the Q-V curve is able to trace what the voltage would be as we increase the load MVAR. With the voltage decreases to a certain value, the MVAR value of the generator will stop decreasing and reach the "bottom" of the Q-V curve. This bottom point

is the maximum load MVAR increase at the bus, and any higher load may cause voltage collapse.

Fig. 7.2 illustrates an unstable situation where the curve does not cross horizontal axis Q = 0. The distance between the bottom point of the curve and the horizontal axis represents the MVARs margin to operability at the bus. It can be used to compute the minimum shunt compensation to restore the system back to voltage stable.

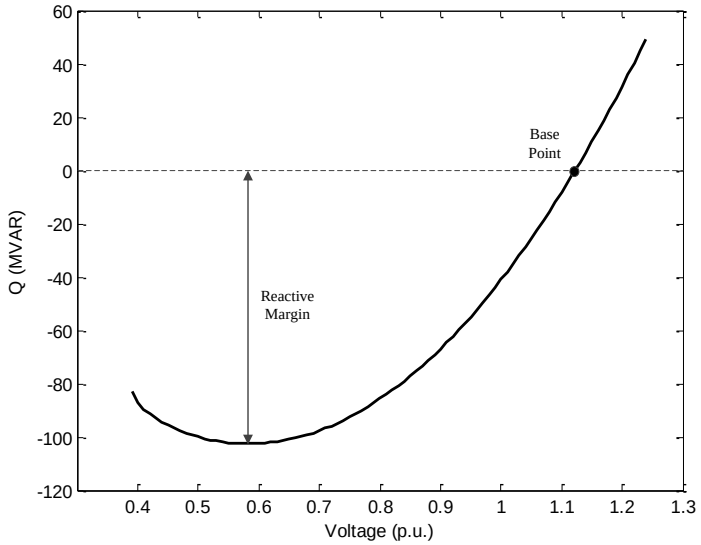

Fig. 7.1 Q-V Curve at a voltage stable bus

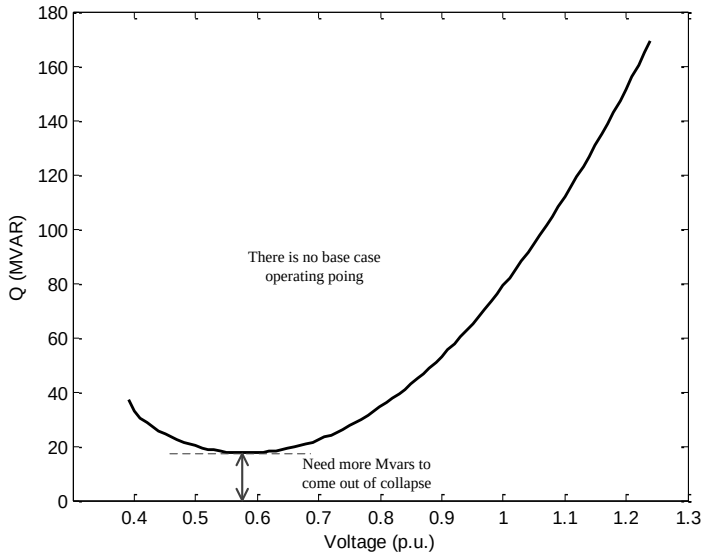

Fig. 7.2 Q-V Curve at a voltage unstable bus

In practice, the Q-V curve can be drawn with a power flow program in the following steps:

a) Modeling a synchronous condenser (SC), i.e., a generator having very wide reactive limits and with P = 0, at the target bus.

b) Setting the bus voltage |V| to a desired value.

c) Solving the system power flow.

d) Reading the MVAR output of the SC.

e) Repeat step b) – d) for a predefined range of voltages.

Note that the Q-V curves are easier to obtain than P-V curves. This is because the standard power flows cannot be solved around/below the "nose point" of PV curves, but they will solve near the "nose point" of Q-V curves. Another point to mention is that reactive power cannot be moved very far in a network, i.e., VARs do not travel, thus a

system may have VAR surplus but experience voltage instability if a local area in it has a VAR deficiency.

7.3 Voltage Instability Performances of SCOPF and RB-SCOPF

7.3.1 System Description

The testing of voltage instability is ongoing on an IEEE 30-bus system. The system diagram and parameter are shown in section 3.5.1. There are 36 contingencies of concern in this system. The original generation cost curves for unit G1, G2, G3, G4, G5 and G6 are shown in Fig. 7.3. For each quadratic curve, we use 3-segment linear curves to approximate it. To better apply the voltage instability analysis, some changes are made to the original data as follows: we increase the voltage level at bus 4 to be 345 kV, which makes it be a high voltage bus. A synchronous condenser with very wide reactive limits (± 1000 MVARs) is located a bus 4 when calculating the power flows.

In order to model losses in the lossless network, a base-case power flow is solved at first. The loss offset is -2.44 MW, which is calculated against the reference bus 1. We have solved the system using RB-SCOPF and using SCOPF. The active power dispatches of all generators are shown in Table 7.1. Since we relaxed the transmission limits by multiplying them with a parameter K_C (>1) in ESM and HEM, they are able to dispatch more MWs from cheaper unit G2.

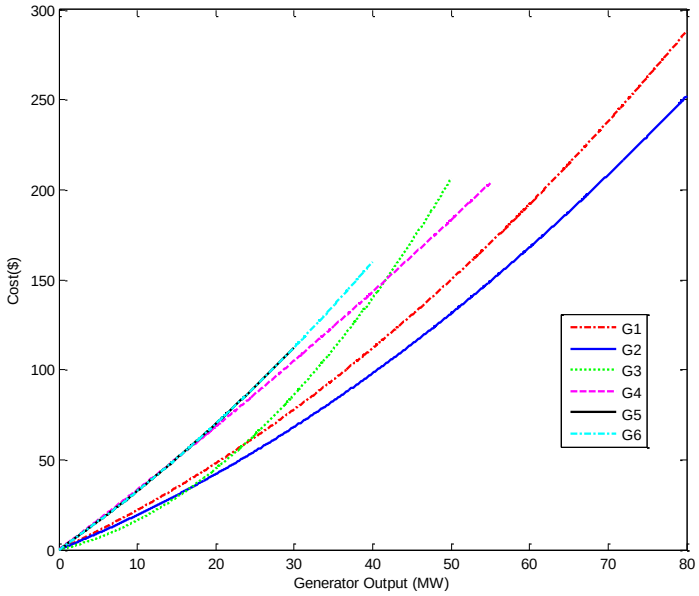

Fig. 7.3 Generation cost curves for unit G1, G2, G3, G4, G5 and G6

Table 7.1 Dispatch of active power for SCOPF and various models of RB-SCOPF

Generator	Dispatch of active power (MW)			
	SCOPF	HSM	ESM	HEM
G1	65.28	66.32	39.17	26.67
G2	0.53	1.08	26.67	37.19
G3	40.00	38.30	38.21	37.91
G4	32.47	32.55	35.07	41.04
G5	10.67	10.67	11.04	12.16
G6	42.70	42.72	41.48	36.67

7.3.2 Voltage instability results

For the IEEE 30-bus system with 36 post-contingency states, we compute the reactive margin using the Q-V curve procedure described above. We do the tests and compare the results in two aspects. First, we compare the Q-V curves for SCOPF, HSM, ESM and HEM without considering contingencies. At a selected bus, we change the voltage and see how the reactive power of the SC changes under each operating mode— this is called **horizontal**

comparison. The selected bus can be PQ bus or PV bus. Then, we select a special bus, and see how the Q-V curves change with a transmission line tripping for SCOPF, HSM, ESM and HEM. The purpose is to see which operating model has strong ability to sustain a contingency— this is called **vertical comparison**.

1) Horizontal comparison

The Q-V curve algorithm is applied on generation bus 2. At base case, the voltages and reactive powers for G1~G6 are shown in Table 7.2. Let's first use G2 as an example to demonstrate how to obtain its Q-V curve. Results on other generators are similar.

Table 7.2 Voltage and unit reactive output at bus 2 for SCOPF, HSM, ESM and HEM

		G1	G2	G3	G4	G5	G6
SCOPF	V (p.u.)	1.060	1.043	1.071	1.033	1.027	1.023
	Q (MVAR)	28.422	39.382	18.023	26.936	-15.093	5.000
HSM	V (p.u.)	1.060	1.043	1.071	1.033	1.027	1.023
	Q (MVAR)	36.678	30.322	18.085	26.005	-14.523	5.754
SEM	V (p.u.)	1.060	1.043	1.071	1.033	1.027	1.023
	Q (MVAR)	40.597	26.451	17.942	23.486	-12.445	5.492
HEM	V (p.u.)	1.060	1.043	1.071	1.033	1.027	1.023
	Q (MVAR)	40.163	28.589	18.262	24.458	-12.415	2.404

Using the method in section 7.1, we plot the corresponding Q-V curve of bus 2, as shown in Fig. 7.4. The voltage changes from 1.25 *p.u.* to 0.35 *p.u.*. We observe the changes of the reactive power at bus 2. In Fig. 7.4, the above picture is an overview all the curves. To see the details at the "nose point", we grasp the curves around the nose point area and demonstrate the details in the below picture of Fig. 7.4. We can observe that the RB-SCOPF dispatch consistently outperforms the SCOPF dispatch in that the RB-SCOPF dispatch shows more reactive margin to voltage instability than the SCOPF dispatch does. ESM and HEM have higher reactive margins than HSM. This is remarkable since RB-SCOPF

dispatch (ESM and HEM) is more economic than the SCOPF dispatch, and ESM and HEM are more economy than HSM. The maximum reactive margins of each case are shown in Table 7.3.

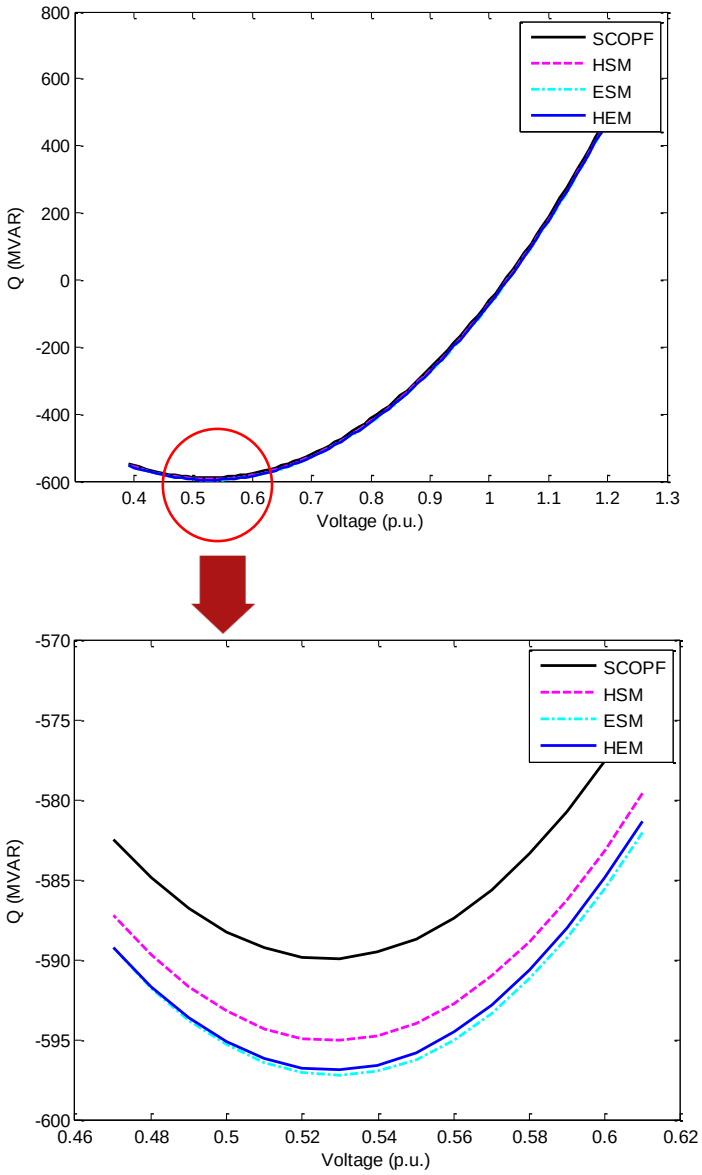

Fig. 7.4 Q-V curves at bus 2

Table 7.3 The maximum reactive margins for SCOPF, HSM, ESM and HEM at bus 2

	SCOPF	HSM	ESM	HEM
Max. reactive Margin (MVAR)	589.9	595.0	597.2	596.9

We also want to demonstrate the Q-V curve on a PQ buses. The bus 4 and bus 12 are selected to analyze. According to the test, they have similar characteristics in Q-V curve: RB-SCOPF has larger reactive margins than SCOPF, and HEM has larger reactive margin than HSM and ESM. Test results on bus 4 are shown in Fig. 7.5 and Table 7.4, and test results on bus 12 are shown in Fig. 6 and Table 7.5. To see the details near the "nose point" of the Q-V curves, we grasp the Q and V around the bottom point of the curve, as shown in the below pictures in Fig. 7.5 and Fig. 7.6. All the evidences demonstrate that RB-SCOPF has better performance on voltage instability analysis.

2) Vertical Comparison

In this part we desire to compare how the performances of SCOPF, HSM, ESM and HEM system change suffering from a single line outage. Not loss of generality, we did the test on bus 4 and see the change of Q-V curves under all the 36 contingencies. Fig. 7.7 shows the Q-V curves on bus 4 under normal state and a "N-1" post-contingency state, i.e., the outage of transmission line 4-12. It can be seen from Fig. 7.7 that for all the operating modes (SCOPF, HSM, ESM and HEM) the reactive margins decrease on bus 4. We are interested in which operating mode has the largest reactive margins when the contingency happens. The result is shown in Fig. 7.8, which has proved that RB-SCOPF has better performance on voltage instability analysis. The interesting point is that the HEM is the most economic operation mode, but it has the largest post-contingency reactive margin.

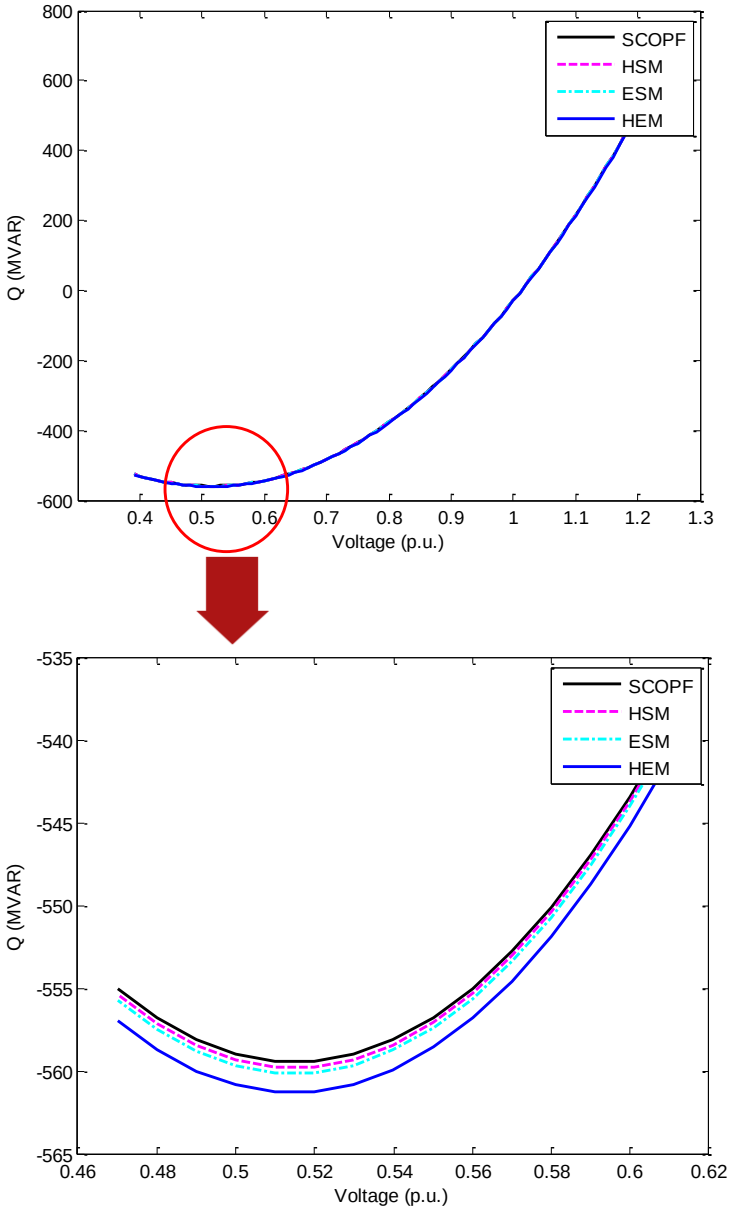

Fig. 7.5 Q-V curves at bus 4

Table 7.4 The maximum reactive margins for SCOPF, HSM, ESM and HEM at bus 4

	SCOPF	HSM	ESM	HEM
Max. reactive Margin (MVAR)	559.47	559.79	560.14	561.35

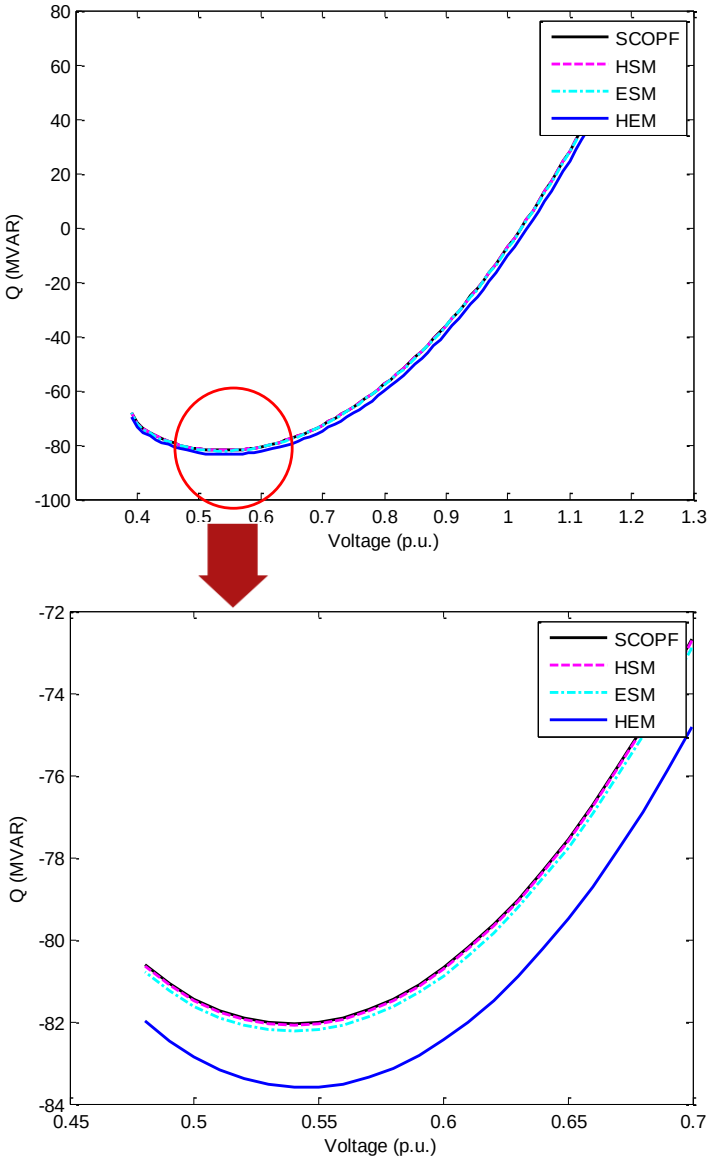

Fig. 7.6 Q-V curves at bus 12

Table 7.5 The maximum reactive margins for SCOPF, HSM, ESM and HEM at bus 12

	SCOPF	HSM	ESM	HEM
Max. reactive Margin (MVAR)	82.06	82.10	82.24	83.65

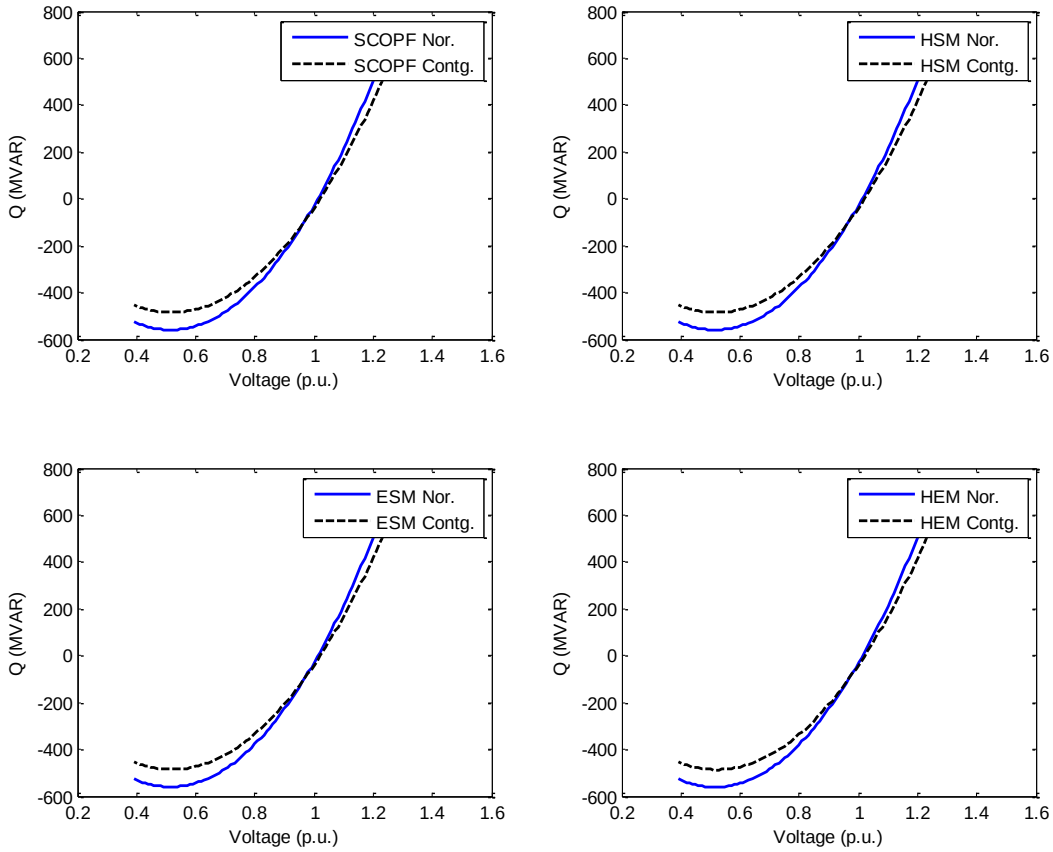

Fig. 7.7 Compare the Q-V curves between normal state and contingency state for SCOPF, HSM ESM and HEM

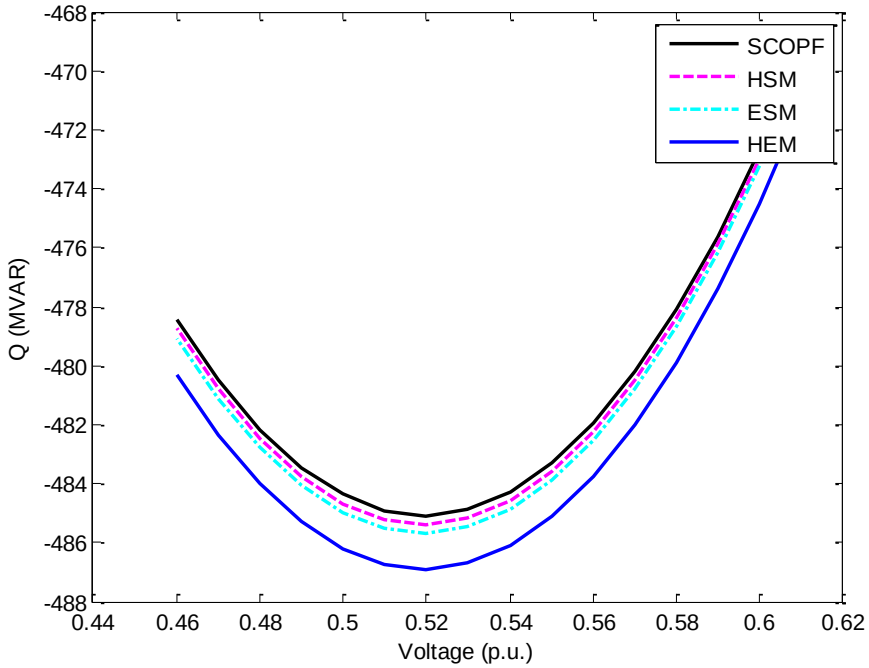

Fig.7. 8 Compare the Q-V curves after a contingency

In Fig. 7.9 we present the reactive margins on bus 4 for all the 36 contingencies. The x-axis is the contingency numbers, and the y-axis is the reactive margins in MVARs. In order to compare the results between RB-SCOPF and SCOPF, we subtract the value of SCOPF from the value of RB-SCOPF. For example, the top line in Fig. 7.9 indicates the reactive margins of HEM minus the reactive margins of SCOPF at bus 4 for all the contingencies. The higher the curve is, the more secure the system is. It is interesting to see that HSM, ESM and HEM have higher reactive margins than SCOPF under all the contingencies. Especially, the HEM is the model with lowest cost yet with the largest post-contingency reactive margins on bus 4.

An important reason for why RB-SCOPF has lager reactive margin than SCOPF is that the former aims at constraining highly-load lines on the system thus the power flows are

more uniformly loaded when compared to the latter. This leads to lower reactive losses on the circuit, thus results in higher reactive margin to voltage instability. Test results shown in Table 7.6 confirm the conclusion. For the dispatch result in Table 7.1, the full AC power flow is applied to the system to calculate the reactive loss. From Table 7.6, the SCOPF has the largest reactive power loss; HSM, ESM and HEM have lower losses than SCOPF, and their losses decrease in sequence.

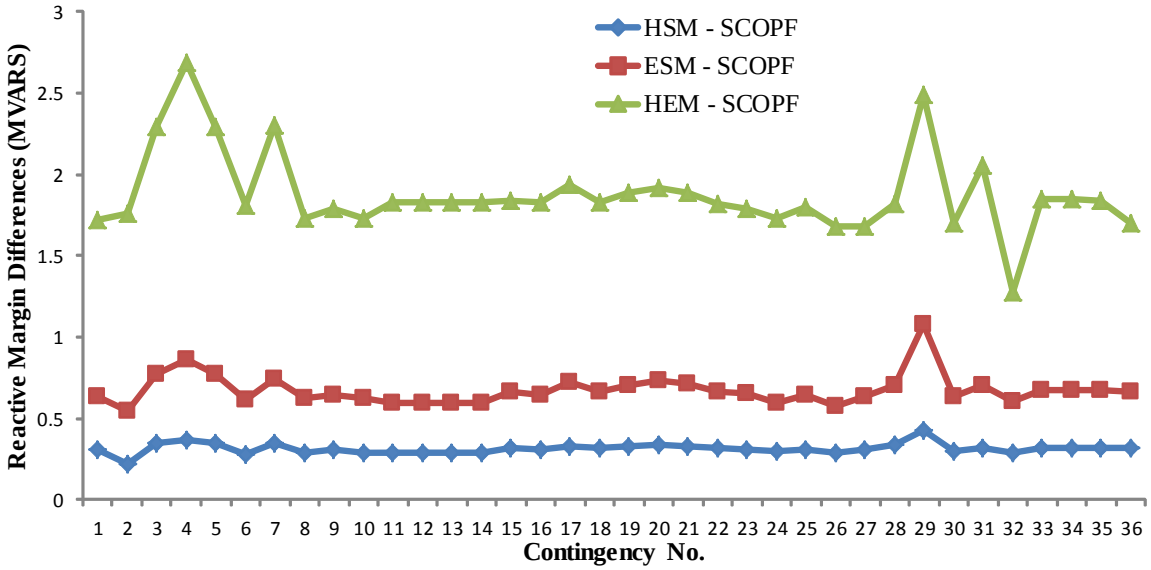

Fig. 7.9 RB-SCOPF reactive margins compared to SCOPF for all the contingencies at bus 4

Table 7.6 Compare the system reactive power loss

	SCOPF	HSM	ESM	HEM
System Q Loss (MVAR)	13.34	12.20	11.41	11.36

7.4 Conclusion

This chapter presents the testing results of voltage stability performance of risk-based security-constrained OPF. The analysis is based on QV curves, which are calculated for a particular bus of interest. We did tests on the IEEE 30-bus system. At first, dispatch solutions on SCOPF, HSM, ESM and HEM are obtained, respectively. Then, we select a single bus and plot the Q-V curves on it based on the different dispatch solutions. At last, we compare the post-contingency Q-V curves on a selected bus. The testing results show that RB-SCOPF has higher reactive margins than SCOPF at both normal state and post-contingency states.

Future research may include analyzing the sensitivity of the reactive margin to the active power output of each unit. This will help understand how the RB-SCOPF causes higher reactive margin than SCOPF.

CHAPTER 8. SUMMARY OF CONTRIBUTIONS AND FUTURE WORKS

8.1 Summary of Contributions

A new philosophy of power system security control has been proposed in this research. Risk, an index to measure the system healthy level, is applied to control the system security. Under the risk framework, the traditional deterministic SCOPF model is evolved into the Risk-based SCOPF (RB-SCOPF) model. Similar to SCOPF, the RB-SCOPF has been formulated into two modes: *preventive* and *corrective*, referred to as PRB-SCOPF and CRB-SCOPF, respectively. This dissertation illustrates the mathematical fundamentals and computational strategies for both PRB-SCOPF and CRB-SCOPF, and explores the application of PRB-SCOPF in the industry. The major contributions of this work are summarized as below.

1. **New approach to handle the piece-wise linearly severity function.** The severity function is piece-wise linear, i.e., its formulation changes with the circuit flow in different intervals, thus it is difficult to handle the severity function during the optimization process. Traditional method to deal with such kind of problems is by introducing integer variables to indicate which interval the severity function is located. This approach is feasible in theory, but is not applicable in reality because the number of circuits and contingency sets is huge in real-world power system. Take the ISO-NE system as an example, millions of integer variables should be introduced if we use the approach. This will cause prohibitive computation time. In this work, a new approach is proposed by transferring the deterministic expression into an optimization problem, which avoids introduction of integer variables. We only need

to solve linear programming (LP) problem by using this new approach. This greatly increases the computational efficiency of RB-SCOPF.

2. **Efficient Computational strategy to solve PRB-SCOPF.** The PRB-SCOPF improves the traditional P-SCOPF in the following two ways: 1) It introduces a risk constraint to control the system's overall risk level at post-contingency states; 2) It enables the system operators control over a tradeoff between the system's *security* and *economy* by adjusting the post-contingency overload rating and the overall risk level. The PRB-SCOPF is difficult to solve because the risk constraint linking every post-contingency state, thus make the size of the programming problem be very large. We have proposed a two-layer nested Benders decomposition approach to solve the PRB-SCOPF. In the first layer, it is similar to solving the SCOPF problem, thus the current framework to solve SCOPF could be used. In the second layer, the problem has some interesting features that we can solve the LP problem algebraically, which has great improved the computation efficiency. Illustration on ISO-NE system illustrates the feasibility of the proposed approach.
3. **Efficient Computational strategy for solving CRB-SCOPF.** The difference between CRB-SCOPF and PRB-SCOPF is that the former allows for post-contingency corrective controls. From the view of mathematics, if Benders decomposition is applied, the CRB-SCOPF is more difficult to solve because we need to solve an individual LP problem for each-contingency state, while in PRB-SCOPF we could solve the LPs algebraically. In real power systems, the contingency set is usually very large, thus the computational burden of CRB-SCOPF is high. In this work, an efficient decomposition based algorithm is proposed to solve CRB-SCOPF

by using Lagrangian relaxation and Benders decomposition. The test results based on the IEEE 30-bus system and the ISO-NE system have demonstrated the feasibility of the proposed approach.

4. **Realization of PRB-SCED in ISO New England bulk system.** The final purpose of this work is to realize the PRB-SCED in the industry (to realize CRB-SCED is a future work). As illustrated above, the PRB-SCED is an improvement of current widely-used SCED, and we can utilize the current SCED framework in the computing procedure. The online RB-SCED software has been developed and realized for the ISO-NE system. The software utilizes *Java* for the computing, GAMS (the General Algebraic Modeling System) for the optimization, and TARA (Transmission Adequacy & Reliability Assessment, software developed by PowerGEM Inn.) for the contingency screening. One important function of TARA is to obtain the shift factors by simultaneous feasibility test (SFT). The test result demonstrates that the RB-SCED can be realized in today's ISO-based power systems.
5. **Research on the coordination of risk and "N-1" criteria.** A visualization diagram, called K_R-K_C coordination diagram, is proposed for decision-support that enables efficient security-economy tradeoff analysis. An efficient algorithm is applied to find "breakpoints" in the KR-KC coordination diagram. The work helps to demonstrate how system risk and post-contingency overload levels on individual circuits are coordinated to enhance both economy and security of a power system in real-time operations and to identify types of conditions for which high-security and high-economy modes would be best suited. Use of RB-SCOPF results in improved long-

term power system performance, for both economics and security. This work provides additional insight on its use to facilitate its eventual adoption by industry.

6. **Research on Risk-based LMP and congestion management.** Traditionally, the LMP is derived from security-constrained economic dispatch model. The LMP formulation can be decomposed into three components: marginal energy price, marginal loss price, and marginal congestion price. In our RB-SCED model, a risk index has been developed for the purpose of quantifying/controlling the system's overall risk level. The locational marginal pricing derived from RB-SCED should contain an additional component, called marginal risk price, and the traditional LMP is extended to risk-based LMP (RLMP). The risk component is a price signal to reflect the system's overall security level. We have examined the features of RLMP and compared it with traditional LMPs.
7. **Research on Voltage Instability Analysis of Risk-based SCOPF**. We compare the voltage stability performance of operating conditions obtained from RB-SCOPF and SCOPF, respectively, using a steady-state voltage instability index. The Q-V curves on a select bus are compared for RB-SCOPF and SCOPF based on the IEEE 30-bus test system. We also compare the post-contingency reactive power margins. The testing result shows that RB-SCOPF has better performance on voltage stability on both normal and post-contingency states.

8.2 Future works

Further develop new security assessment tools, focused on the risk-based security-constrained optimal power flow, illustrate its effectiveness in enhancing system security

levels, and explore the applicability for of RBOPF under the market environment. The following topics may be of interest.

8.2.1 Effects of Risk-based LMPs on congested lines causing high LMPs

Traditionally, LMPs are calculated based on the security constrained economic dispatch (SCED) in day-ahead and real-time electricity markets. The LMP calculated from SCED is composed of three components: marginal energy price, marginal loss price and marginal congestion price. Use of the RB-SCED in electricity markets will result in LMPs that include these three components and one more associated with the system risk constraint. This risk component is a price signal to reflect the system's overall security level. It is expected that by properly choosing KR and KC values, high LMPs caused by highly congested lines will decrease. The RB-SCED model imposes control in proportion to the amount of post-contingency flows on lines that need to have flow reduction; this is unlike SCED which imposes control to satisfy each line's post-contingency flow constraint. This unique feature of RB-SCED tends to decrease system losses and further decrease LMPs. We will study the effects of RB-SCED on LMPs, particularly for congested cases. Some issues of particular interest include: 1) Does RB-LMP stabilize price volatility for small increase in risk? 2) Given its economic benefits, we will explore the effects on dynamic security associated with the RB-SCED solutions.

8.2.2 Extension of the risk concept

Risk assessment (RA) has been widely used in other industries such as nuclear, aerospace, oil, food, public health, information technology and finance engineering. It is an

emerging new topic in power engineering. The successful application of RA in other areas has provided valuable experience for the implementation of risk-based approach in power systems. Thus, we may extend our risk concept in the following ways: 1) Take a consideration of today's mature risk management measures such as CVAR and chance-constrained programming. 2) Enforce several risk indices in the dispatch problem, in which each risk index describes one aspect of operational risk. For example, we could use LOLE as a risk index to measure the generation system adequacy. 3) Compare the benefits of various risk measurements.

8.2.3 Security assessment of risk-based approach

We would like to see an improvement of the system's security level if we transfer from deterministic SCED to RBSCED approach. The security assessment study, on both static security and dynamic security, should be enforced to compare the performance of the two different dispatch tools. The assessment results are useful for our decision on adopting the risk-based approach. Suggested measurement metrics are: 1) Static security: overload, cascading overload, low voltage and voltage collapse. 2) Dynamic security: perform dynamic security assessment on the system. 3) Demonstrate that RBOPF will decrease the system losses, because it inherently makes the distribution of power flow more evenly on the system. 4) Test on the previously defined indices such as ASI (Angular Separation Index) and CEI (Cascading Expectation Index).

8.2.4 Uncertainties of power system

The power system is facing new challenge as the supply and demand uncertainty increases significantly due to the integration of renewable energy resources and price responsive demand. The risk-based dispatch approach should consider these uncertainties. Suggested uncertainty sources may come from: 1) Loss of a generation resources. 2) Uncertainty on load forecasting, especially when wind is high. 3) Uncertainty on demand response.

BIBLIOGRAPHY

[1] International Energy Agency (IEA), "What can I do to save energy?" Available: http://www.iea.org/efficiency/whatcanido.asp.

[2] V. Miranda and L. M.Proenca, "Why risk analysis outperforms probabilistic choice as the effective decision support paradigm for power system planning," IEEE Trans. Power Syst., vol.13, no. 2, pp.643-648, May 1998.

[3] P. Linares, "Multiple criteria decision making and risk analysis as risk management tools for power systems planning," IEEE Trans. Power Syst., vol.17, no. 3, pp. 895-900, Aug. 2002.

[4] W. Li, P. Choudhury, D. Gillespie, and J. Jue, "A Risk Evaluation Based Approach to Replacement Strategy of Aged HVDC Components and Its Application at BCTC", IEEE Trans. Power Delivery, vol. 22, no. 3, pp. 1834 – 1840, 2007.

[5] A. Janjic and D. Popovic, "Selective Maintenance Schedule of Distribution Networks Based on Risk Management Approach", IEEE Trans. Power Syst., vol. 22, no. 2, pp.597-604, 2007.

[6] G. Strbac, R. Moreno, D. Pudjianto, and M. Castro, "Towards a risk-based network operation and design standards," IEEE Power and Energy Society General Meeting, Detroit, MI, July 2011.

[7] T. Zheng and E. Litvinov, "Operational risk management in the future grid operation," IEEE Power and Energy Society General Meeting, Detroit, MI, July 2011.

[8] P.R. Varaiya, F.F. Wu, and J.W. Bialek, "Smart Operation of Smart Grid: Risk-limiting Dispatch," Proc. of IEEE, Vol. 99, No. 1, pp. 40-57, Jan. 2011.

[9] NERC, Reliability Assessment Guidebook, version 2.1, May 2010.

[10] P. Kunder, Power System Stability and Control, McGraw-Hill press, 1994.

[11] D.S. Kirschen. K.R.W. Bell, D.P. Nedic, D. Jayaweera and R.N. Allan, "Computing the value of security," IEE Proc. Gener Transm. Dltrrib., Vol 150, No. 6, pp. 673-678, Nov. 2003.

[12] Mario A. Rios, Daniel S. Kirschen, Dilan Jayaweera, Dusko P. Nedic, and Ron N. Allan, "Value of Security: Modeling Time-Dependent Phenomena and Weather Conditions," IEEE TRANSACTIONS ON POWER SYSTEMS, VOL. 17, NO. 3, pp. 543-548, AUGUST 2002.

[13] K. Morison, L. Wang, and P. Kunder, "Power system security assessment," IEEE Power & Energy Magazine, vol.2, no. 5, pp, 30-39, 2004.

[14] N. Balu, et al., "On-Line Power System Security Analysis," Proceedings of The IEEE, Vol. 80, no. 2, pp. 262-279, Feb. 1992.

[15] S. Weerasooriya, M.A. El-Sharkawi, M. Damborg, et al., "Towards static-security assessment of a large-scale power system using neural networks," IEE Proceedings Generation, Transmission and Distribution, vol. 139, no. 1, pp. 64-70, Jan. 1992.

[16] M.J. Laufenberg and M.A. Pai, "A new approach to dynamic security assessment using trajectory sensitivities," 20th International Conference on Power Industry Computer Applications., May 11-16, Columbus, OH, USA, 1997.

[17] R. Billinton, Y. Gao, and R. Karki, "Application of a Joint Deterministic-Probabilistic Criterion to Wind Integrated Bulk Power System Planning," IEEE Trans. Power Systems, vol. 25, no. 3, pp. 1384-1392, Aug. 2010.

[18] D. Niebur and A.J. Germond, "Power system static security assessment using the Kohonen neural network classifier," IEEE Trans. Power Systems, vol. 7, no. 2, pp. 865-872, May 1992.

[19] J. Zhihong and B. Jeyasurya, "Contingency ranking for on-line voltage stability assessment," IEEE Trans. Power Systems, vol. 15, no. 3, pp. 1093-1097, Aug. 2000.

[20] A.P.S. Meliopoulos, G.J. Cokkinides, and X.Y. Chao, "A new probabilistic power flow analysis method," IEEE Transactions on Power Systems, vol. 5, no. 1, pp. 182-190, Feb. 1990.

[21] J. Endrenyi, G.J. Anders, and A.M. Leite da Silva, "Probabilistic evaluation of the effect of maintenance on reliability—An application to power systems," IEEE Transactions on Power Systems, vol. 13, no. 2, pp. 576-583, May 1998.

[22] R. Allan and R. Billinton, "Probabilistic assessment of power systems," Proceedings of the IEEE, Vol. 88, no. 2, pp. 140-162, Feb. 2000.

[23] R.R. Booth, "Power System Simulation Model Based on Probability Analysis," IEEE Transactions on Power Apparatus and Systems, Vol. PAS-91, no. 1, pp. 62-69, Jan. 1972.

[24] J. McCalley, et al., "Probabilistic security assessment for power system operations," IEEE Power Engineering Society General Meeting, June 6-10, 2004.

[25] Hyungchul Kim and Chanan Singh, "Power system probabilistic security assessment using Bayes classifier," Electric Power Systems Research, Vol. 74, no. 1, pp. 157–165, April 2005.

[26] E. Ciapessoni, D. Cirio, S. Grillo, S. Massucco, A. Pitto, and F. Silvestro, "Operational Risk Assessment and control: A probabilistic approach," IEEE PES Innovative Smart Grid Technologies Conference Europe (ISGT Europe), Milan, Italy, 11-13 Oct. 2010.

[27] M.V.F. Pereira, M.E.P. Maceira, G.C. Oliveira,and L.M.V.G. Pinto, "Combining analytical models and Monte-Carlo techniques in probabilistic power system analysis," IEEE Transactions on Power Systems, Vol. 7, no. 1, pp. 265-272, Feb. 1992.

[28] Daniel S. Kirschen, Dusko P. Nedic, and Ron N. Allan, "A Probabilistic Indicator of System Stress," IEEE Transactions on Power Systems, Vol. 19, No. 3, pp. 1650-1657, AUGUST 2004.

[29] Hyde M. Merrill and Allen J. Wood, "Risk and uncertainty in power system planning," International Journal of Electrical Power & Energy Systems, Vol. 13, no. 2, pp. 81–90, April 1991.

[30] E.O. Crousillat, P. Dorfner, P. Alvarado, and H.M. Merrill, "Conflicting objectives and risk in power system planning," IEEE Transactions on Power Systems, Vol. 8, no. 3, pp. 887-893, Aug. 1993.

[31] J.D. McCalley, A.A. Fouad, V. Vittal, A.A. Irizarry-Rivera, and B.L. Agrawal, "A risk-based security index for determining operating limits in stability-limited electric power systems," IEEE Transactions on Power Systems, Vol. 12, no. 3, pp. 1210-1219, Aug. 1997.

[32] D.S. Kirschen and D. Jayaweera, "Comparison of risk-based and deterministic security assessments," IET Gener. Transm. Distrib., vol. 1, no. 4, pp. 527–533, 2007.

[33] J. He, L. Cheng, D.S. Kirschen, and Y. Sun, "Optimising the balance between security and economy on a probabilistic basis," IET Gener. Transm. Distrib., Vol. 4, Iss. 12, pp. 1275–1287, 2010.

[34] J.D. McCalley, V. Vittal, and N. Abi-Samra, "An overview of risk based security assessment," IEEE Power Engineering Society Summer Meeting, Edmonton, Alta., Canada, 18-22 July, 1999.

[35] Hua Wan, McCalley, J.D. Vittal, V., "Risk based voltage security assessment," IEEE Transactions on Power Systems, Vol.15, no. 4, pp. 1247-1254, Nov. 2000.

[36] M. Ni, J. McCalley, V. Vijay, and T. Tayyib, "On-line risk-based security assessment," IEEE Trans. Power Syst., vol. 18, no. 1, pp.258–265, Feb. 2003.

[37] Qiming Chen and J.D. McCalley, "Identifying high risk N-k contingencies for online security assessment," IEEE Transactions on Power Systems, Vol. 20, no. 2, pp. 823-834, May 2005.

[38] S.K. Mukherjee, A. Recio, and C. Douligeris, "Optimal power flow by linear programming based optimization," IEEE Southeastcon Proceedings, Birmingham, AL, USA, Apr 1992.

[39] M. Olofsson, G. Anderson and L. Soder, "Linear Programming Based Optimal Power Flow Using Second Order Sensitivities," IEEE Transactions on Power Systems, Vol. 10, No. 3, pp. 1691-1697, August 1995.

[40] D.S. Kirschen, and H.P. Van Meeteren, "Further developments in LP-based optimal power flow," IEEE Transactions on Power Systems, Vol. 3 no. 2, pp. 481-489 , May 1988.

[41] G.L. Torres and Quintana, V.H., "An interior-point method for nonlinear optimal power flow using voltage rectangular coordinates," IEEE Transactions on Power Systems, vol. 13, no. 4, pp. 1211-1218, Nov 1998.

[42] R.A. Jabr, A.H. Coonick, and B.J. Cory, "A primal-dual interior point method for optimal power flow dispatching," IEEE Transactions on Power Systems, vol. 17, no. 3, pp. 654-662, Aug. 2002.

[43] F. Capitanescu, M. Glavic, D. Ernst, and L. Wehenkel, "Interior-point based algorithms for the solution of optimal power flow problems," Electric Power Systems Research, vol. 77, no. 5, pp. 508-517, April 2007.

[44] G. P. Granelli and M. Montagna, "Security constrained economic dispatch using dual quadratic programming", Electric Power System Research, vol 56, pp. 71-80, 2000.

[45] R.D. Zimmerman, C.E. Murillo-Sánchez, R.J. Thomas, "MATPOWER: Steady-State Operations, Planning, and Analysis Tools for Power Systems Research and Education," IEEE Transactions on Power Systems,vol. 26, no. 1, pp. 12-19, Feb. 2011.

[46] Y.H. Song M.R. Irving, "Optimization techniques for electrical power systems Part 2: Heuristic optimization methods," Power Engineering Journal, vol. 15, no. 3, pp. 151-160, June 2001.

[47] Y. Li and J. McCalley, "Decomposed SCOPF for Improving Efficiency," IEEE Trans. Power Syst., vol. 24, no. 1, pp. 494- 495, Feb. 2009.

[48] F. Capitanescu, M. Glavic, D. Ernst, and L.Wehenkel, "Contingency Filtering Techniques for Preventive Security-Constrained Optimal Power Flow," IEEE Trans. Power Syst., vol. 22, no. 1, pp. 1690-1697, Nov. 2007.

[49] H. Yamin, K. Al-Tallaq, and S. Shahidehopur, "A Novel Approach for Optimal Power Flow Using Bender's Decomposition in a Deregulated Power Market," Elect. Power Components and Syst., vol. 31, no. 1, pp. 1179-1192, 2003.

[50] J. Benders, "Partitioning procedures for solving mixed-variables programming problems". J. Numer. Math., vol. 4, no. 1, pp. 238–252, Dec. 1962.

[51] A. Geoffrion, "Generalized Benders decomposition," J. Optim. Theory Appl., vol. 10, no. 4, pp. 237-260, 1972.

[52] J. Zhu and K. Cheung, "Flexible Simultaneous Feasibility Test in Energy Market," IEEE Power and Energy Society General Meeting, Minneapolis, MN, July 2010.

[53] X., Luo and O. Obadina, "Security assessment and enhancement in real-time operations of ERCOT nodal electricity market," 2010 IEEE Power and Energy Society General Meeting, Minneapolis, MN, 25-29 July, 2010.

[54] Fei Xiao and James D. McCalley, "Risk-Based Security and Economy Tradeoff Analysis for Real-Time Operation," IEEE Trans. Power Syst., Vol. 22, No. 4, pp. 2287-2288, Nov. 2007.

[55] Slava Maslennikov and Eugene Litvinov, Enhancement of Dispatch by Utilization of Adaptive Transmission Rates (ATR), Available: http://www.ferc.gov/eventcalendar/Files/20100623161839-Maslennikov,%20ISO-NE%206-23-10.pdf.

[56] R. Billinton and R. Allan, Reliability Evaluation of Engineering Systems, 2nd ed. New York: Plenum Press, 1996, pp. 1-16.

[57] A. J. Wood and B. F. Wollenberg, Power Generation, Operation and Control, 2nd ed. New York: Wiley, 1996, pp. 501-550.

[58] W.Y. Li, Risk Assessment of Power Systems: Models, Methods, and Applications. New York: Wiley, 2005, pp. 89-125.

[59] G.C. Ejebe and B.F. Wollenberg, "Automatic Contingency Selection," IEEE Trans. Power Apparatus and Syst., vol. PAS-98, no.1, pp. 97-109, Jan. 1979.

[60] O.Alsac and B. Stott, "Optimal Load Flow with Steady-State Security," IEEE Trans. Power Apparatus and Systems, vol. PAS-93, no. 3, pp. 745-751, May 1974.

[61] C. W. Sanders,and C. A. Monroe, "An algorithm for real-time security constrained economic dispatch," IEEE Trans. Power Syst., vol. PWRS-2, no. 4, pp. 1068-1074, 1987.

[62] L.G. Dias and M.E. Elhawary, "Security-constrained OPF: influence of fixed TAP transformer fed loads," IEEE Trans. Power Syst., vol. 6, no. 4, pp. 1366-1372, 1991.

[63] C. Lehmköster, "Security Constrained Optimal Power Flow for an Economical Operation of FACTS-Devices in Liberalized Energy Markets," IEEE Trans. Power Deliv., vol. 17, no. 2, pp. 603-608, 2002.

[64] A. Berizzi, M. Delfanti, P. Marannino, M. Pasquadibisceglie, and A. Silvestri, "Enhanced Security-Constrained OPF With FACTS Devices," IEEE Trans. Power Syst., vol. 20, no. 3, pp. 1597-1605, 2005.

[65] F. Milano, C. A. Cañizares, and A. J. Conejo, "Sensitivity-Based Security-Constrained OPF Market Clearing Model," IEEE Trans. Power Syst., vol. 20, no. 4, pp. 2051-2060, 2005.

[66] Y. Li and J. McCalley, "Risk-based Optimal Power Flow and System Operation State," in IEEE Power & Energy Society General Meeting, Calgary, July 2009.

[67] F. Xiao and J. McCalley, "Power System Risk Assessment and Control in a Multi-objective Framework," IEEE Trans. Power Syst., Vol. 24, No. 1, Feb. 2009, pp 78-87.

[68] R. Dai, H. Pham, Y. Wang and J.D. McCalley, "Long Term benefits of online risk-based DC optimal power flow", Journal of Risk and Reliability (Part O of the Proceedings of the Institution of Mechanical Engineers): Special Issue on "Risk and reliability modeling of energy systems", vol. 226, no. 1, pp. 65-74, Feb. 2012.

[69] M. Ni, J. McCalley., V. Vijay, et al. "Software implementation of online risk-based security assessment," IEEE Trans. Power Syst., vol. 18, no. 3, 2003, pp. 1165-1172.

[70] G.R. GRIMMETT and D.R. STIRZAKER, Probability and Random Processes, 3rd ed., Oxford University Press, 2001.

[71] F. Xiao, J. McCalley, Y. Ou, et al., "Contingency Probability Estimation Using Weather and Geographical Data for On-Line Security Assessment," Int. Conf. on Prob. Methods Applied to Power Syst., Stockholm, June 2006.

[72] J. McCalley, F. Xiao, Y. Jiang, et al., "Computation of Contingency Probabilities for Electric Transmission Decision Problems," Proc. of the 13th Int. Conf. on Intelligent Syst. Appl. to Power Syst., Arlington, Nov. 2005.

[73] S. Maslennikov and E. Litvinov, “Adaptive Emergency Transmission Rates in Power System and Market Operation,” IEEE Trans. Power Syst., vol. 24, no. 2, pp. 923 – 929, 2009.

[74] ISONE. Operating Procedure (No. 19), Effective on Feb. 1, 2005. [Online]. Availabl e: http://www.iso-ne.com/rules_proceds/operating/isone/op19/op19b_rto_final.pdf

[75] ERCOT, EMS. Dynamic Ratings Requirements (09Q2) v3.0. [Online]. Available: http://nodal.ercot.com/docs/pd/ems/index.html#req

[76] PJM Manual 03: Transmission Operations, Nov. 16, 2011. [Online]. Available: http://pjm.com/~/media/documents/manuals/m03.ashx

[77] California Energy Commission, Dynamic Circuit Thermal Line Ratings, Oct. 1999. [Online]. Available: http://www.energy.ca.gov/reports/2002-01-10_600-00-036.pdf

[78] F. Xiao, "Risk based multi-objective security control and congestion management," Ph.D. dissertation, Dept. Elect. and Comput. Eng., Iowa State Univ., Ames, IA, 2007.

[79] E. Litvinov, T. Zheng, G. Rosenwald, and P. Shamsollahi, “Marginal loss modeling in LMP calculation,” IEEE Trans. Power Sys, vol. 19, no. 2, pp. 880-888, 2004.

[80] Y. Fu, M. Shahidehpour, and Z. Li, “AC Contingency Dispatch Based on Security-Constrained Unit Commitment,” IEEE Trans. Power Syst., vol. 21, no. 2, pp. 897-908, 2006.

[81] N. Alguacil and A. J. Conejo, “Multiperiod Optimal Power Flow Using Benders Decomposition,” IEEE Trans. Power Syst., vol. 15, no. 1, pp. 196-201, 2000.

[82] P.Yumbla, J.M. Ramirez, and C. Coello, “Optimal Power Flow Subject to Security Constraints Solved With a Particle Swarm Optimizer,” IEEE Trans. Power Syst., vol. 23, no. 1, pp. 33-40, 2008.

[83] V. Sarkar and S. A. Khaparde, “Optimal LMP Decomposition for the ACOPF Calculation,” IEEE Trans. Power Syst., vol. 26, no. 3, pp. 1714-1723, 2011.

[84] FERC report, Recent ISO software enhancements and future software and modeling plans, Nov. 2011. Available at: http://www.ferc.gov/industries/electric/indus-act/rto/rto-iso-soft-2011.pdf.

[85] M. Shahidehopour and Y. Fu, “Benders decomposition: applying Benders decomposition to power systems,” IEEE Power Energy Mag., vol. 3, no. 2, pp. 20–21, Mar./Apr. 2005.

[86] A. Monticelli, M. V. F. Pereira, and S. Granville, "Security-Constrained Optimal Power Flow with Post-Contingency Corrective Rescheduling," IEEE Trans. Power Syst., vol. 2, no. 1, pp. 175-180, 1987.

[87] Y. Fu, and M. Shahidehpour, "Fast SCUC for Large-Scale Power Systems," IEEE Trans. Power Syst., vol. 22, no. 4, pp. 2144-2151, 2007.

[88] P. Anderson and A. Fouad. Power System Control and Stability, 2nd ed. Wiley-IEEE Press, 2003, pp.33-48.

[89] N. KARMARKAR, "A new Polynomial-time Algorithm for Linear Programming," Combinatorica, vol.4, no. 4, pp. 373-395, 1984.

[90] Qin Wang, James D. McCalley, T. Zheng and E. Litvinov, "A Computational Strategy to solve preventive risk-based security constrained OPF," IEEE Trans. on power systems, vol. 28, no. 2, pp. 1666-1675, May 2013.

[91] H.W. Dommel and W.F. Tinney, "Optimal power flow solutions," IEEE Trans. Power App. Syst., vol. PAS-87, no. 10, pp. 1866-1876, Oct. 1968.

[92] D.I. Sun, B. Ashley, B. Brewer, A. Hughes and W.F. Tinney, "Optimal power flow by Newton approach," IEEE Trans. Power App. Syst., vol. PAS-103, no. 10, pp. 2864-2875, Oct. 1984.

[93] F. Capitanescu, J.L.M. Ramos, P. Panciatici, et al., "State-of-the-art, challenges, and future trends in security constrained optimal power flow," Electric Power Systems Research, vol. 81, no. 8, pp. 1731-1741, Aug. 2011.

[94] M.S. Bazaraa, H.D. Sherali and C.M. Shetty, Nonlinear programming: theory and algorithms, 3rd ed. New York: Wiley, 2006, pp.257-313.

[95] A.J. Conejo, E. Castillo, R. Minguez, and R.G. Bertrand, Decomposition techniques in mathematical programming: engineering and science application, Berlin: Springer, 2006, pp.187-239.

[96] Luenberger, D.G. Linear and Nonlinear Programming, 2nd ed. Addision-Wesley Reading, MA, 1984.

[97] A.J. Conejo and J.A. Aguado, "Multi-area coordinated decentralized DC optimal power flow," IEEE Trans. Power Syst., vol. 13, no. 4, 1998, pp. 1272-1278.

[98] R. E. Perez-Guerrero and G. T. Heydt, "Distribution system restoration via subgradient-based Lagrangian relaxation," IEEE Trans. Power Syst., vol. 23, no. 3, pp. 1162-1169, Aug. 2008.

[99] K.S. Hindi and M. Ghani, "Dynamic economic dispatch for large scale power systems: a Lagrangian relaxation approach," Int. Journal of Elec. Power & Energy Systems, vol. 13, no. 1, pp.51-56, Feb.1991.

[100] Y. Fu, M. Shahidehpour, and Z. Li, "Long-term security-constrained unit commitment: hybrid Dantzig-Wolf decomposition and subgradient approach," IEEE Trans. Power Syst., vol. 20, no. 4, Nov. 2005, pp. 2093-2106.

[101] N.J. Redondo and A.J. Conejo, "Short-term hydro-thermal coordination by Lagrangian relaxation: solution of the dual problem," IEEE Trans. Power Syst., vol. 1, no. 4, pp. 89-95, 1999.

[102] H.Y. Yamin, K. Al-Tallaq, S.M. Shahidehpour, "New approach for dynamic optimal power flow using Benders decomposition in a deregulated power market," Electric Power Systems Research, vol. 65, no. 2, pp. 101-107, May 2003.

[103] S. Binato, M.V.F. Pereira, and S. Granville, "A new Benders decomposition approach to solve power transmission network design problem," IEEE Trans. Power Syst., vol. 16, no. 2, pp. 235-240, 2001.

[104] H. Ma and S.M. Shahidehpour, "Transmission constrained unit commitment based on Benders decomposition," Elect. Power Energy Syst., vol. 20, no. 4, pp. 287-294, May 1998.

[105] M. Shaaban, W. Li, H. Liu, Z. Yan, Y. Ni and F. Wu, "ATC calculation with steady-state security constraints using Benders decomposition," IEE Proceedings on Generation, Transmission and Distribution, vol. 150, no. 5, pp. 611-615, Sept. 2003.

[106] T. Gomez, I.J. Perez-Arriaga, J. Lumbreras, and V.M. Parra, "A security-constrained decomposition approach to optimal reactive power planning," IEEE Trans. Power Syst., vol. 6, no. 3, pp. 1069-1076, Aug. 1991.

[107] The Joint Board for the PJM/MISO Region, Report on Security Constrained Economic Dispatch, Submitted to the Federal Energy Regulatory Commission on May 24, 2006.

[108] W.H. Fu and J.D. McCalley, "Risk based optimal power flow," IEEE Porto Power Tech Proceedings, Porto, Portugal, Sep. 2001.

[109] A. Dissanayaka, U.D. Annakkage, B. Jayasekara, and B. Bagen, "Risk-Based Dynamic Security Assessment," IEEE Trans. Power Sys, vol. 26, no. 3., pp. 1302-1308, 2011.

[110] 2009 Annual Markets Report, ISO New England, May 18, 2010.

[111] State of the Markets Report, New York ISO, 2009.

[112] 2010 State of the Market Report State of the Market Report, Midwest ISO, May 2011.

[113] PJM Training Materials (LMP 101), PJM.

[114] B.B. Chakrabarti, C. Edwards, C. Callaghan, and S. Ranatunga, Alternative Loss Model for the New Zealand Electricity Market using SFT, 2011 IEEE Power and Energy Society General Meeting, Detroit, USA.

[115] L. Chen, H. Suzuki, T. Wachi, and Y. Shimura, "Components of Nodal Prices for Electric Power Systems," IEEE Trans. Power Sys., vol. 17, no. 1, pp. 41-49, 2002.

[116] T. Orfanogianni and G. Gross, "A General Formulation for LMP Evaluation," IEEE Trans. Power Sys., vol. 2, no. 3, pp. 1163-1173, 2007.

[117] A. Conejo, E. Casillo, R. Minguez, and F. Milano, "Locational Marginal Price Sensitivities," IEEE Trans. Power Sys., vol. 20, no. 4, pp. 2026-2033, 2005.

[118] J. E. Price, "Market-Based Price Differentials in Zonal and LMP Market Designs," IEEE Trans. Power Sys., vol. 22, no. 4, pp. 1486-1494, 2007.

[119] Q. Wang and J. McCalley, "Risk and 'N-1' Criteria Coordination for Real-time Operations," Accept for publication by IEEE Trans. Power Sys., 2013.

[120] J. B. Cardell, "Marginal Loss Pricing for Hours with Transmission Congestion," IEEE Trans. Power Sys., vol. 22, no. 4, pp. 1466-1474, 2007.

[121] ISONE. Operating Procedure (No. 19), Effective on Feb. 1, 2005. [Online]. Availabl e: http://www.iso-ne.com/rules_proceds/operating/isone/op19/op19b_rto_final.pdf

[122] PJM Interconnection LLC, "LMP/FTR trainning". [Online]. Available: http://pjm.com/training/~/media/training/core-curriculum/ip-lmp-101/lmp-ftr-101-training.ashx

[123] F. X. Li and R. Bo, "DCOPF-Based LMP Simulation: Algorithm, Comparison with ACOPF, and Sensitivity," IEEE Trans. Power Sys, vol. 22, no. 4, pp. 1475-1485, 2007.

[124] F. X. Li , "Continuous Locational Marginal Pricing (CLMP)," IEEE Trans. Power Sys., vol. 22, no. 4, pp. 1638-1646, 2007.

[125] E. Litvinov, "Design and operation of the locational marginal prices-based electricity markets," IET Gen., Trans. & Dist., vol. 4, no. 2, pp. 315-323, 2010.

[126] T. Wu, “Locational marginal price calculations using the distributed-slack power-flow formulation,” IEEE Trans. Power Sys, vol. 20, no. 2, pp. 1188-1190, 2005.

[127] C. Xu and T. J. Overbye, “An energy reference bus independent LMP decomposition algorithm,” IEEE Trans. Power Sys, vol. 21, no. 3, pp. 1041-1049, 2006.

[128] G. Hamoud and I. Bradley, “Assessment of Transmission Congestion Congestion Cost and Locational Marginal Pricing in a Competitive Electricity Market,” IEEE Trans. Power Sys., vol. 19, no. 2, pp. 769-775, 2004.

[129] V. Sarkar, and S.A. Khaparde, "Reactive Power Constrained OPF Scheduling With 2-D Locational Marginal Pricing," IEEE Trans. Power Sys., vol. 28, no. 1, pp. 503-512, 2013.

[130] T. Van Cutsem, “A method to compute reactive power margins with respect to voltage collapse,” IEEE Trans. Power Syst., vol.6, no. 1, pp. 145-156, Feb. 1991.

[131] P. Sauer and M. Pai, “Power System Steady-State Stability and the Load Flow Jacobian,” IEEE Trans. Power Syst., vol.5, no. 4, pp. 1374-1383, Nov. 1990.

[132] V. Ajjarapu, and C. Christy, “The continuation power flow: a tool for steady state voltage stability analysis,” IEEE Trans. Power Syst., vol.7, no. 1, pp. 416-423, Feb. 1992.

[133] Scott Greene, Ian Dobson and Fernando L. Alvarado, “Sensitivity of the loading margin to voltage collapse with respect to arbitrary parameters,” IEEE Trans. Power Syst., vol.12, no. 1, pp. 262-272, Feb. 1997.

[134] A.K. Sinha, D. Hazarika, “A comparative study of voltage stability indices in a power system,” Electrical Power and Energy Systems, vol. 22, pp. 589-596, 2000.

[135] Scott Greene, Ian Dobson and Fernando L. Alvarado, “Contingency Ranking for Voltage Collapse via Sensitivities from a Single Nose Curve,” IEEE Trans. Power Syst., vol.14, no. 1, pp. 232-240, Feb. 1999.

[136] Hsiao-Dong Chiang, Rene Jean-Jumeau, “Toward a Practical Performance Index for Predicting Voltage Collapse in Electric Power Systems,” IEEE Trans. Power Syst., vol.10, no. 2, pp. 584-590, May. 1995.

[137] Z. Feng and W. Xu, “Fast computation of post-contingency system margins for voltage stability assessments of large-scale power systems,” IEE Proc, Transm, Distrib, vol. 147, no. 3, pp. 76-80, March 2000.

[138] Arthit Sode-Yome, N. Mithulananthan, and K. Y. Lee, “A Maximum Loading Margin Method for Static Voltage Stability in Power Systems,” IEEE Trans. Power Syst., vol.21, no. 2, pp. 799-808, May 2006.

[139] Wenjuan Zhang, Fangxing Li and Leon M. Tolbert, "Review of Reactive Power Planning: Objectives, Constraints, and Algorithms," IEEE Trans. Power Syst., vol.22, no. 4, pp. 2177-2186, Nov. 2007.

[140] Haifeng Liu, et al., "Planning Reconfigurable Reactive Control for Voltage Stability Limited Power Systems," IEEE Trans. Power Syst., vol.24, no. 2, pp. 1029-1038, May 2009.

[141] M. Beiraghi and A.M. Ranjbar, "Online Voltage Security Assessment Based on Wide-Area Measurements," IEEE Trans. Power Delivery, vol. 28, no. 2, pp. 989-997, Apr. 2013.

[142] Thierry Van Cutsem, "Voltage Instability: Phenomena, Countermeasures, and Analysis Methods," Proceedings of the IEEE, vol. 88, no. 2, pp. 208-227, Feb. 2000.

[143] F. W. Mohn and A. C. Zambroni de Souza, "Tracing PV and QV curves with the help of CRIC continuation Method," IEEE Trans. Power Syst., vol.21, no. 3, pp. 1115-1122, Aug. 2006.

[144] B. H Chowdhury and C. W. Taylor, "Voltage Stability Analysis: V-Q Power Flow Simulation Versus Dynamic Simulation," IEEE Trans. Power Syst., vol.15, no. 4, pp. 1354-1359, Nov. 2000.

[145] A.C. Zambroni de Souza, Fritz W. Mohn, Isabella F. Borges, and Tito R. Ocatiz, "Using PV and QV curves with the meaning of static contingency screening and planning," Electric Power Systems Research, vol. 81, pp. 1491-1498, 2011.